FLUID FLOW AND SOUND GENERATION AT HYDROTHERMAL VENT FIELDS

by

Sarah Alden Little

B.S. (1981) Stanford University

Submitted in Partial Fulfillment
of the Requirements for the Degree of

Doctor of Philosophy
at the
Massachusetts Institute of Technology
and the
Woods Hole Oceanographic Institution

April 8, 1988

Signature of Author _____
Woods Hole Oceanographic Institution / Massachusetts Institute of Technology Joint Program in Oceanography, Woods Hole, MA 02543.

Certified by _____
Keith D. Stolzenbach, Thesis Co-Supervisor
Department of Civil Engineering, MIT

Certified by _____
G. Michael Purdy, Thesis Co-Supervisor
Department of Geology and Geophysics, WHOI

Accepted by _____
Marcia McNutt, Chairman
Joint Committee for Marine Geology and Geophysics, MIT/WHOI

CONTENTS

FLUID FLOW AND SOUND GENERATION AT HYDROTHERMAL VENT FIELDS

by

SARAH ALDEN LITTLE

Submitted to the Department of Earth, Atmosphere and Planetary Sciences
on April 8, 1988
in partial fulfillment of the requirements for the
Degree of Doctor of Philosophy in
Marine Geophysics

ABSTRACT

Several experiments are presented in this thesis which examine methods to measure and monitor fluid flow from hydrothermal vent fields.

Simultaneous velocity, temperature, and conductivity data were collected in the convective flow emanating from a hydrothermal vent field located at $10^{o}56'N$, $103^{o}41'W$ on the East Pacific rise. The horizontal profiles obtained indicate that the flow field approaches an ideal plume in the temperature and velocity distribution. Such parameters as total heat flow and maximum plume height can be estimated using either the velocity or the temperature information. The results of these independent calculations are in close agreement, yielding a total heat flow from this vent site of 3.7 ± 0.8 MW and a maximum height of 150 ± 10 m. The nonlinear effects of large temperature variations on heat capacity and volume changes slightly alter the calculations applied to obtain these values.

In Guaymas Basin, a twelve day time series of temperature data was collected from a point three centimeters above a diffuse hydrothermal flow area. Using concurrent tidal gauge data from the town of Guaymas it is shown that the effects of tidal currents can be strong enough to dominate the time variability of a temperature signal at a fixed point in hydrothermal flow and are a plausible explanation for the variations seen in the Guaymas Basin temperature data.

Theoretical examination of hot, turbulent, buoyant jets exiting from hydrothermal chimneys revealed acoustic source mechanisms capable of producing sound at levels higher than ambient ocean noise. Pressure levels and frequency generated by hydrothermal jets are dependent on chimney dimensions, fluid velocity and temperature and therefore can be used to monitor changes in these parameters over time.

A laboratory study of low Mach number jet noise and amplification by flow inhomogeneities confirmed theoretical predictions for homogeneous jet noise power and frequency. The increase in power due to convected flow inhomogeneities, however, was lower in the near field than expected.

Indirect evidence of hydrothermal sound fields (Reidesel et al., 1982; Bibee and Jacobson, 1986) showing anomalous high power and low

frequency noise associated with vents is due to processes other than jet noise.

On Axial Seamount, Juan de Fuca Ridge, high quality acoustic noise measurements were obtained by two hydrophones located 3 m and 40 m from an active hydrothermal vent, in an effort to determine the feasibility of monitoring hydrothermal vent activity through flow noise generation. Most of the noise field could be attributed to ambient ocean noise sources of microseisms, distant shipping and weather, punctuated by local ships and biological sources. Water/rock interface waves of local origin, were detected which showed high pressure amplitudes near the seafloor and, decaying with vertical distance, produced low pressures at 40 m above the bottom.

Detection of vent signals was hampered by unexpected spatial non-stationarity due to shadowing effects of the caldera wall. No continuous vent signals were deemed significant based on a criterion of 90% probability of detection and 5% probability of false alarm. However, a small signal near 40 Hz, with a power level of 1×10^{-4} Pa^2/Hz was noticed on two records taken near the Inferno black smoker. The frequency of this signal is consistent with predictions and the power level suggests the occurrence of jet noise amplification due to convected density inhomogeneities.

Ambient noise from the TAG (Trans-Atlantic Geotraverse) hydrothermal area on the Mid-Atlantic Ridge near $26^{o}N$, in the frequency band 1-30 Hz at a range of 0.75-14 km from the site of an extremely active high temperature hydrothermal vent field (Rona, 1986) was examined. The ambient noise field exhibits great temporal and spatial variations attributed in part to typical ocean noise sources such as distant shipping and microseisms. Power spectral levels as measured at each of six ocean bottom hydrophones (OBH) were used to estimate the location of point sources of sound in the area, if any.

The hydrothermal vent did not produce enough sound to be located as a point source using data from the OBH array. The only consistently identifiable point source found with the data set was generating sound in a 0.8-3.5 Hz bandwidth and located outside the median valley. It appears to be harmonic tremor associated with the tip of a ridge on the western side of the spreading axis and may be volcanic in origin.

BIOGRAPHICAL NOTE

Education:

B.S. Physics, Stanford University, Phi Beta Kappa, 6/81
Ph.D. Marine Geophysics, Massachusetts Institute of Technology, Woods Hole Oceanographic Institution Joint Program in Oceanography, 4/88

Positions:

Optical engineer at MIT Lincoln Laboratory, 10/81-9/82
Summer Student Fellowship in Ocean Engineering, WHOI, 6/81-9/81
Center for Analysis of Marine Systems fellowship, 9/82-1/85

Publications:

Little, S.A. and R.A. Stephen, 1985, The Costa Rica Rift Borehole Seismic Experiment, DSDP Hole 504B, Leg 92. Deep Sea Drilling Project Initial Reports, Vol. 83, p517-528.

Little, S.A., K.D. Stolzenbach, and R.P. Von Herzen, Measurements of Plume Flow from a Hydrothermal Vent Field. J. Geophys. Res., 92, B3, p2587-2596.

Research Cruises:

1983, April: Two weeks on the Ellen B. Scripps, to rendezvous with the Glomar Challenger and conduct the borehole seismic experiment south of the Costa Rica Rift in DSDP Hole 504B (chief scientist: R.A. Stephen).

1984, May: Ten days on the Atlantis II to dive with the DSV Alvin on a hot vent and survey a hydrothermal plume on the East Pacific Rise at 11^{o}N (chief scientist: M.J. Mottl).

1985, December: Four weeks on the RV Melville, to survey 10^{o}N-12^{o}N on the East Pacific Rise with the towed televiewer ARGO (chief scientist: R.D. Ballard); Little conducted a passive acoustic survey of hydrothermal vents.

1987, September: Three weeks on the Atlantis II, to dive with the DSV Alvin on Ashes Vent Field on Axial Seamount, Juan de Fuca Ridge (chief scientist: S. Hammond) to emplace and recover a hydrothermal acoustic monitoring instrument.

ACKNOWLEDGEMENTS

Since my work has taken me across disciplines, from geology and geophysics to engineering and physical oceanography, I have had the dubious pleasure of asking favors of more people than most graduate students even know. Luckily, the people at WHOI are extremely generous in coming to the aid of the underclass citizen which is a graduate student. I could present a complete list of those who have helped me during my graduate career, but a WHOI directory has already been published. I will, therefore, limit myself to acknowledging here those whose generosity struck me as being far beyond the call of duty.

First, and foremost, I wish to recommend Keith Stolzenbach to any graduate student who is in search of an advisor who can walk the fine line between guidance and freedom; who repays conscientious work with prompt and even handed criticism; and who genuinely and willingly develops from mentor and advocate, to colleague.

Second, I always have and always will be indebted to my family, but the special recognition they deserve in this thesis is embodied in my oft-used phrase " family technical." It is no understatement to say that without Jack's Matlab software, coupled with his generous and lucid explanations of signal processing, I would still be analyzing data (yes, even as you read this), writing Fortran until I was blue in the face (which doesn't take too long), and wondering how to solve a multivariable, non-linear set of equations (hint: type "help nelder").

Also, I discovered that work can be quite enjoyable when tackling technical problems with the help of a clever physicist who thinks along the same lines as I do - and I wouldn't have known this if Ruel hadn't come by my lab to check out what was happening with my experiment. That got him interested in my project, interested enough to spend many of his nights and weekends building and programming the hydrothermal acoustic monitor instrument. Without his help the CHAMP (Calibrated Hydrothermal Acoustic Monitor) would have been SPAM (Sarah's Permanent Acoustic Monitor) and my blood pressure would have been a lot higher.

Finally, John, Elizabeth, Nancy and Tom, making up the rest of the family technical team, all managed to set me straight more than once while I searched for math, hardware, programming or organizational help.

My committee, Keith Stolzenbach, Mike Purdy, Spahr Webb, Joe Cann, and Dick Von Herzen, deserves tremendous thanks for helping me formulate and carry out my thesis. Even though it was outside the research bounds of any one member they were very supportive and allowed me to pursue my own interests despite the risks involved.

As for the rest, I present in no particular order, a few people whose help with my work has left me quite deeply in debt: Joe Cann, Hugh Milburn, Jerry Dean, Chris Bradley, Laura Kong, Ed Mellinger, Josh Hoyt, Franz Hover, Karlen Wannop, Jim Newman, Chris Fox, Doug Hersh, and Debbie Smith.

This work was supported by the WHOI/MIT Education Office, the Center for Analysis of Marine Systems, the National Science Foundation (grant OCE83-10175), WHOI Sea Grant (R/6-14), the Office of Naval Research, and the NOAA Vents Program.

INTRODUCTION

The interaction of a complex set of geological, biological, chemical and fluid dynamical processes create the life supporting environment called earth. Except for the influx of solar radiation, the earth is basically a self-contained, internally cycling system upon which a great diversity of life depends. The different cycles occur on all scales and levels of interaction. Slow, large scale geologic processes such as continental formation and drift, seafloor creation, and mountain building interact with similar scale processes in other fields: species evolution in biology, mantle convection in fluid dynamics, to create long time period trends in the environment. Medium scale variations seen in ocean chemical composition, hydrothermal activity, sea level, biological extinction and global climate are clearly cyclic and interdependent. And on the small scale, volcanic eruptions, earthquakes, storms, pollution, and species blooms and extinctions interact to produce a challenging, rapidly changing habitat. The ability to predict and control changes in this environment is necessary for our survival on such a planet, especially as we begin to participate, through technology and increased population, in the cycles and processes themselves.

The ambitious task of understanding the earth as a system must be approached by breaking down the problem into a set of studies of individual processes which can then be related to the interdisciplinary, global view. In this way, a large number of scientists from many fields

contribute to a level of understanding necessary to prevent adverse changes and precipitate beneficial ones in this self-contained system.

In the context of earth system science, an important, individual process is the circulation of seawater through oceanic lithosphere, a process which transfers heat and chemicals from the mantle to the oceans and enables them to react with and influence the biosphere. Over 30 active hydrothermal vent sites have been found to date, both in the Atlantic and Pacific oceans. It is becoming increasingly apparent that hydrothermal systems permeate a large portion of the Mid-Ocean Ridge system, and may significantly contribute to the chemical composition of the ocean and atmosphere.

Hydrothermal circulation begins as cold seawater seeps into the exposed, fractured basalt found along mid-ocean ridges. The shallow magma chambers and intruded lavas characteristic of these ocean floor spreading centers provide heat to drive the seawater in a convection system within the crust. Unreacted seawater enters a broad downflow zone which extends kilometers along and away from the unsedimented spreading axis. As the cool water descends and approaches the heat source, its temperature and reactability increase and it rapidly leaches minerals from the surrounding rock. Upon descending to the top of a magma chamber, 2-4 km into the crust, the water, now rich in minerals, turns and rises through narrow upflow zones a few tens of meters wide and exits onto the sea floor. The surface expression of these hydrothermal vents is a spectacular manifestation of the importance of the heat and mass load of the fluid. The precipitation of minerals that occurs when the hot vent fluid mixes with cold, ambient seawater forms tall, 15-20 m high

sulfide chimneys out of which spews 350°C black, particle laden smoke. Fluid that has mixed in the subsurface with ambient seawater and has lost its mineral load issues from cracks and fissures around these chimneys as cooler, clear fluid. The hydrogen sulfide present in vent water provides the primary energy source for a suite of unique organisms which colonize hydrothermal vents. Massive ore deposits of iron, copper and zinc sulfide are formed by continuous deposition of the mineral content of vent fluid. And the plume of warm, particle rich fluid that rises above a vent field can be detected many kilometers away and may drive local ocean circulation.

Studies of hydrothermal circulation have relied on instantaneous measurements of surface characteristics like morphology, biota, temperature, chemical composition, and flow velocity, which are then can be used to model subsurface chemical and flow processes. Even these measurements are difficult to obtain, requiring the use of a submersible for most sampling. The high pressure, hot water, particle precipitation and corrosive fluids make long-term measurements even more scarce. In designing a method to determine simply the temperature field, for example, one is faced with numerous difficulties starting with the complex and variable morphology of vent fields. Flow ranges in character from 10°C water slowly seeping through cracks, fissures, masses of tube worms, and bacterial mats, to hot, 350°C water jetting out of narrow, 5 cm diameter sulfide chimneys at 2-3 m/s. The sensor must be able to withstand high temperature and also cover an area of extremely variable flow and temperature. Long-term measurements are even more problematic, as they are complicated by the fact that chimneys grow, fall and

effectively change position, that many materials degrade under vent conditions, and that variable cross-currents move the plume of hot water back and forth over the vent field.

The full impact of hydrothermal fluxes of heat and chemicals on biogeochemical cycles can only be assessed by determining both the total spatial extent and temporal variability of hydrothermal vents, neither of which are presently well known. The overall purpose of the work contained in this volume was to examine heat and fluid fluxes from hydrothermal vents, and to develop methods with which to measure these, both instantaneously and over the long-term.

The first study was directed at measuring instantaneous heat flux from a black smoker vent field. Velocity and temperature measurements were taken in the convective flow emanating from a hydrothermal vent field and used with plume theory to estimate total heat flux from the site. The close agreement between heat flux calculations using velocity and independent calculations using temperature justified the validity of this method for estimating instantaneous hydrothermal vent heat flux.

The second study examined cross-current effects on temperature measurements made in diffuse hydrothermal flow. A twelve day time series of temperature from a few centimeters above an area of diffuse flow showed significant temporal variations which seemed to be correlated with tide. It was shown through a boundary layer flow model that the effects of tidal currents can be strong enough to dominate the time variability of a temperature signal at a fixed point in hydrothermal flow. The results show the necessity of recording simultaneous bottom currents when

trying to use temperature measurements to determine variations in hydrothermal flow caused by subsurface processes.

The three other studies which make up this work were concentrated on determining the feasibility of monitoring high temperature, high velocity fluid flux through passive acoustic measurements of hydrothermally generated sound. They include a theoretical examination of sound source mechanisms, a laboratory experiment to determine the acoustic behavior of low Mach number, an examination of noise recorded near hydrothermal vents by microearthquake surveys, and a field experiment designed to measure the sound produced at a hydrothermal vent jet.

Theoretical examination of hot, turbulent, buoyant jets exiting from hydrothermal chimneys revealed acoustic source mechanisms capable of producing sound at levels higher than ambient ocean noise. Pressure levels and frequency generated by hydrothermal jets are dependent on chimney dimensions, fluid velocity and temperature and therefore can be used to monitor changes in these parameters over time.

A laboratory study of low Mach number jet noise and amplification by flow inhomogeneities confirmed theoretical predictions for homogeneous jet noise power and frequency. The increase in power due to convected flow inhomogeneities, however, was lower in the near field than expected.

Indirect evidence of hydrothermal sound fields showing anomalous high power and low frequency noise associated with vents is due to processes other than jet noise.

Direct measurements of hydrothermal vent sound fields show that frequency and power levels are comparable to ambient ocean noise and are consistent with jet quadrupole near-field sound which has been amplified

by the dipole behavior of convected flow inhomogeneities. This near-field amplification is not as great as that predicted for the far-field but is consistent with theoretical considerations for near-field dipole and quadrupole behavior.

Hydrothermal systems are extremely variable, complex, inaccessible and difficult to characterize. Yet, they embody a process through which significant quantities of heat and chemicals enter the ocean, massive ore deposits are formed, and on which unique vent communities depend. The value of studying them outweighs the difficulties inherent in such studies. The work presented here has provided a method with which to measure instantaneous heat flux from black smoker vent fields. The proportion of heat loss from diffuse flow to that of total flux remains unknown, however. The importance of measuring cross-currents in long-term monitoring has been illuminated. The method of examining long-term variability in flow through passive acoustic monitoring has been shown to be theoretically possible, but given the levels of ambient ocean noise, not a simple tool useful at all vent sites.

The development of hydrothermal vent monitoring techniques is still an active field where many important problems remain unsolved.

JOURNAL OF GEOPHYSICAL RESEARCH, VOL. 92, NO. B3, PAGES 2587-2596, MARCH 10, 1987

Measurements of Plume Flow From a Hydrothermal Vent Field

SARAH A. LITTLE

Woods Hole Oceanographic Institution, Massachusetts

KEITH D. STOLZENBACH

Ralph M. Parsons Laboratory, Department of Civil Engineering
Massachusetts Institute of Technology, Cambridge

RICHARD P. VON HERZEN

Woods Hole Oceanographic Institution, Massachusetts

Simultaneous velocity, temperature, and conductivity data were taken in the convective flow emanating from a hydrothermal vent field located at 10°56'N, 103°41'W on the East Pacific Rise. The horizontal profiles obtained indicate that the flow field approaches an ideal plume in the temperature and velocity distribution. Such parameters as total heat flow and maximum plume height can be estimated using either the velocity or the temperature information. The results of these independent calculations are in close agreement, yielding a total heat flow from this vent site of 3.7 ± 0.8 MW and a maximum height of 150 ± 10 m. The nonlinear effects of large temperature variations on heat capacity and volume changes slightly alter the calculations applied to obtain these values.

INTRODUCTION

Near midocean ridges (MOR's), cold seawater seeps into unsedimented crust and is heated by the shallow magma chambers and intruded lavas of newly formed oceanic lithosphere in the process called hydrothermal circulation. The hot water, rich in minerals, rises buoyantly through the crust and exits through hydrothermal vents located on the ridge axis. These relatively sparsely distributed and inaccessible vents are geologically, chemically, and biologically active areas currently under intense study.

Active hydrothermal vents have been found in the Pacific Ocean on medium to fast spreading ridges near the Galapagos at 86°W, along the East Pacific Rise (EPR) at 20°S, 11°N, 13°N, and 21°N, in the Guaymas Basin, and on the Gorda and Juan de Fuca ridges between 40° and 50°N [*Green et al.*, 1981; *Baker et al.*, 1985; *Francheteau and Ballard*, 1983; *Crane et al.*, 1985; *Rona et al.*, 1985]. Numerous extinct vent sulfide chimneys have also been found in these areas. In the Atlantic Ocean, vents have been photographed at 23°N and 26°N on the Mid-Atlantic Ridge [*Rona et al.*, 1984 and R. Detrick, personal communication, 1985].

The processes of hydrothermal convection can be separated into three distinct scales of venting. The smallest scale is that of flow from a single opening on a hydrothermal sulfide edifice. Vents on this scale are often called smokers (due to the particulates in the venting fluid) and typically have openings 2-8 cm in diameter [*Converse et al.*, 1984]. The next scale is that of a vent field or vent area. This includes all the hot smokers (30-420°C) on the sulfide structure as well as the cooler (5-30°C) diffuse flow from cracks and crevices in the vicinity of the main sulfide edifice. A typical vent field is 100 x 100 m and is usually defined by the lateral extent of thermal anomalies and the associated animal communities [*Francheteau and Ballard*, 1983]. The largest scale of hydrothermal venting is that of an active ridge segment. On this scale of tens of kilometers, hydrothermal deposits and venting sites appear on regularly spaced (30-80 km) topographic highs [*Francheteau and Ballard*, 1983; *Schouten et al.*, , 1985]. These highs are thought to overlie sites of geologically recent (thousands of years) magma injection [*Schouten et al.*, 1985]. This scale could include 10-100 km of midocean ridge crest containing 20-30 active vent areas.

Attempts to determine the thermal output of hydrothermal vents have been limited in accuracy by either the very small scale (e.g., a single vent orifice) or the very large scale (e.g., a midocean ridge segment) of the measurements. *Macdonald et al.* [1980] used vent exit velocities and an orifice diameter estimated from video tapes coupled with assumed exit temperatures to calculate a heat flow of 60 MW from a single smoker at the National Geographic vent site at 21°N on the East Pacific Rise. *Converse et al.* [1984] measured flow rates and temperatures at 21°N by inserting a small vane-type flowmeter into individual smokers, estimating orifice diameters, and using buoyant plume theory to obtain values of heat flow ranging from 0.5 to 10 MW for individual smokers. These heat flow estimates depend on measurements made near the plume source and are thus highly sensitive to both the location of velocity and temperature measurements and visual estimates of the vent exit geometry. In addition, subsequent estimates of total heat flow from the vent field obtained by multiplying an individual smoker's heat flow by the number of observed orifices can neither account for the variations of individual smoker size nor the contribution to heat flow from diffuse flow.

On the large scale, *Crane et al.* [1985] estimated heat loss from ridge segments by applying buoyant plume theory and a gross heat balance to temperature measurements obtained by a ship-towed sensor array. Their estimates varied by a factor of more than 100, between 13,000 and 1,560,000 MW, for 141 km of the Juan de Fuca Ridge, largely as a result of the sensitivity of heat flow calculations to the resolution of horizontal and vertical positioning of temperature measurements and to uncertainties in the magnitude of regional ocean currents and hydrography.

Paper number 6B6258.
0148-0227/87/006B-6258$05.00

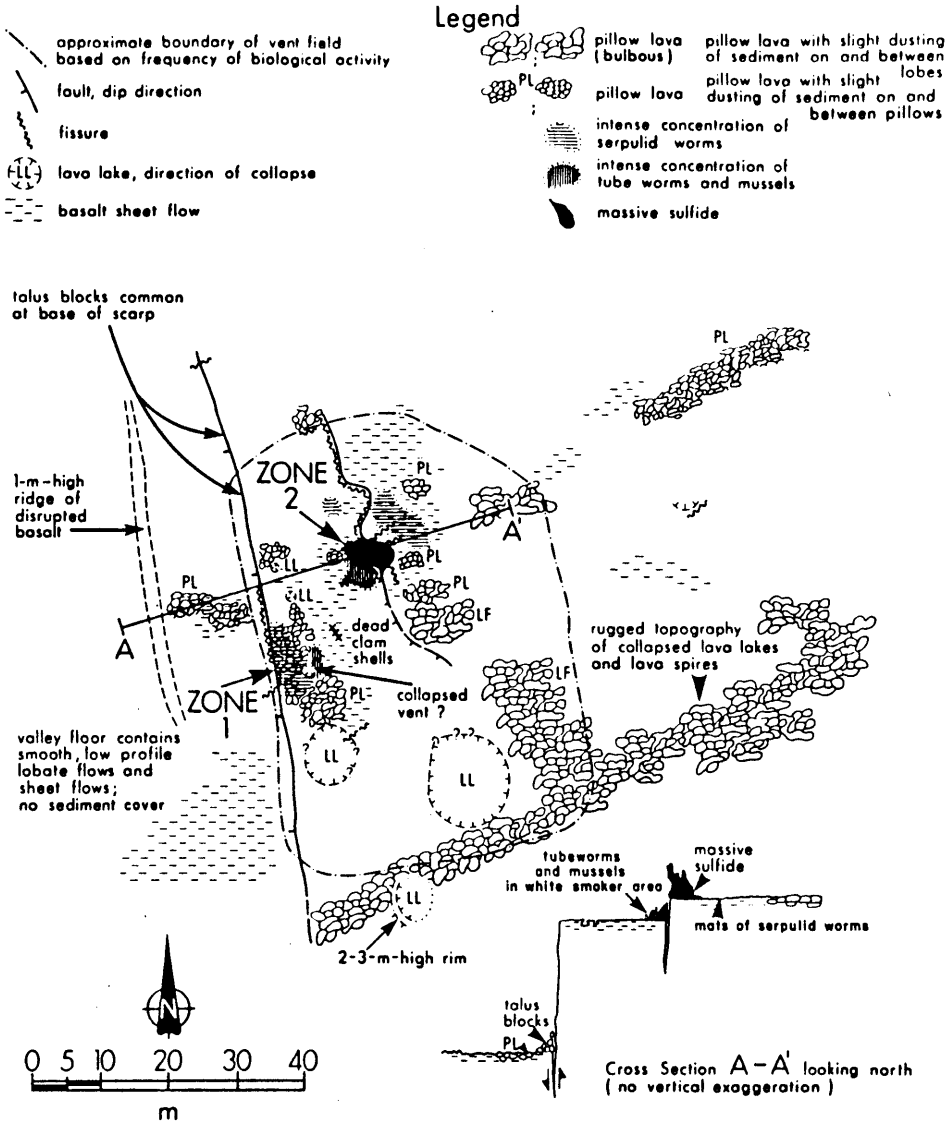

Fig. 1. Map of vent field at 10°55.73'N, 103°40.6'W showing sulfide structure on edge of fault scarp [from *McConachy et al.*, 1986]. Zone 1 depicts the location of warm water seeps; zone 2 shows the location of the main sulfide edifice with black smokers.

Our objectives were to obtain more accurate heat flow estimates and to characterize the fluid flow from a vent field by measuring the three-dimensional structure of the convective flow above a vent field at a scale (meters) between that of MacDonald and Converse et al. (centimeters) and Crane et al. (kilometers). Measurements made at the scale of a vent field can avoid problems due to sensitivity to vent exit quantity and geometry, and depend minimally on estimates of oceanic conditions such as ambient current and stratification. Precise mapping of temperature anomalies also permits the quantification of the relative contributions of high-temperature smokers and lower temperature diffuse flow to the total heat flow. To collect the appropriate data, the DSV *Alvin* and R/V *Atlantis II* visited 11°N on the EPR in May 1984 to survey chemically and physically the water above a vent field composed of both black smokers and the more diffuse warm vents. Temperature, pressure, conductivity, and velocity were measured at various heights above this vent field and used to determine the physical structure of the flow and to calculate maximum plume height and total advective heat flow.

SITE DESCRIPTION

The target vent field, located at 10°55.73'N, 103°40.6'W at a depth of 2531 m (see Figure 1), contains an actively venting sulfide edifice surrounded by patches of warm venting. The 65 x 45 m vent field lies along the eastern edge of the rift valley against a 20 m-high north-south trending fault scarp [*McConachy et al.*, 1984, 1986]. The vent area is comprised of pillow lava, basalt sheet flows, lava lakes with lava spires, and talus blocks of sulfide near the smokers. The chimney structure, consisting of both dead and broken spires and several active regions, reaches a height of approximately 8 m and is 3-4 m wide

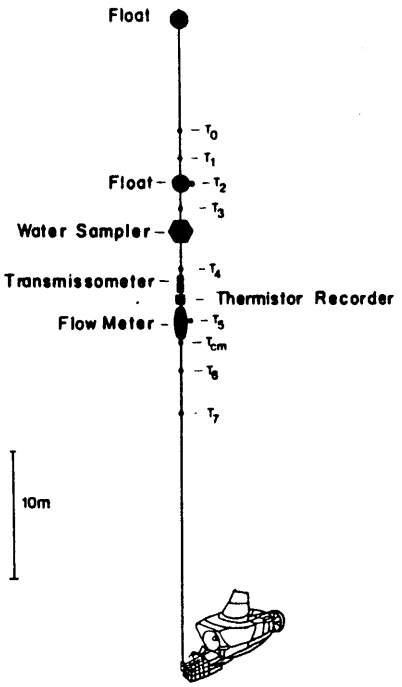

Fig. 2. Diagram of 50 m cable array deployed from the DSR/V *Alvin* with a water sampler, transmissometer, current meter and nine thermistors.

at the base. Hot, gray-black water flowed from the base from three main and three or four lesser openings 2-8 cm in diameter, all within 1 m of the seafloor. Shimmering, milky white water seeped out several meters from the base through beds of vestimentiferan tube worms.

EQUIPMENT

The temperature, conductivity, and velocity fields above the hydrothermal vent field were sampled with an array of sensors deployed vertically from the DRV *Alvin* (Figure 2). The instruments used in this work included a vertically mounted seven-thermistor chain surrounding a self-contained flowmeter, which recorded three-component current velocity, temperature, conductivity, pressure, tilt, and compass heading. The flowmeter was positioned 24 m above the sampling basket attached to base of the submarine; the thermistors were mounted at 40.5, 38.2, 35.6, 34.2, 30.1, 25.4, and 22.5 m above the base.

The flowmeter, built by J. Dean at the Woods Hole Oceanographic Institution, operates in the range of 1-100 cm/s [*Weller et al.*, 1985]. Its four fans, each 22 cm in diameter, detect two vertical (for redundancy) and two horizontal components of velocity. A tilt meter and a compass enable the measured velocities to be transposed into an earth-based reference frame despite rotations of the flowmeter. The thermistor response time is 7 s with a resolution of 0.005°C. Tilt, temperature, and pressure are each averaged over 5 s, conductivity over 3.6 s, and the current velocities over the entire 14 s sampling interval.

The thermistor chain, consisting of seven thermistors and a self-contained, internally recording package, was deployed on dive 1386. A data sample with a resolution of 0.001°C was recorded from each thermistor every 24 s.

EXPERIMENTAL PROCEDURE

The 50 m cable, with its attached flowmeter, thermistor chain, and flotation, was connected by a quick release mechanism to the basket of *Alvin* prior to launch. During descent, temperature, conductivity, and pressure were recorded to obtain the ambient stratification of the water column. Following descent, each dive consisted of several stations in the vicinity of the active main sulfide edifice. At each station the submarine remained stationary on the bottom for 5-30 min to allow the instrument array to stabilize in a vertical position and to record the time variability of the turbulent fluctuations in the plume. The submarine moved between stations while remaining as close to the bottom as possible, usually within 1-2 m. This resulted in flowmeter positioning of 24 ± 2 m above the seafloor during most of the dives. Larger excursions can be seen by examining the pressure records. All stations were conducted in the vent field at distances of 1-35 m from the chimney. Navigation was by dead reckoning. Video and still pictures were taken of the chimney structure and environs.

Three dives were completed with a fully operational, continuously recording flowmeter (1384, 1385, 1386), and on the last of these the thermistor chain internally recorded temperature at seven points along the vertical array.

DATA REDUCTION

The experiment resulted in a data set that includes seven simultaneous temperature profiles of the plume from one dive and three sets of temperature, conductivity, pressure, three-component velocity, tilt, and compass taken at 24 m above the bottom from each of three dives.

Salinity was calculated via a salinity algorithm [*Fofonoff and Millard*, 1983] using the temperature, conductivity, and pressure records. The few-second time lag between measurements of temperature and conductivity was sufficient to cause errors in salinity calculations in the rapidly varying plume environment. However, the chloride content of a water sample from this vent taken on dive 1377, several weeks earlier, was found to be only 3‰ higher than that of the ambient water (J. Edmond, personal communication, 1985). Accordingly, it was assumed in further data analysis that the plume salinity was equal to the ambient value of 34.651‰ obtained during the dive series 1384-1386.

Plume density was calculated employing an equation of state for seawater, [*Fofonoff and Millard*, 1983] and assuming a constant ambient salinity and pressure (2535 x 10^4 Pa).

Corrections are applied in order to recover the true vertical plume velocities in cases when the instrument array was moving up or down in response to the submarine motion. These vertical motions are removed from the measured vertical velocities to obtain true vertical plume velocities by subtracting the rate of pressure change of the instrument from the measured velocities. This procedure introduces an unwanted but tractable amount of noise (±4 cm/s) into the resulting vertical plume velocities due to the limited resolution of the pressure sensor.

Both the vertical and horizontal velocities have been put in an earth-based reference frame by using the compass and tilt records to remove the effects of spinning and tipping. These horizontal velocity records were used to calculate approximate instrument trajectories because an operational bottom navigation system was unavailable during the dives. The trajectories were reconstructed by estimating the ambient current from the long-term stations and subtracting this from the horizontal velocity data. The resultant velocities were integrated to obtain the relative positions of the instrument during a given dive. By

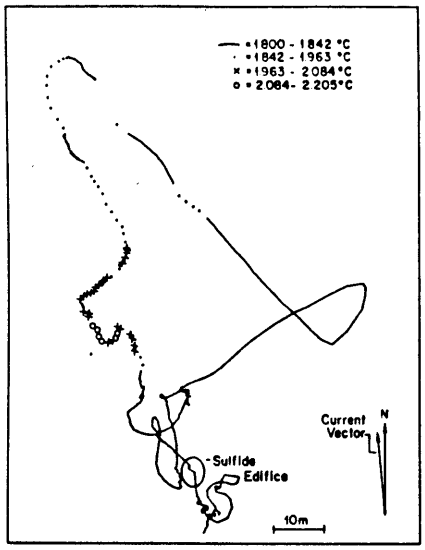

Fig. 3. Approximate dive track from dive 1384 shown with annotated temperatures and ambient current vector (0.24 cm/s W, 3.4 cm/s N). Track obtained from horizontal current records (accurate to 10 m). The approximate location of the main sulfide chimney is outlined with a circle.

combining temperature records with these positions we were able to make an approximate, two-dimensional map of the measured temperature anomalies 24 m off the bottom (see Figure 3). The major source of error in position (on the order of 10 m) results from the assumption of constant ambient current, which ranged from 3 to 4 cm/s toward the north to northwest during the dive.

RESULTS AND DISCUSSION

In order to characterize the fluid flow from a hydrothermal vent field and improve the accuracy of quantifying advected heat flow it is important to determine the extent to which the advective flow is plumelike and how it may be complicated by multiple sources, diffuse flow, ambient stratification, or shear flow caused by cross currents.

To determine the form of the convected flow, it is noted that when the instruments intersect the vent field at a height of 24 m above the bottom, the data show constant ambient values of 1.83°C punctuated by sharp peaks in temperature, velocity, and conductivity (see Figures 4-7). The data obtained from the thermistors at seven different heights also show this pattern with similarly shaped anomalous peaks in temperature. This indicates a plumelike structure, characterized by positive, peaked anomalies, where the overall structure of each anomaly is present at more than one height (Figure 7) with a general decrease in amplitude as height increases.

The four complicating factors mentioned above are all present at this vent site and must initially be addressed to determine the applicability of simple plume theory at this site, and later will be tested more rigorously with the specific values calculated from the theory. (1) Multiple sources: Photos show three strongly venting orifices and three or four weaker ones located at various levels on the main sulfide deposit within 3 m horizontally of each other. (2) Diffuse flow: Several pockets of cooler

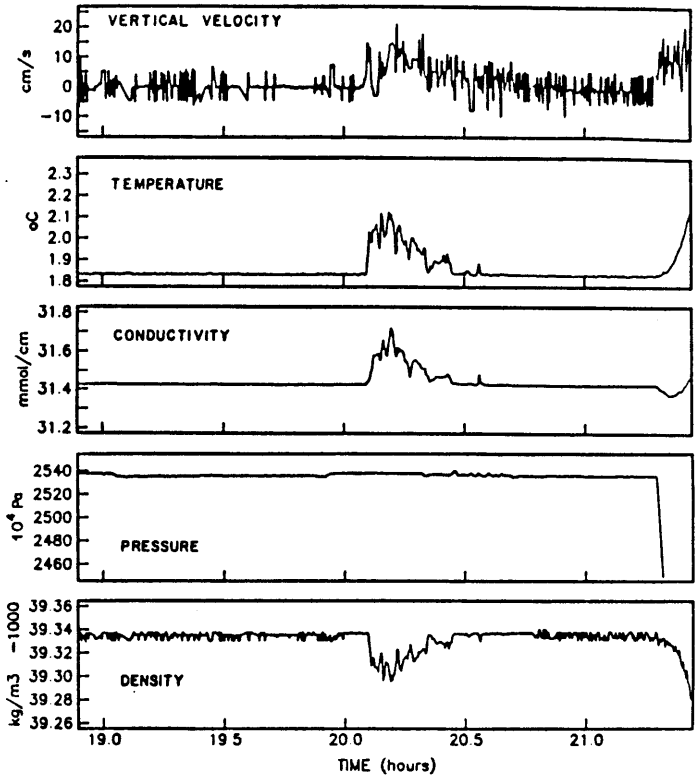

Fig. 4. Dive 1384 vertical velocity, temperature, conductivity, pressure,and density profiles through the vent field. The ascent at the end of the dive can be seen at 21.5 hours. The spikes in the velocity result from the corrections applied to compensate for the vertical motions of the submarine (±4 cm/s).

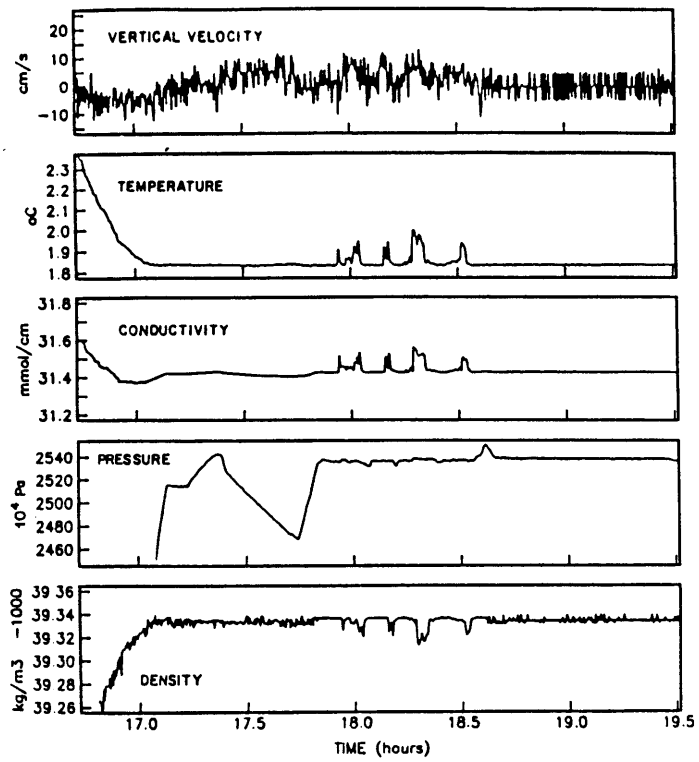

Fig. 5. Dive 1385 vertical velocity, temperature, conductivity, pressure, and density data profiles through the vent field. The descent at the beginning of the dive can be seen at 17 hours. The pressure drop indicates the occurrence of a submarine reconnaissance excursion off the seafloor.

diffuse flow are visible within 20 m of the base of the sulfide edifice. (3) Ambient stratification: Ambient stratification monitored during ascent and descent indicated that the ambient density of 1039.3330 kg/m³ at 2535 m remained constant up to a height of 75 m off the bottom, after which it dropped steadily (in 50 m averages) to 1039.3185 kg/m³ at 2235 m. (4) Shear flow: The ambient current remained fairly constant during the 3 days at 3-4 cm/s toward the north to northwest.

If each of the six or seven orifices was emitting a single plume, the diameters of each would be approximately 5 m at a height of 24 m above the base of the sulfide edifice. The plume centerlines, however, are no more than 3 m apart, so by 24 m, the plumes will have merged to some extent. The temperature sampling interval of 14 s coupled with a bottom speed ranging from 5 to 50 cm/s resulted in a typical sample spacing of from 0.7 to 7.0 m. This makes it difficult to determine whether unique signatures of the plumes from individual orifices exist at 24 m. No evidence of a distributed, diffuse, convective flow is observed in the recorded data. The effects of the diffuse flow are either below the limits of detection or have been incorporated through entrainment into the main plume. On the basis of these measurements, we hypothesize that at this vent site the convective heat transport is primarily in the form of a single plume created by the merging of multiple individual smokers. Furthermore, although the plume was measurably deflected by a lateral current (no anomalies were found when the submarine was on the south side of the smokers), it is hypothesized that this current has no significant effect on calculations yielding heat flow and maximum plume height. Finally, there is very little ambient density stratification over the height range of measurements (50 m). This characterization of the vent field flow provides the basis for heat flow estimates developed in the next section.

Simple Plume Approximation

In a pure ideal plume, the gravitational force acts on density differences between the source fluid and its environment and, for a buoyant source fluid, an upwardly expanding plume results. In a pure jet, fluid enters an ambient fluid of equal density, and the flow is governed entirely by the initial momentum. Many flows, called buoyant jets, fall somewhere between the two, with both initial momentum and either positive or negative buoyancy relative to the ambient fluid. Although jets and plumes behave differently near the source, all buoyant jets will emulate ideal plumes at distances far from the source [*Turner*, 1973]. In the following formulation we use simple plume theory to examine quantitatively the hypothesis that our vent field plume can be considered an ideal plume exiting into a uniform, quiescent environment.

The behavior of these plumes can be approximated for small temperature differences by simple plume theory [*Fischer et al.*, 1979] in which the plume is characterized by a given initial buoyancy flux from a point source:

$$B_o = (\alpha g H)/(C_p \rho) \quad (1)$$

where H is the heat flux added by the source, α is the density of the fluid, α is the coefficient of thermal expansion (1.48×10^{-4} °C^{-1} at ambient temperature), g is gravitational acceleration, and C_p is the specific heat (4200 J kg^{-1}°C^{-1} at ambient temperature). In a simple plume, with no initial momentum flux, dimensional analysis results in equations relating the centerline axial velocity, W, to initial buoyancy flux B_o and height Z above a

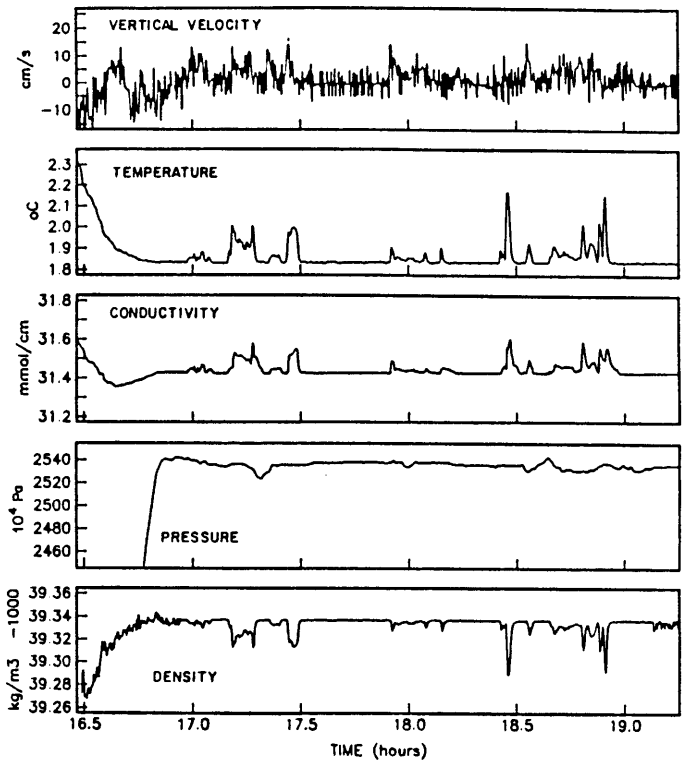

Fig. 6. Dive 1386 vertical velocity, temperature, conductivity, pressure, and density profiles through the vent field. The descent at the beginning of the dive can be seen at 16.5 hours.

point source:

$$W = C_1(B_o/Z)^{1/3} \quad (2)$$

and centerline temperature T, to initial buoyancy flux and height:

$$T = C_2(B_o^2 Z^{-5})^{1/3}/(\alpha g) \quad (3)$$

The dimensionless constants C_1 and C_2 have been obtained empirically: 4.7 for C_1 by *Rouse et al.*, [1952] and 9.1 for C_2 [*Chen and Rodi*, 1980]. Real plumes do not exit from point sources, but *Morton et al.* [1956] have demonstrated that all plumes exiting from finite sources can be modeled as flows generated from virtual sources a distance Z_o below the real source. To obtain other plume parameters, the equations relating initial volume flux, Q_o, and specific momentum flux M_o to buoyancy flux and height are

$$Q_o = C_3 B_o^{1/3} Z_o^{5/3} \quad (4)$$

$$M_o = C_4 B_o^{2/3} Z_o^{4/3} \quad (5)$$

In addition, the plume radius can be related to Q and W:

$$R = [Q/(\pi W)]^{1/2} \quad (6)$$

where C_3 and C_4, obtained using an assumption of Gaussian profiles for temperature and velocity [*Fischer et al.*, 1979], are 0.15 and 0.315, respectively. (The value of C_4 is slightly different from that given by Fischer et al. because we have taken into account the contribution of both mean and turbulent fluxes.) The initial values of plume parameters such as buoyancy flux (B_o), volume discharge (Q_o), specific momentum discharge (M_o), radius (R_o), and velocity (W_o) can be calculated given an initial temperature (T_o), and either the centerline temperature or velocity at a known height. An average centerline temperature anomaly of 0.27 ± 0.09° C at 24 m above the bottom and an average centerline velocity of 0.15 ± 0.03 m/s at 24 m have been

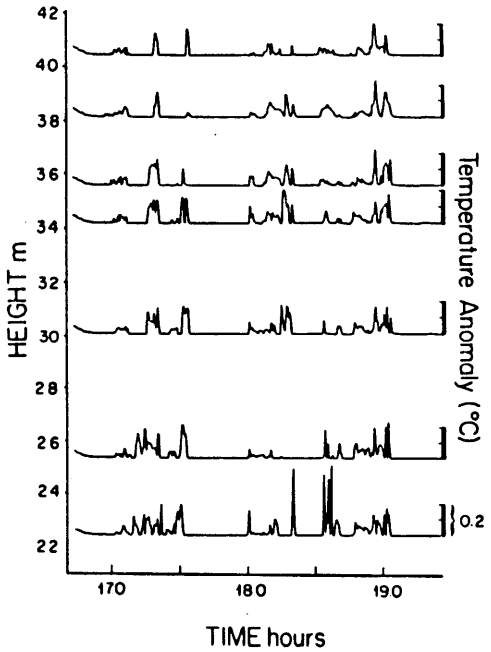

Fig. 7. Simultaneous temperature profiles as a function of height from dive 1386. Profiles were taken at 22.5, 25.4, 30.1, 34.2, 35.6, 38.2, and 40.5 m above the *Alvin* sampling basket. Bars on right indicate a 0.20° C temperature differential. The abruptness of the temperature peaks is due to the sharpness of the hot/cold boundary characteristic of plumes, coupled with the length of sampling interval compared with the width of the plume.

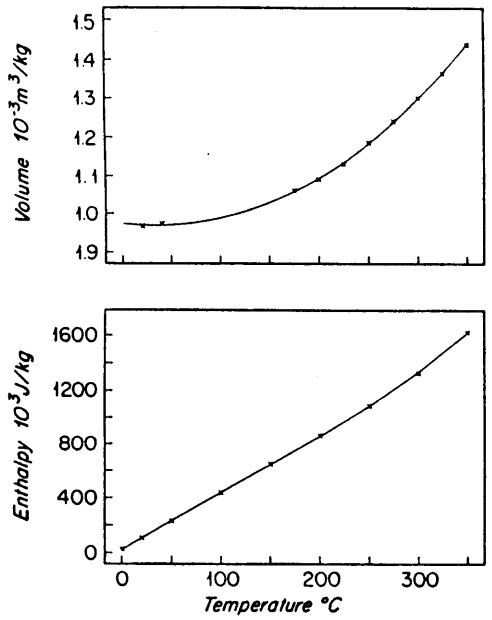

Fig. 8. (Top) Volume versus temperature for NaCl solution lower points (0-40°C) from *Fofonoff and Millard* [1984], upper points from *Chen* [1981]. Solid curve depicts function used for modeling. (Bottom) Enthalpy versus temperature for H_2O solution from *Keenen* [1969].

calculated using the maximum values from the data shown in Figures 4-6. A vent exit temperature of 338°C was measured with the submarine's high temperature probe at one of the orifices. Using the above equations and the average centerline temperature, the following values for the relevant plume parameters are obtained:

$$Z_o = 0.33 \text{ m}$$
$$W_o = 0.63 \text{ m/s}$$
$$R_o = 0.033 \text{ m}$$
$$B_o = 7.9 \times 10^{-4} \text{ m}^4/\text{s}^3$$
$$Q_o = 2.2 \times 10^{-3} \text{ m}^3/\text{s}$$
$$M_o = 6.1 \times 10^{-4} \text{ m}^4/\text{s}^2$$

These values are consistent (within 10%) with those calculated from the average centerline velocity. These initial values can now be used to check the validity of certain assumptions made when the simple equations presented above were applied to this vent. These assumptions relate to the effects of source geometry, initial momentum, viscosity, ambient stratification, and shear flow on plume behavior.

The simple plume relationships presented above may be applied to observed plumes provided that the comparisons with measurements are made beyond the distance $l_Q = Q_o/M_o^{1/2}$, within which the source geometry is important, and $l_m = M_o^{3/4}/B_o^{1/2}$ within which initial momentum influences the plume [*Fischer et al.*, 1979]. Using the above values for the hydrothermal vents studied here, it is found that $l_Q = 0.09$ m and $l_m = 0.14$ m. The data in this experiment were collected well beyond these distances. The effects of viscosity can be neglected provided that the Reynolds number

$$Re = (\pi R^2 W^2)^{1/2}/\nu \qquad (7)$$

(where ν is the kinematic viscosity) is greater than about 4000 [*Labus and Symons*, 1972]. The Reynolds number at the exit of the hydrothermal vent is about 4×10^4 ($\nu = 1 \times 10^{-6}$ m^2/s).

The effect of the 3-4 cm/s lateral current on the heat flow estimates is negligible because at 24 m the (calculated) initial vertical velocity of 63 cm/s has been reduced to a (measured) value 15 cm/s, which is still a factor of 4 times the magnitude of the ambient cross current. Plume deflections at this height are estimated to be of the order of 10 m, which is consistent with the observed horizontal distribution of anomalies.

The maximum height of the plume in a stratified environment can be calculated from the heat flow and density stratification. Specifically, from *Campbell et al.* [1985],

$$Z_{max} = 5(B_o/\pi)^{1/4}N^{-3/4} \qquad (8)$$

where Z_{max} is the maximum height off the bottom and N is the buoyancy frequency

$$N = [(-g d\rho)/(\rho dz)]^{1/2} \qquad (9)$$

where ρ is a reference density of seawater.

Using data obtained on dive descent and ascent, an average density gradient of 4.8×10^{-5} kg/m^4 for the bottom 300 m was recorded (averaging in 50 m intervals). With a buoyancy flux of 7.9×10^{-4} m^4/s^3 and $N = 6.8 \times 10^{-4}$ Hz, the plume should reach maximum height of 150 m, at which point the plume density reaches ambient density and it begins to spread laterally. Since the plume does not begin to spread until 150 m, simple plume theory (which ignores density stratification effects) can be used at heights below this and is valid for the range of measurements in this experiment (up to 50 m).

NONLINEAR PLUME MODEL

The discussion above justifies the neglect of plume momentum, ambient stratification, and horizontal currents in analyzing the plume data. A potential problem with using the simple plume model is that the environment of hydrothermal plumes comprises seawater, high pressure (2500×10^4 Pa), and large temperature gradients (2-350°C). The specific volume (V) and the enthalpy (E) are nonlinear functions of temperature (see Figure 8) and, in the temperature and pressure ranges at a hydrothermal vent, linear approximations to V and E cannot be used (i.e., the coefficient of thermal expansion α and the specific heat C_p of seawater are not constant). As a consequence, the plume buoyancy flux is not conserved but varies with height. *Kotsovinos* [1975] has shown that corrections should be made in plume behavior models for even moderate differences in temperature. Instead of *a posteriori* use of nonlinear temperature-density or temperature-enthalpy relationships (as was done by *Converse et al.* [1984]) to correct a model based on buoyancy flux conservation, a plume model based on enthalpy conservation that takes into account the nonlinear dependence of enthalpy and volume with temperature must be used. This more general approach to the buoyant plume problem uses the *Morton et al.* [1956] entrainment hypothesis coupled with an assumption of similarity of horizontal profiles of velocity and temperature. This method, which uses a differential formulation, is described in the appendix. This approach also allows plume and environmental parameters such as ambient stratification or cross flow to enter the problem as initial conditions, boundary conditions and coefficients in a system of differential equations, although such calculations are not presented in this paper.

The numerical solution of the differential model yields the same results as the simple plume model when the coefficients of thermal expansion and specific heat are held constant. When they are allowed to vary as expected, a comparison of simple plume theory with nonlinear formulation indicates that the nonlinear variation of density and enthalpy with temperature has some effect on the plume temperature and velocity profiles

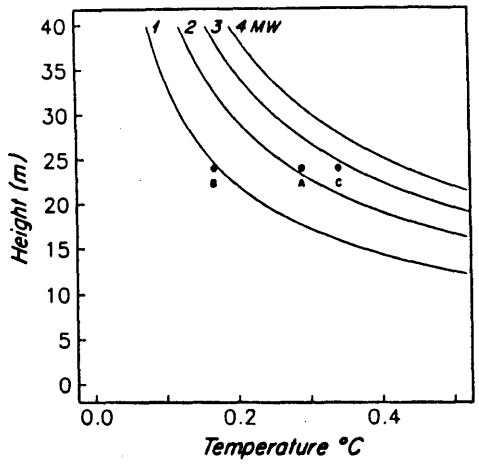

Fig. 9. Height versus temperature for initial heat flow values of (from left to right) 1, 2, 3, and 4 MW obtained using the nonlinear model. Peak temperature values from dives 1384 (point A), 1385 (point B) and 1386 (point C) taken at 24 m above the submarine.

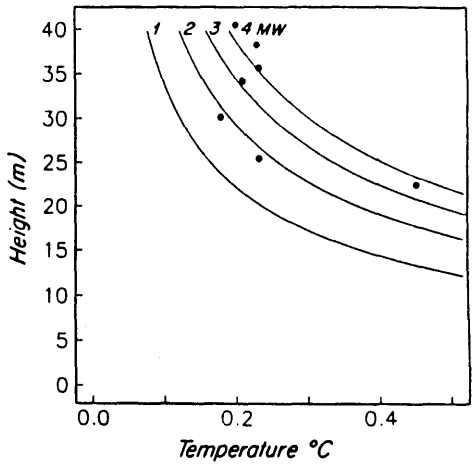

Fig. 11. Height versus velocity for initial heat flow values of (from left to right) 1, 2, 3, and 4 MW obtained using the nonlinear model. Peak temperatures from dive 1386 taken at 40.5, 38.2, 35.6, 34.2, 30.1, 25.4 and 22.5 m above the submarine.

when applied to a vent field. For a vertical velocity of 14.4 cm/s at 24 m, the simple plume model predicts a heat flow of 2.02 MW, while the nonlinear model predicts 1.97 MW, a difference of 3%. For a temperature anomaly at 24 m of 0.341°C, the simple plume model yields 3.40 MW, whereas the nonlinear one produces 2.76 MW, a difference of 20%. While these differences are modest compared with possible errors in the measurements, the nonlinear model provides, at reasonable computational cost, a theoretically consistent prediction of plume temperature and velocity. Accordingly, the nonlinear model will be used in the next section to estimate heat flows.

HEAT FLOW ESTIMATES

Heat flow values using the nonlinear model can be obtained by fitting *either* T versus Z or W versus Z to the peak temperature and velocity data. Heat flow estimates resulting from using T and W are independent of each other, and their comparison can be used as a measure of confidence in the final heat flow estimate. Maximum peak values of temperature anomaly and vertical velocity from each of three dives were used in the model; it is assumed that the lesser peaks on the T (or W) versus time records were due to passing through the plume but not through its center. To obtain the heat flow, the maximum temperatures (Figure 9) and velocities (Figure 10) measured with the flowmeter from each of three dives are plotted with the calculated temperature versus height and velocity versus height curves for various initial heat flows generated by the nonlinear enthalpy and thermal expansion model. The seven-thermistor chain used on dive 1386 yields additional temperature maxima at different heights (Figure 11). A summary of the data and resultant heat flow is given in Table 1.

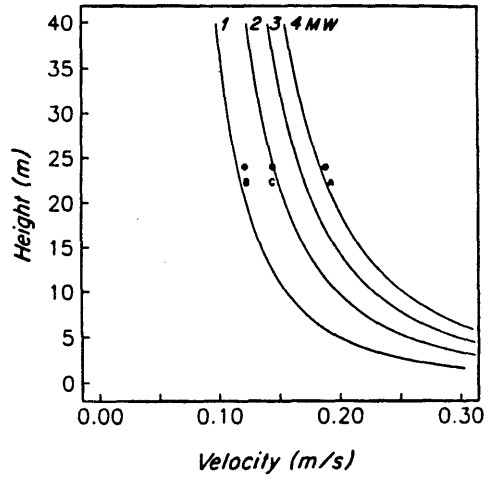

Fig. 10. Height versus velocity for initial heat flow values of (from left to right) 1, 2, 3, and 4 MW obtained using the nonlinear model. Peak velocity values from dives 1384 (point A), 1385 (point B), and 1386 (point C) taken at 24 m above the submarine.

The final estimate of the total heat flow must take into account the need of the plume models for an input of *centerline* temperature or velocity. Since real-time temperature was not available during the dive, we cannot be sure that the peak values were centerline values. It is likely that some of the peak temperature values were recorded off-centerline and thus are lower than the true centerline temperatures. This would imply that the maximum temperature recorded during the experiment should be chosen and, consequently, the maximum heat flow obtained with the nonlinear plume model. However, the models also assume that the centerline value is a mean value, averaged over a long time to remove the effects of turbulent fluctuations. Unfortunately, again because electronics problems in *Alvin* eliminated real-time readouts, we were not able to position the sensor in one spot of the plume for the necessary amount of time. Therefore the temporal temperature variability of the plume due to turbulent fluctuations is not known. If the absolute peak temperature measured during the experiment is chosen as a representative mean centerline temperature, too high a heat flow estimate may result. However, because the temperature and velocity values are so sensitive to lateral position in the plume, it is more likely that the heat flow values are biased on the low side. The average value of all the heat flow estimates is 2.8 MW and the maximum value is 4.6 MW. Given the uncertainties mentioned above, a reasonable heat flow estimate for the vent field is 3.7 ± 0.8 MW.

Heat flow can also be calculated directly by multiplying point

TABLE 1. Nonlinear Model Heat Flow (Maximum Value From Each Dive)

Dive	Height* m	Temperature Anomaly °C	Heat Flow MW	Velocity cm/s	Heat Flow MW
1384	24.0	0.290	2.2†	18.8	4.2†
1385	24.0	0.168	0.9†	12.1	1.2†
1386	24.0	0.341	2.8†	14.4	2.0†
	40.5	0.201	4.4		
	38.2	0.230	4.6		
	35.6	0.233	4.1		
	34.2	0.210	3.1		
	30.1	0.179	1.9		
	25.4	0.232	1.8		
	22.5	0.453	3.7		

* *Above submarine.*
† Value derived from data obtained by flowmeter instrumentation.

velocity and temperature measurements. This is a relatively inaccurate procedure, in part because temperature and velocity are correlated in turbulent plumes, and errors due to sparse sampling of turbulent fluctuations are multiplied. To illustrate, temperature and velocity are known at 24 m, and we estimate the plume radius to be about 2.5 m at this height (using simple plume relations, $R \simeq 0.1Z$). Multiplying temperature and velocity at each point and taking the average of this value, we can obtain an estimate of heat flow (using $C_p = 4200$ J/kg^{-1} °C^{-1}, density 1000 kg/m^3) ranging from 0.04 to 0.59 MW for the three dives. These estimates are up to a factor of 50 times lower than of any of the temperature or velocity heat flow estimates, and they illuminate some of the difficulties in using the technique of averaging flow through a surface for turbulent plumes without sufficient spatial resolution.

CONCLUSIONS

We obtained the first simultaneous velocity, temperature, and conductivity data to be taken in the convective flow emanating from a hydrothermal vent field. The single temperature, velocity, and conductivity profiles at 24 m and the seven simultaneous temperature profiles at various heights indicate that the flow field forms a single plume.

The flow characteristics and surrounding environment are such that simple plume formulas can be applied to predict such plume behaviors as maximum height and total heat flow. The nonlinear effects of large temperature variations have been considered here as far as they relate to using plume theory to predict heat flow. The good agreement between heat flow estimates from vertical velocity and from temperature anomalies supports the heat flow estimate of 3.7 ± 0.8 MW for this vent field.

APPENDIX: CALCULATIONS FOR PLUMES WITH VARIABLE NONLINEAR PARAMETERS

The primary variables of the plume model are the total fluxes of volume, specific momentum, and enthalpy, integrated over the plume cross section:

Volume flux

$$Q = \int_0^\infty 2\pi r w \, dr \tag{10}$$

Specific momentum flux

$$M = \int_0^\infty 2\pi r w^2 \, dr \tag{11}$$

Enthalpy flux

$$E = \int_0^\infty 2\pi r w \, \Delta h \, dr \tag{12}$$

where r is radial distance from the plume centerline, w is vertical velocity, and Δh is specific enthalpy.

The time-averaged tracer concentration (temperature, density, or velocity) across a turbulent plume exhibits essentially Gaussian distributions [*Fischer et al.*, 1979]. These mean velocity and concentration profiles are self-similar with height, enabling tracer distributions to be expressed only in terms of maximum (centerline) values and some measure of width (the point off-axis where the vertical velocity w falls to $e^{-1} = 0.37$ of the centerline velocity W for Gaussian distributions).

$$w = W \exp(-r^2/R^2) \tag{13}$$

$$\Delta h = \Delta h_{max} \exp[-r^2/(R^2\lambda^2)] \tag{14}$$

where $\lambda = 1.2$ [*Fischer et al.*, 1979]. With these assumptions, the integrated flux parameters become

$$Q = \pi R^2 W \tag{15}$$

$$M = K_m \pi R^2 W^2/2 \tag{16}$$

$$E = K_e \pi \lambda^2 R^2 W \Delta h_{max}/(1 + \lambda^2) \tag{17}$$

where the constant coefficients $K_m = 0.89$ and $K_e = 1.24$ have been included to account for the additional transport of momentum and enthalpy by turbulent fluctuations rather than by mean motions [*Fischer et al.*, 1979].

Following *Fischer et al.* [1979], differential conservation equations for Q, M, and E are given by

$$dQ/dz = 2\pi\sigma RW \tag{18}$$

$$dM/dz = \pi g \delta \lambda^2 R^2 \tag{19}$$

$$dE/dz = 0 \tag{20}$$

Equation (18) states that increase in specific volume flux Q is the result of entrainment, which is in turn proportional to the local centerline plume velocity where the constant of proportionality σ is the entrainment coefficient. The value of σ for buoyant jets lies between that of jets ($\sigma_j = 0.0535$) and plumes ($\sigma_p = 0.0833$). *Priestly and Ball* [1955] found that, to a good approximation

$$\sigma = \sigma_{jet} - (\sigma_{jet} - \sigma_{plume})(Ri/Ri_p)^2 \tag{21}$$

where Ri_p is the plume Richardson number, with a value of 0.557 [*Fischer et al.*, 1979]. Ri is the local Richardson number given by

$$Ri = \{[4(2\pi)^{1/2}\lambda^2/(1 + \lambda^2)][gR\delta/W^2]\}^{1/2} \tag{22}$$

Equation (19) states that the vertical buoyancy force acting per unit height of the jet equals the rate of change of vertical momentum flux. The quantity δ is the specific density anomaly $(\rho_a - \rho_{max})/\rho_a$ at the plume centerline. For the nonlinear plume this must be calculated as a function of the centerline temperature (or enthalpy).

Equation (20) expresses conservation of enthalpy flux E across any horizontal plane in the plume. The maximum enthalpy anomaly Δh_{max} is in general a nonlinear function of the plume centerline temperature difference ΔT_{max}. Only for small values of ΔT_{max} and thus constant C_p is

$$E = \rho C_p \pi \lambda^2 W \Delta T_{max}/(1 + \lambda^2) \tag{23}$$

The system of equations ((18)-(20)) can be solved relatively easily by using an explicit, first-order, numerical formulation. Specific volume values for temperatures of NaCl solutions greater than 40°C were obtained from *Chen* [1981] and enthalpy values for pure water from *Keenen et al.* [1969].

Acknowledgments. We would like to thank the captain and crew of the R/V *Atlantis* and the DSR/V *Alvin* pilots R. Hollis, D. Foster, and D. Collasius. In addition, the assistance of J. Dean with his current meter/CTD was extremely valuable to the ultimate success of this experiment. Erika Francis completed the initial steps in the data reduction. We also appreciate the work provided by co-chief scientist M. J. Mottl in cruise organization and manuscript suggestions. Figure 1 was kindly provided by T. F. McConachy. This work was supported by NSF grant OCE83-10175 and the WHOI/MIT Joint Program in Oceanography. Woods Hole Oceanographic contribution 6268.

REFERENCES

Baker, E., R. Collier, D. Kadko., G. Massoth, T. Nelsen,P. Rona, and J. Trefy, Hydrothermal activity on the Gorda Ridge, Eos, *Trans. AGU,67*, 523, 1985.

Campbell, I. H., T. J. McDougall, and J. S. Turner, A note on fluid dynamic processes which can influence the deposition of massive sulfides, *Econ. Geol., 79*, 1905-1913, 1984.

Chen, C. J., and W. Rodi, Vertical turbulent buoyant jets: a review of experimental data, Science and Applications of Heat and Mass Transfer. Series, V4. Ed. D. B. Spalding. Pergammon Press, 1980.

Chen, C.-T. A., Geothermal systems at 21°N, *Science, 211*, 298, 1981.

Converse, D. R., H. D. Holland, and J. Edmond, Flow rates in the axial hot springs of the East Pacific Rise (21°N): Implications for the heat budget and the formation of massive sulfide deposits, *Earth Planet. Sci. Lett., 69*, 159-175, 1984.

Crane, K., F. Aikman, R. Embley, S. Hammond, A. Malahoff, and J. Lupton, The distribution of geothermal fields on the Juan de Fuca Ridge, *J. Geophys. Res., 90* 727-744, 1985.

Fischer, H. B., J. E. List, R. C. Koh, J. Imberger, and N. H. Brooks, *Mixing in Inland and Coastal Waters*, pp. 315-389, *Academic*, New York, 1979.

Fofonoff, N. P., and R. C. Millard, Algorithms for computation of fundamental properties of seawater, *UNESCO Tech. Pap. Mar. Sci., 44*, 153, 1983.

Francheteau J., and R. Ballard. The East Pacific Rise near 21°N, 13°N, and 20°S: Inferences for along-strike variability of axial processes of the mid-ocean ridge, *Earth Planet Sci. Lett., 64*, 93-116, 1983.

Green, K. E., R. P. Von Herzen, and D. L. Williams, The Galapagos spreading center at 86° W: A detailed geothermal field study, *J. Geophys. Res., 86*, 979-986, 1981.

Keenen, J. H., F. G. Keyes, P. G. Hill, and J. G. Moore, *Steam Tables*, p. 162, John Wiley, New York, 1969.

Kotsovinos, N. E., A study of the entrainment and turbulence in a plane buoyant jet, Ph.D. thesis, Cal. Inst. of Technol., Pasadena, 1975.

Labus, T. L., and E. P. Symons, Experimental investigation of an axisymmetric free jet with an initially uniform velocity profile, *NASA Tech Note TN D-6783*, 1972.

MacDonald, K. C., K. Becker, R. N. Spiess, and R. D. Ballard, Hydrothermal heat flux of the "black smoker" vents on the East Pacific Rise, *Earth Planet Sci. Lett., 48*, 1-7, 1980.

McConachy, T. F., M. J. Mottl, and R. P. Von Herzen, Geological form and setting of a recently discovered hydrothermal vent field at 10°56'N, 103°41'W. East Pacific Rise, *Eos Trans. AGU, 65*,(45), 1124, 1984.

McConachy, T. F., R. D. Ballard, M. J. Mottl, and R. P. Von Herzen, The geological form and setting of a hydrothermal vent field at 10°56'N, East Pacific Rise: A detailed study using *Angus* and *Alvin*, *Geology, 14*,(4), 295-298, 1986.

Morton, B. R., G. Taylor, and J. S. Turner, Turbulent gravitational convection from maintained and instantaneous sources, *Proc. R. Soc. London, Ser. A, 234*, 1-23, 1956.

Priestly, C. H. B., and F. K. Ball, Continuous convection from an isolated source of heat, *Q. J. R. Meteorol. Soc., 81*(348), 144-157, 1955.

Rona, P. A., G. Thompson, M. J. Mottl, J. A. Karson, W. J. Jenkins, D. Graham, M. Mallette, K. Von Damm, and J. M. Edmond, Hydrothermal activity at the TAG hydrothermal field, Mid-Atlantic Ridge crest at 26°N, *J. Geophys. Res., 89*, 11365, 1984.

Rona, P., E. Baker, R. Collier, D. Kadko, G. Massoth, T. Nelsen, and J. Trefry, Hydrothermal activity on the Gorda Ridge, *Eos, Trans. AGU, 66*(27), 523, 1985.

Rouse, H., C.-S. Yih, and H. W. Humphreys, Gravitational convection from a boundary source, *Tellus, 4*, 201-210, 1952.

Schouten, H., K. D. Klitgord, and J. A. Whitehead, Segmentation of mid-ocean ridges, *Nature, 317*(6034), 225-229, 1985.

Turner, J. S., *Buoyancy Effects in Fluids*, Cambridge University Press, New York, 1973.

Weller, R. A., J. P. Dean, J. Marra, J. F. Price, E. A. Francis, and D. C. Boardman, Three-dimensional flow in the upper ocean, *Science, 227*, 1552-1556, 1985.

S. A. Little and R. P. Von Herzen, Woods Hole Oceanographic Institution, Woods Hole, MA 02543.

K. D. Stolzenbach, Ralph M. Parsons Laboratory, Department of Civil Engineering, Massachusetts Institute of Technology, Cambridge, MA 02139.

(Received August 20, 1986;
revised November 17, 1986;
accepted November 18, 1986.)

TIDAL CURRENT EFFECTS ON TEMPERATURE MEASUREMENTS IN DIFFUSE HYDROTHERMAL FLOW: GUAYMAS BASIN

Sarah A. Little

Dept. of Geology and Geophysics

Woods Hole Oceanographic Institution

Frederick J. Grassle

Dept. of Biology

Woods Hole Oceanographic Institution

Keith D. Stolzenbach

Dept. of Civil Engineering

Massachusetts Institute of Technology

ABSTRACT

A twelve day time series of temperature data was collected from a point three centimeters above a diffuse flow area at a Guaymas Basin hydrothermal site. Using concurrent tidal gauge data from the town of Guaymas it is shown that the effects of tidal currents can be strong enough to dominate the time variability of a temperature signal at a fixed point in hydrothermal flow and are a plausible explanation for the variations seen in the Guaymas Basin temperature data.

INTRODUCTION

The high heat flow, high permeability and low sedimentation of the world's Mid-Ocean Ridge system support hydrothermally active regions of the seafloor in localized sites encompassing areas as large as $10^4 m^2$. The process of hydrothermal circulation transfers heat and material from the lithosphere into the oceans, influencing oceanic composition as well as creating massive ore deposits on the seafloor. The significance and global impact of this process are determined by the heat and mass flux from individual sites, the number of hydrothermal sites, and the variation of these fluxes over time.

Recent efforts have focussed on characterizing temporal changes in hydrothermal activity. Hydrothermal vent fields evolve continually, in flow rates, size, geometry and biological composition (Hekinian et al, 1983; Johnson and Tunnicliffe, 1985), the most direct evidence being both the existence of numerous extinct fields and apparently young fields uncolonized by biota. Possible mechanisms for reducing flow include the blocking of flow channels by hydrothermal precipitates, exhaustion of the underlying heat source, reduction of porosity by mineralization, and obstruction of flow paths due to tectonic activity. On the other hand, increase in flow may result from tectonic activity and magma injection. Periodic oscillation in flux may be produced by tidal forcing either indirectly through tectonic activity or directly through pressure effects on the flow. Cataclysmic changes are possible based on models of heat transfer near the magma-water interface of the convective system which predict sudden changes in flow due to the behavior of seawater as it

reaches the two-phase region of pressure and temperature (Cann et al., 1985).

Quantifying even the instantaneous heat and mass flux from individual sites is difficult due to the complexity of flow systems typically encountered in hydrothermal fields. In a single field the flow can range in character from warm, 10°C water slowly seeping through large masses of tube worms and bacterial mats, to hot, 350°C water jetting from narrow sulfide chimneys only 0.05 m in diameter. The most straightforward flux measurements to make are those of well-defined plumes emanating from single chimneys. These measurements are achieved by obtaining temperature, flow rate and exit area at a vent orifice using conventional thermistors and mechanical flow meters (Converse et al., 1984; Macdonald et al., 1980). Only slightly more complex is measuring temperature and velocity above a multiple outlet sulfide structure and using plume theory to derive heat flux from the entire edifice (Little et al., 1987).

Much more difficult to quantify is the diffuse flow emanating from cracks, fissures and biological masses at velocities of less than about 0.1 m/s because the velocity and temperature signals are low and unevenly distributed over a large area. Diffuse flow is visually identified by the presence of shimmering water, upward moving particles, hydrothermal mineral deposits and an abundance of biota. Measuring instantaneous, point temperature is reasonably simple although typical non-uniform distributions require many measurements. Velocity is quite difficult to obtain because the flow is heterogeneous over scales as small as a few centimeters and the flow velocity is low and on the same order of

magnitude as ocean currents (0.05-0.10 m/s) which can dominate hydrothermal fluid related flow.

Measurements of temporal changes in hydrothermal activities require some means of obtaining time-series data within the difficult constraints of deployment, recovery, power consumption, data storage, and instrument reliability. Little (in prep) has explored the use of passive acoustic monitoring for this purpose. However, until this method is proven, temperature may be the parameter of choice, especially for low temperature diffuse flow.

When making temperature measurements in a hydrothermal environment, care must be taken to separate out the effects of changes in hydrothermal flow and temperature from changes in ambient currents. In this article we examine a time-series of temperature data collected near a diffuse flow area at a Guaymas Basin hydrothermal site. We will show that the effects of tidal currents can be strong enough to dominate the time variability of a temperature signal at a fixed point in hydrothermal flow, and are a plausible explanation for the variations seen in the Guaymas Basin temperature data. This study points out the necessity to measure lateral currents whenever temperature measurements made in hydrothermal vent fields are used to examine time variability of venting.

MEASUREMENTS AND RESULTS

The experiment site was a hydrothermally active area located in the Southern Trough of Guaymas Basin in the Gulf of California at $27^{o}00'N$, $111^{o}24'W$ (figure A1) where vents flow through a thick layer of pelagic sediment before breaking out onto the seafloor. In an effort to

characterize temporal variability of diffuse hydrothermal flow, a temperature probe was placed 0.03 m above the sediment surface in an approximately 5x5 m zone characterized by bacterial mat, whitish mineral deposition and patches of shimmering water. A few meters from the thermistor site was a particularly dense bacterial mat in and above which temperatures were greater than 30°C (the upper limit of the temperature probe) and perhaps as high as 230 °C as evidenced by charring of the recording instrument's wooden base. In the vicinity of the study area were broad areas of hydrothermal discharge covered with living bacterial mat whose temperatures were measured from the submarine at less than 11°C above ambient at a depth of 0.08 m below the sediment surface and 78°C above ambient at a depth of 0.50 m in the sediments. Numerous 270°C vents were associated with mounds and chimneys that rose up to 25 m above this sediment pond area (Lonsdale and Becker, 1985).

The thermistor was deployed with a submersible and left in place for 12.5 days from July 17, 1985 to July 28, 1985, during which time temperatures were recorded every 5 minutes for a total of 3790 points. The ambient temperature in this area as measured during descent of the instrument package was 2.85°C. The maximum recorded temperature for this deployment was 20°C, which occurred during deployment probably as the probe touched or came very close to the sediment surface. We will use this value for sediment surface temperature in calculations that follow.

Tidal high and low water surface elevations were obtained from the town of Guaymas, Mexico, approximately 100 km away, for the same time period. A cubic spline is subsequently used to interpolate this temporally unevenly spaced data. Tidal currents measured at 10 m above

bottom in the troughs of Guaymas Basin have reversing northwest-southeast flow with velocities of up to 0.12 m/s (Lonsdale and Becker, 1985). Current speed was not recorded at the vent site and will be derived from tidal heights recorded at the town of Guaymas.

The most prominent feature of the raw temperature data (figure A2) is the strong semi-diurnal oscillation, which exhibits a temperature range from a minimum of 3.05°C to a maximum of 4.87°C. The concurrent tide data (also figure A2) show that the dominant tide in this region is diurnal. Closer examination reveals that the temperature reaches a peak when the tide is at a minimum or maximum, and reaches a low when the tide is at an inflection-point.

DISCUSSION

From the observations follows the hypothesis that temperature is influenced by tidal current speed, a process which can have a 90° phase lag to tidal height and which peaks twice as often as tidal elevation. To test this hypothesis we will compare the frequency spectra of temperature and tide to determine whether correlations at frequencies higher than diurnal exist. Following this, we will estimate current speed from tidal height, use this in a simple model of boundary layer flow and compare the results with the measured temperature data.

To compare temperature and tidal frequencies under the supposition that tidal periods are twice that of temperature, we have presented the frequency spectra with the tidal period axis divided by two (figure A3). The tidal spectrum was calculated after cubic spline interpolation (see figure A2). The temperature spectrum was produced by first dividing the

data set into fourteen, 256 point segments by sub-sampling the full set every fourteen points. The new segments, with points separated by 70 min., are used to produce an averaged spectrum with a minimum resolvable period of 2.33 hours. The power levels are not normalized so comparison only can be made of the peak period locations, not amplitudes. There are striking similarities between the two spectra, especially at the 12 and 6 hour periods but also at the shorter periods such as 4 and 3 hours, indicating that tidal current speed, which peaks twice as often as tidal height, may be influencing temperature.

Now we turn to a boundary layer flow model to examine the effects of current speed on temperature at a fixed point above a heated surface. When a current passes over a heated surface, a thermal boundary layer is produced whose thickness increases with distance downstream from the leading edge of the plate. There are two ways that a vector current can influence temperature at a point inside a thermal boundary layer. First, if the heated surface is asymmetrical and finite and the sensor is located off center then rotating the direction of the current vector while maintaining a constant current magnitude will change the effective distance between the sensor and leading edge of the surface. As boundary layer thickness is a function of this distance, a current rotation will result in a change of boundary layer thickness and hence the recorded temperature. Such temperature variations would have frequencies correlated with the tides. However, it would be pure chance if the phases of variation coincided - there would be no reason to expect a temperature low at a tidal inflection point since the timing of the variation would depend only on sensor position within the hot plate.

The second mode of current influence on temperature depends on the fact that thermal boundary layer thickness is a function of current magnitude, and temperature at a fixed point above the surface depends on boundary layer thickness. We suggest that this mode is operating and temperature variations seen are due to the fact that the thermistor is in an area where a thickening and thinning of the boundary layer is caused by changes in current magnitude.

To examine how temperature relates to flow we first assume a general form for the dependence of the boundary layer thickness, δ, on flow velocity, v:

$$\delta = Cv^{-\frac{1}{2}} \qquad (1)$$

This functional relationship is consistent with a thermal boundary layer development in a flow with a uniform velocity and a constant diffusivity (Fischer et al., 1979). The constant C will be determined by calibration with the temperature and velocity measurements, and will be limited in resolution to an order of magnitude because surface temperature and bottom current speed are not well constrained. These approximations do not affect comparisons of temporal variability so much as comparisons of absolute temperatures.

To relate temperature to the position of a measurement point within the boundary layer we assume a parabolic for the temperature profile:

$$T(y) = Ts-(Ts-Ta)\left[\frac{2y}{\delta} - \frac{y^2}{\delta^2}\right] \qquad (2)$$

Where Ts is the surface temperature (=20°C), Ta is the ambient temperature (=2.85°C), and y is distance from surface (=0.03m). This profile reflects the general characteristics of the temperature

variations within a thermal boundary layer (Schlicting, 1968). A simpler linear functionality yielded less satisfactory results.

The flow speed over the heated surface, v, was assumed to be proportional to the first derivative of tidal height as measured at Guaymas. To obtain a functional form for v, the interpolated tide data was harmonically decomposed using a least squares sine fit such that:

$$h = K_o \sum_i A(i)\sin[\theta(i)t + \phi(i)] \qquad (3)$$

where A(i), θ(i) and ϕ(i) are the amplitude, frequency, and phase of each component (see table 1). The flow speed υ is then modelled as being linearly dependent on the absolute value of the time derivative of equation 3 for h:

$$v = K_o \, \mathrm{abs}\{ \sum_i A(i)\theta(i)\cos[\theta(i)t + \phi(i)] \} + K_1 \qquad (4)$$

The constants K_o and K_1 are determined to match estimated values of the maximum and minimum current speeds, υ_{max} and υ_{min} at the height of the sensor. υ_{max} is estimated from the maximum free stream velocity measured at 0.12 m/s at 10 m above bottom (Lonsdale and Becker, 1985). Using a logarithmic velocity profile between two points above the bottom:

$$\frac{U1}{U2} = \frac{\ln(z1)-\ln(zo)}{\ln(z2)-\ln(zo)} \qquad (5)$$

where zo =roughness height/25 (Townsend, 1980). For a roughness height of 0.05 m we estimate zo to be 0.002m. Using z1=0.03m, z2=10 m, U2=0.12 m/s in equation 3 results in an order of magnitude estimate for U1 = υ_{max} = 0.05 m/s. This value of υ_{max} may be used directly in conjunction with

TABLE 1

Period (hours)	Amplitude (meters)	Phase (degrees)
4.00	0.010	166
4.14	0.002	230
6.10	0.010	206
6.21	0.002	344
6.27	0.009	273
8.18	0.013	120
11.97	0.939	230
12.00	1.032	57
12.42	0.317	13
12.66	0.164	289
23.93	1.451	3
24.07	1.184	188
25.82	0.204	102
26.87	0.160	60
327.90	0.101	40
661.30	0.140	289

the observed temperature minimum T_{min} = 3.05°C and equation 1 and 2 to calculate C=7.5x10^{-3} m$^{3/2}$/s^{½}. Using the same equations with this value of C and T = T_{max} = 4.87°C yields an estimate of υ_{min} = 0.03m/s. Correspondingly, the values of K_o = 9.27 and K_1 = 0.03 m/s may be obtained. In addition, with the above values for C and υ, δ_{min} = 0.033 m and δ_{max} = 0.043 m.

The time series of velocities obtained from equation 4 may now be substituted into equation 1 and 2 to obtain an estimate of temperature at the sensor height (figure A4a and A4b). A detailed examination shows extremely good correlation between predicted and actual temperatures between 0 and 150 hours. Following this, a notable difference arises where from 150-290 hours maximum temperature peaks decrease and the variations get slightly out of phase. This is probably due to the fact that tides can have a rotational component which is not considered here, ie they are not exactly reversing and the minimum current increases during these periods. This causes disagreement between the estimated T(h), which is forced to a constant minimum set by scaling to υ_{min}.

CONCLUSIONS

The important measurements of temperature variation over space and time for the purpose of estimating heat flux and flux variability from hydrothermal vents should be pursued, however, this analysis shows that temperature variability measured near a source of diffuse hydrothermal flow can be produced by tidal currents. A time series of temperature from a hydrothermal area in the Guaymas Basin can be explained in a large part, if not entirely, by invoking boundary layer theory and tidal cross

currents. These results point out the importance of collecting simultaneous temperature and bottom current velocities to allow unambiguous interpretation of the data.

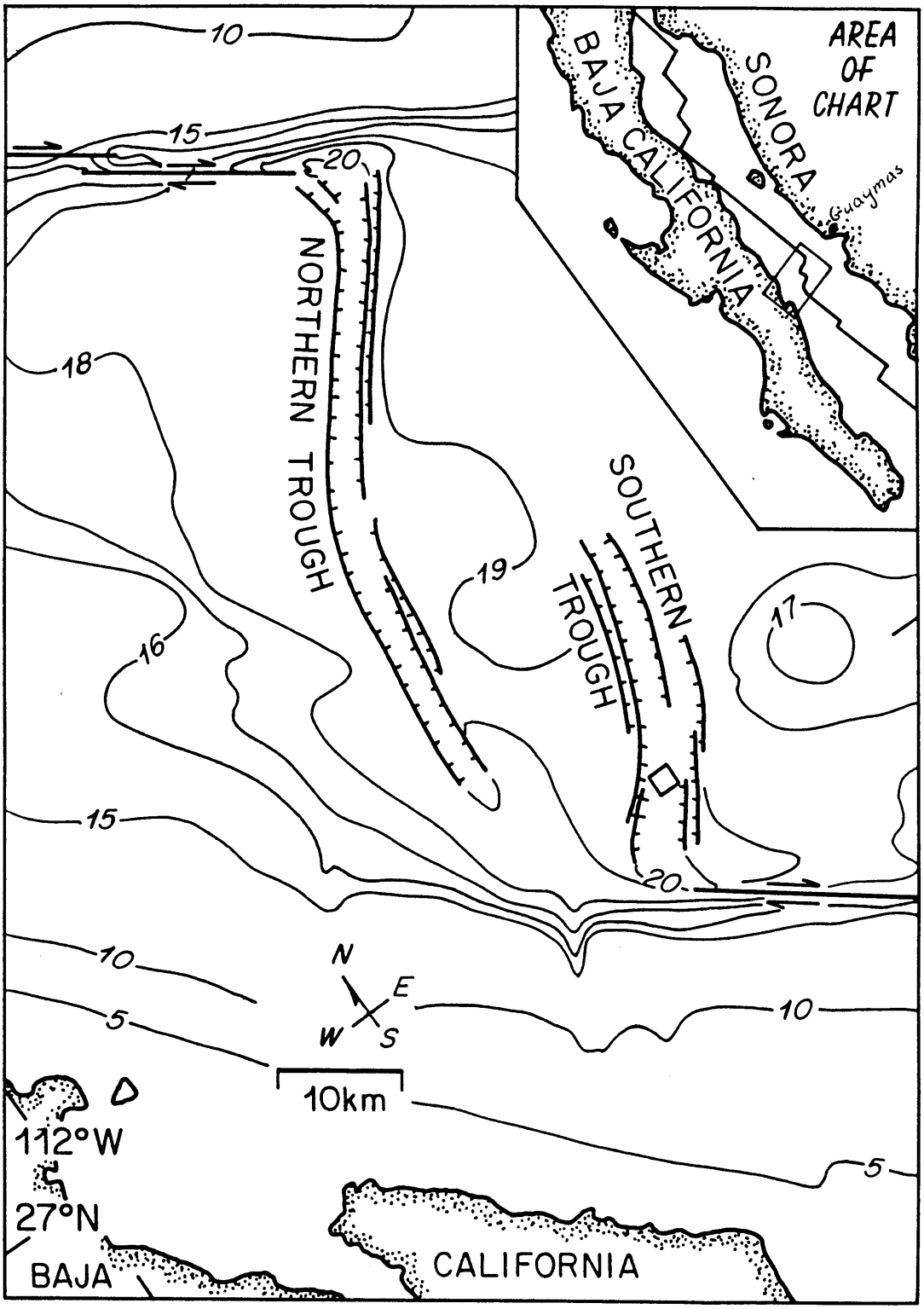

Figure A1

Map showing location of hydrothermal vent site (small box) in the Southern Trough of Guaymas Basin in the Gulf of California. Units on contours are in 100 m. Town of Guaymas, marked on inset, is about 100 km away.

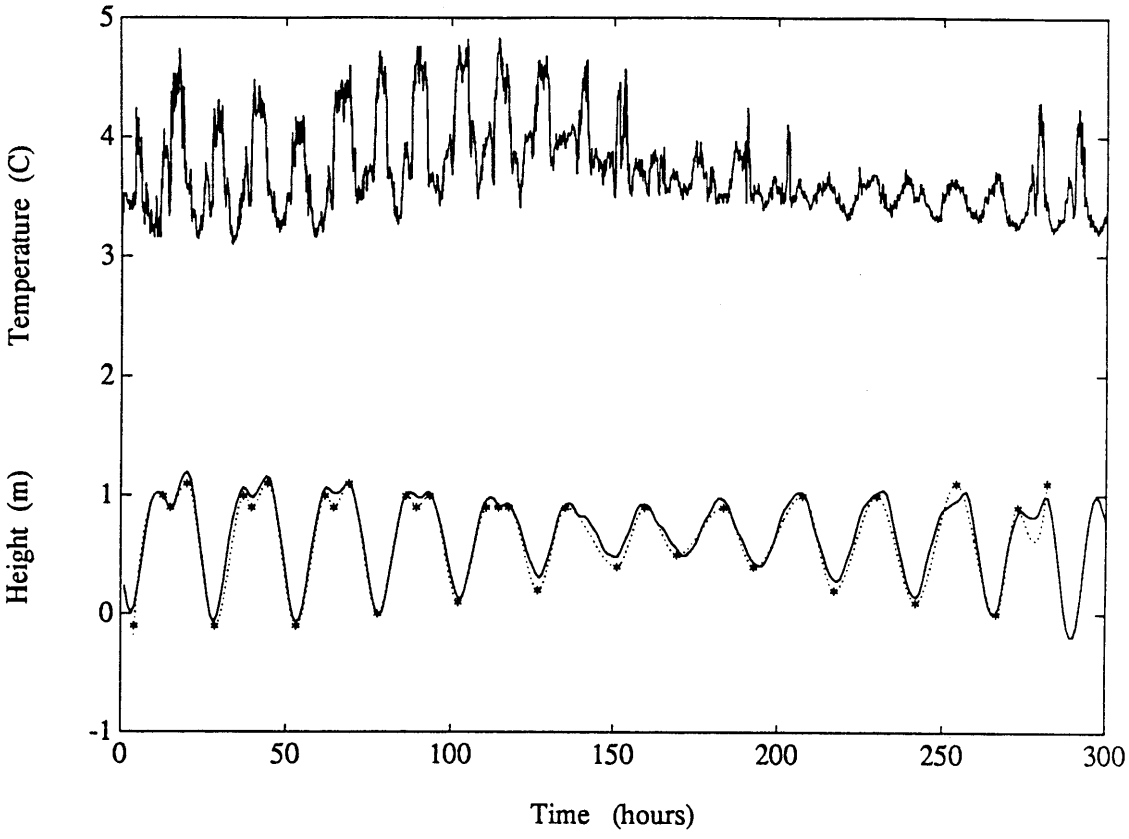

Figure A2

Upper - Raw temperature data recorded by T1, 3 cm above diffuse flow, samples every 5 minutes, showing semi-diurnal variations.
Lower - Tidal maxima and minima above mean low water, recorded at the town of Guaymas (stars). A cubic spline interpolation between data points (dotted line) is then fitted with tidal harmonics to approximate a functional form for the tide. This will then be used to arrive at tidal velocities which are applied to a boundary layer model.

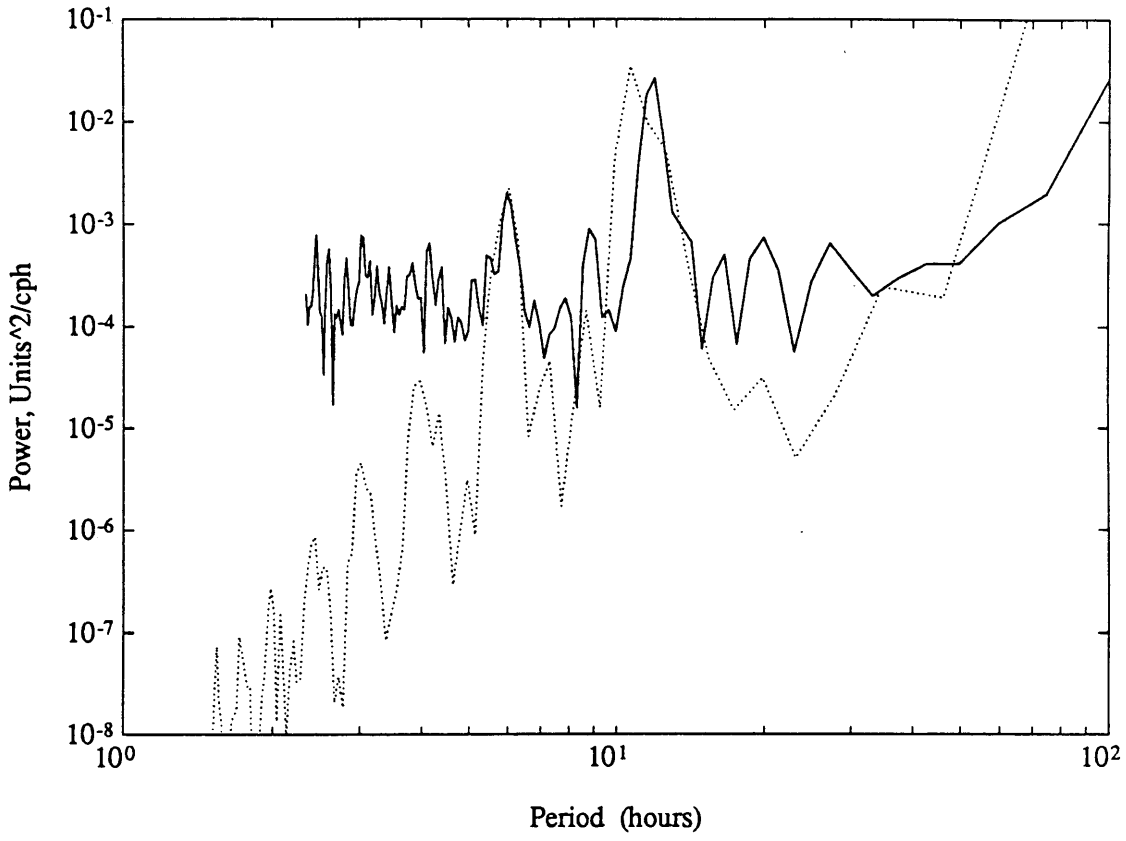

Figure A3

Frequency spectra from raw temperature data, solid line, and cubic spline fit to tides, dotted line. The frequency axis for the tidal spectrum has been divided by two to show good comparison of estimated tidal current spectrum with temperature spectrum. The y-axis units are useful only for comparing relative power levels within a single spectrum.

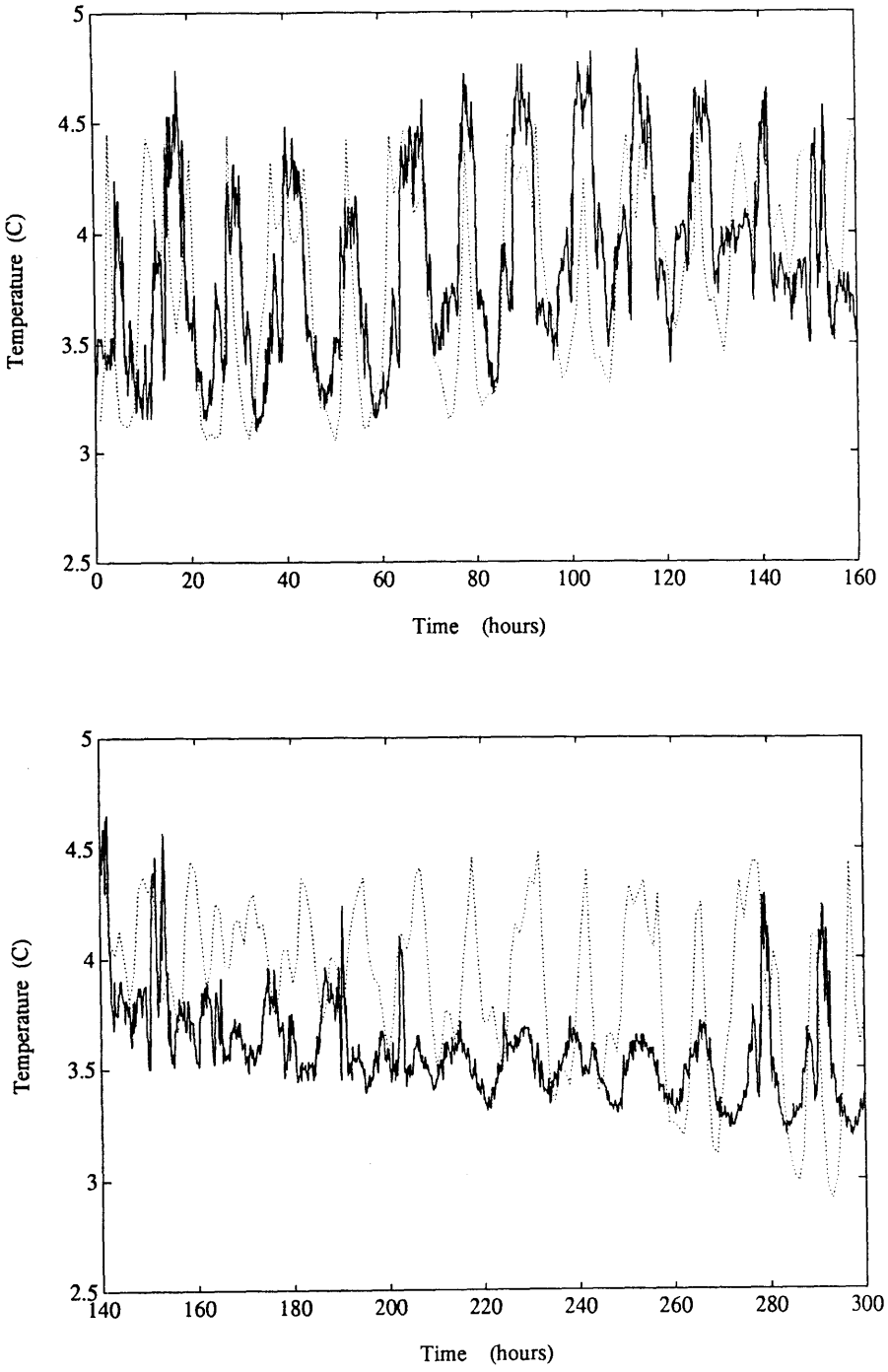

Figure A4

a) Raw temperature (solid line) and temperature estimated from boundary layer flow model and tidal currents (dotted line), shows remarkable similarity in both relative amplitude and temporal variation for the first half of the thermistor deployment.
b) Raw temperature (solid line) and temperature estimated from boundary layer flow model and tidal currents (dotted line) from second half of data record shows differences in relative amplitude and less agreement in phase. These differences are probably due to the use of the first order approximation that currents are the first derivative of height.

SOUND PRODUCTION BY HYDROTHERMAL VENTS

ABSTRACT

Theoretical examination of hot, turbulent, buoyant jets exiting from hydrothermal chimneys revealed acoustic source mechanisms capable of producing sound at levels higher than ambient ocean noise. Pressure levels and frequency generated by hydrothermal jets are dependent on chimney dimensions, fluid velocity and temperature and therefore can be used to monitor changes in these parameters over time.

A laboratory study of low Mach number jet noise and amplification by flow inhomogeneities confirmed theoretical predictions for homogeneous jet noise power and frequency. The increase in power due to convected flow inhomogeneities, however, was lower in the near field than expected.

Indirect evidence of hydrothermal sound fields (Reidesel et al., 1982; Bibee and Jacobson, 1986) showing anomalous high power and low frequency noise associated with vents is due to processes other than jet noise.

Direct measurements of hydrothermal vent sound fields show that frequency and power levels are comparable to ambient ocean noise and are consistent with jet quadrupole near-field sound which has been amplified by the dipole behavior of convected flow inhomogeneities. This near-field amplification is not as great as that predicted for the far-field but is consistent with theoretical considerations for near-field dipole and quadrupole behavior.

INTRODUCTION

The global transport of heat and chemicals from the earth's interior through the seafloor and into the biosphere depends on the movement of water through oceanic lithosphere. At the crests of the world's mid-ocean ridge (MOR) system, cold seawater seeps into the permeable, unsedimented crust and is heated by the shallow magma chamber and intruded lavas of newly formed oceanic lithosphere in the process called hydrothermal circulation. The hot water, rich in minerals, rises buoyantly in narrow upflow zones from crustal depths of 2-4 km (Macdonald, 1982) and exits at hydrothermal vents located on the ridge axis (figure B1). Upon mixing with the cold, ambient ocean bottom water, metals and sulfides precipitate, depositing zinc, copper and iron sulfides and forming the massive sulfide deposits characteristic of hydrothermal vent sites. It is becoming increasingly apparent that hydrothermal systems permeate a large portion of the Mid-Ocean Ridge system and may significantly contribute to the chemical composition of the oceans and atmosphere.

To date, active hydrothermal vents have been found (Hoagland and Broadus, 1987) in the Pacific Ocean on medium to fast spreading ridges: at the Galapagos Rift area near 86^{o}W (Ballard et al., 1982), along the East Pacific Rise (EPR) at 20^{o}S, 11^{o}N (McConachy et al., 1986), 13^{o}N, and 21^{o}N (Ballard et al., 1981; Ballard et al., 1984; Francheteau and Ballard, 1983; Hekinian et al., 1983b; RISE, 1980), in the Guaymas Basin (Peter and Scott, 1985), on the Explorer Ridge (Scott et al., 1984), the Juan de Fuca Ridge (CASM, 1985; Hammond et al., 1984; Crane et al.,

1985; Normark, 1986), the Gorda Ridge (USGS, 1985), the Lau Basin (Hawkins, 1986; Craig, 1987), and in the Sea of Okhotsk (Ocean Science News, 1986). Numerous extinct vent sulfide chimneys have also been found in these areas. On the slow spreading Mid-Atlantic Ridge (MAR) active vents have been located near the TAG (Trans-Atlantic Geotraverse) area at 26°N and at 23°N (Rona, 1984; Rona, 1985).

Vent fields, ranging in area from 10 to 10,000 m^2, form in the narrow active volcanic regions of ridge crests. The fields are characterized by sulfide structures up to 15 m high, surficial sulfide deposits and sedimentation, and are usually found hosting a suite of organisms whose primary food source is hydrogen sulfide from vent fluid. The flow regime is often quite complex and depends on the subsurface geological structure as well as sediment cover. The highest velocity and hottest flow emanates from sulfide chimneys, with typical velocities of 1-3 m/s, temperatures of 250-350 °C, and exit areas of 10-30 cm^2 (Converse et al., 1984; Little et al., 1987). This type of flow originates from near the top of the magma chamber, with hot fluid moving upward through the crust in a relatively unobstructed path (Cann, 1982). The rest of the vent field encompasses areas of diffuse flow emanating from cracks and fissures. In this case, the high temperature fluid has premixed with ambient seawater that has seeped several tens of meters into the subsurface. The fluid is therefore cooler, 10-30°C, and has precipitated most of its sulfides before exiting the sea floor.

The full impact of hydrothermal fluxes of heat and chemicals on biogeochemical cycles can only be assessed by determining both the total spatial extent and temporal variability of hydrothermal vents, neither of

which are presently well known. Vent sites are typically found by towing cameras, nephelometers, CTDs (conductivity, temperature, depth recorders), or taking hydrocasts to locate the plume of hydrothermal fluid found above active vents. Measurements of instantaneous morphology, chemical composition, mineralogy, temperature, flow rates and biota, have generally been done with a submersible, a method which results in short time samples and sparse lateral coverage along the ridge axis (Backer et al., 1985; Hekinian et al., 1983a; Karsten et al., 1984; Tivey and Delaney, 1985; Hessler et al., 1985). In addition, both the difficulty in location vents and the harsh environment they comprise have resulted in an unusual dearth of information on vent activity. The high temperatures and particle precipitation at vents make conventional direct sensing instruments such as thermistors and flow meters ineffective for long-term measurements (none have operated for more than a few days; Converse et al., 1984). Also, these instruments need to be precisely placed by a submarine with a manipulator arm inside an active sulfide chimney, and the results are strongly dependent upon the position of the sensor in the chimney.

There is at present a strong scientific need for methods with which to measure the long-term (days to years) variations in hydrothermal vent activity. Calculations of vent lifetime based on such indirect estimates as vent fauna age and size of heat source in the ocean crust range from one to 10^4 years (Converse et al., 1984; Hekinian et al., 1983b; Macdonald, 1982). Hydrothermal vent fields evolve continually, in flow rates, size, geometry and biological composition (Hekinian et al., 1983a; Johnson and Tunnicliffe, 1985), the most direct evidence being the

existence of numerous extinct fields. Possible mechanisms for reducing flow include the blocking of flow channels by hydrothermal mineralization, exhaustion of underlying heat source (Cann and Strens, 1982), reduction of porosity, and closing of flow paths by tectonic activity. On the other hand, flow may increase as a result of tectonic activity or magma injection. Periodic oscillation in flow may be produced by tidal forcing either indirectly through tectonic activity or directly through pressure effects on flow. Cataclysmic changes are possible based on models of heat transfer at the base of the convective system which predict sudden changes in flow due to the behavior of seawater as it reaches the high temperature two-phase region of pressure and temperature (Cann et al., 1986). Measurements of flow variations are needed to constrain these and other models of hydrothermal processes.

Long-term monitoring of fluid fluxes within the severe environmental conditions at vents requires the development of a remote sensing technique that can be located away from hydrothermal fluid. This article will examine the applicability of a method to acoustically monitor fluid flow by recording the sound field generated by hydrothermal vents. The sound field of a hot, turbulent jet is known to be related to fluid efflux velocity, fluid temperature, and orifice diameter (Lighthill, 1952). The monitoring of jet sound power and frequency can be used to detect changes in fluxes at a particular site. In addition, a detailed understanding of sound source mechanisms and vent geometry can theoretically allow vent sound fields to be used to determine the absolute velocity, diameter, and temperature of fluid discharge. Long-term monitoring of this sound field will give information on the

variation of these parameters over time and thus provide data on the variations of vent fluid fluxes over the life cycle of a particular vent field.

The use of passive remote acoustic monitoring with available technology alleviates many of the degradation problems associated with instrumentation placed directly in hydrothermal flow. In this paper we will examine evidence for hydrothermal sound generation and assess the technique of determining the long-term behavior of heat, chemical and mass fluxes from the active hydrothermal vents found along Mid-Ocean Ridges by acoustically monitoring the sound produced by hot, turbulent, hydrothermal vent jets. Included in this presentation are a theoretical examination of sound source mechanisms, a laboratory study of jet noise, and a summary of results of noise measurements made near hydrothermal vent sites (Riedesel et al., 1982; Bibee and Jacobson, 1986; Little, in prep.)

THEORETICAL SOURCE MECHANISMS

Sound production by moving fluids occurs through the conversion of kinetic energy into acoustic energy (Dowling and Ffowcs Williams, 1983). The kinetic energy of a moving fluid is attributed to hydrodynamic motions and inertial effects and depends on fluid density and velocity, whereas acoustic energy is stored in the elastic forces of the fluid and depends on its compressibility. Pressure variations occur in all unsteady flows; sometimes they are confined to the flow and balance fluctuations of local momentum, and sometimes they propagate away from the flow as sound (Ffowcs Williams, 1969). Propagating and non-

propagating pressure fields (often designated sound and pseudo-sound, respectively) are sensed in the same way by hydrophones, but they behave differently. The non-propagating pressure field defines the near-field and does not radiate; it is a hydrodynamic pressure field in which compressibility effects are negligible. The propagating pressure field makes up the far-field, or radiated pressure field, which behaves as a classical acoustic wave whose speed depends on the compressibility of the fluid. The non-propagating pressure level is proportional to the dynamic head of the flow, which is ρV^2, where ρ is fluid density and V is fluid velocity.

The basic physical processes which transfer inertial to elastic energy and generate a radiating pressure field in a fluid primarily do so through mechanisms (figure B2) described as monopoles, dipoles, and quadrupoles (or more generally, multipoles). The monopole radiator arises through volume or mass fluctuations, such as expanding and collapsing bubbles. Also, if mass flux from a hydrothermal vent is not constant, but varies in a regular way, then conditions exist for monopole sound production. The dipole radiator is generated by external force fluctuations which result in variations of momentum, such as vibrations of an object in a fluid. Vibrations of the chimney induced by the flow of turbulent hydrothermal fluid would produce dipole sound radiation. The quadrupole is produced by fluctuations of the rate of momentum across a fixed surface, such as turbulent shear stress in the mixing region of a jet. In the mixing region of turbulent jets where shear stress is high, kinetic energy is converted to sound through fluctuations in momentum

flux. Quadrupole sources also can be considered formed from the opposing dipoles of vortices found on the edges of the jet (Powell, 1964).

Generally, in dividing multipole pressure fields into the two regions of differing behavior (radiating and non-radiating), the near-field is chosen as less than one wavelength from the source and the far-field as beyond one wavelength, although the change is not abrupt. A single monopole radiates a pressure wave equally in all directions. The amplitude decays as 1/r, where r is radial distance from the source and it has no near-field component. A dipole, made of two equal but opposite polarity monopoles, has a two-dimensional radiation pattern and is a less efficient radiator due to cancellation effects of the two monopoles. The near-field of a dipole, however, has a higher amplitude than that of a monopole of the same source strength, and decays as $1/r^2$ until $r=\lambda$ (λ = wavelength). In the far-field, the amplitude of the dipole pressure wave decays as 1/r. A quadrupole has a three-dimensional radiation pattern and, being formed from two equal but opposite dipoles, is the least efficient radiator. However, the near-field of a quadrupole has the highest amplitude of these multipoles and it decays as $1/r^3$. Its far-field decays as 1/r but is the weakest of the three poles. Monopole radiation, if present, will dominate the far-field acoustic signal, followed by dipole radiation. Quadrupole radiation will be significant only at high fluid exit velocities if the other sources are not present, or in the near-field.

At hydrothermal vents it is possible that all three sources are present and that they are site specific. Monopole radiation can be produced by cavitation, boiling, pulsating exit flows, or resonance in

subsurface cavities. Dipole radiation will arise from vibrations of the chimney, interaction of the turbulent flow with a rigid surface, or convection of flow inhomogeneities. Quadrupole radiation will emanate from the shear stress produced in the turbulent mixing region of the free hydrothermal jet. Estimates of the contribution of these sources to a hydrothermal acoustic pressure field follow.

Sound production by hydrothermal vents is theoretically a function of fluid exit velocity (V), temperature (T), density (ρ), sound speed (c), orifice diameter (D), and sulfide chimney dimension (L). The dependence of sound on these parameters varies according to the particular source mechanism involved. These parameters are difficult to measure, and vary from site to site, but estimates have been obtained in several experiments (Converse et al., 1984, Little et al., 1987; Tivey and Delaney, 1986). The following nominal values are used in this discussion of acoustic source mechanisms:

Velocity:	$V = 2$ m/s
Temperature:	$T = 350\ ^{o}C$
Density:	$\rho = 1000\ kg/m^3$
Diameter:	$D = 0.05$ m
Length:	$L = 3$ m
Sound Speed:	$c = 1500$ m/s

Monopole

i) Pulsating Exit Flow

The sound generated from this type of pulsating flow from a pipe can be treated as if it was produced by the motions of a baffled piston (Ross, 1976). The pressure field from such a source is approximated as:

$$P(r) = \frac{3\pi D P_i f(\theta)}{16r} \qquad (1)$$

where P_i is the rms pressure fluctuations, $f(\theta) = 1$ for $\lambda > 0.5$m. The pressure produced by the mean flow of a jet is approximately ρV^2 where V is the mean exit velocity. If we assume that P_i is 10% of the mean flow, then

$$P_i = 0.1\rho V^2 = 400 \text{ Pa} \qquad (2)$$

and

$$P(r) = \frac{12}{r} \text{ Pa}\cdot\text{m} \qquad (3)$$

ii) Subsurface Cavity Resonance

Hydrothermal vents are generally found on fresh basalt flows which often contain numerous drained lava lakes and collapse pits. Recent efforts to drill into zero-age crust at a hydrothermal site were hampered by the presence of subsurface cavities (ODP, 1986). These cavities are capable of resonating and producing considerable sound if excited at the proper frequency. Fluid moving in and out of a cavity provides mass while the flexibility of the cavity walls provides the spring action to sustain resonance. Flow excitation of the cavity occurs through interaction of turbulent flow with the walls as the fluid enter the

volume. If the dominant frequency of turbulence approaches the resonance frequency of the cavity, the cavity will begin to pulsate, which, in turn, will strengthen production of that very frequency of turbulence (Laufer and Yen, 1983). Such flow excited resonance will radiate a strong tonal component (Ross, 1976). The frequency of such acoustic radiation, being dependent on cavity size, rigidity, and geometry, is difficult to predict since very little information on subsurface cavity structure in hydrothermal systems exits. The magnitude of radiated power depends on how close the bandwidth of the excitation frequency is to the resonant frequency of the cavity. This type of sound would be extremely site specific in hydrothermal systems.

iii) Cavitation

Cavitation is the formation of a macroscopic bubble at a liquid-liquid or liquid-solid interface caused by a local drop in pressure (Ross, 1976; Urick, 1975). Such local pressure drops occur when a moving fluid is forced to accelerate around a bend or past a fixed object. The magnitude of this pressure drop is a function of the density and velocity of the fluid and is approximately equal to $\rho V^2/2$, which for hydrothermal vents is about 2000 Pa. Cavitation inception depends on the existence of submicroscopic voids, called cavitation nuclei, in the liquid. When pressure outside a nucleus drops below the surface tension of the bubble, rapid vaporization can occur and the bubble will rupture, expand and then collapse, producing significant monopole sound. The rates of growth and collapse, which determine acoustic frequency and power, are affected by the interaction of the pressure and velocity fields at the moving

boundary, surface tension, evaporation, dissolved gas content, heat conduction, viscosity and compressibility. Dissolved gas in the fluid has the effect of cushioning the collapsing bubble, causing multiple rebounds, and reducing sound production.

The peak frequency of cavitation is inversely related to bubble radius α which is likely to be small given the depth and large static pressure at vents:

$$f = \frac{1}{2\alpha} \sqrt{\frac{\overline{P}}{\rho}} \qquad (4)$$

where

$$P = p(a)-p(\infty), \qquad (5)$$

$p(\infty)$ is ambient pressure, $p(a)$ is the pressure in the liquid just outside the liquid-gas surface, and ρ is ambient fluid density. Low frequency broad band noise dominates when the gas content of the bubble is high. Sharp, high amplitude peaks are characteristic of cavitation due to water vapor only. The inception of cavitation has been experimentally determined to depend on a cavitation parameter:

$$K = (P(\infty)-P_v-P_g)/(0.5\rho V^2) \qquad (6)$$

where P_v is vapor pressure in the bubble, and P_g is gas pressure in the bubble. If K is greater than 4, cavitation will not occur (Ross, 1976). Hydrothermal vents have been found at depths of 1500-3700 m which

correspond to ambient pressures of $1.5x10^7$-$3.7x10^7$ Pa. The vapor pressure of seawater at 350°C is about $1.5x10^7$ Pa. The dissolved gas content will effectively increase the pressure inside the bubble. It is therefore possible that cavitation occurs at shallow vent sites where $P(\infty)-P_v < 8000$ Pa. However, it is highly unlikely for cavitation to be a source of sound at greater depths.

iv) Boiling

Boiling differs from cavitation in that the enlargement of bubbles occurs due to an increase in temperature and hence vapor pressure, rather than a decrease in local outside pressure. Sound production will depend on the temperature of the hydrothermal fluid and the depth of the vent. Most systems will not exhibit appreciable sound due to boiling. Some of the shallower vent sites could, however, experience two-phase separation and generate some sound through growth and collapse of bubbles. This process, being monopole in nature, could be of primary importance in hydrothermal sound generation, if present. Recent studies north of Iceland (Jon Olafsson, personal communication) have visually documented boiling at discharge sites of hydrothermal vents at a depth of 100 m. These vents will have a distinctive acoustic signature.

Dipole

i) Chimney Vibrations

It is possible for turbulent flow through sulfide chimneys to induce vibrations in their structures. The frequency of oscillation depends on the stiffness and length of the chimney. The amplitude depends, as in

cavity resonance, on mean flow velocity and on how close the forcing frequency is to the natural frequency of the chimney. A way to estimate pressure from a vibrating chimney is to use the general description of dipole resonance coupled with a frequency estimate from theories of structural vibrations for circular beams (Ross, 1976). The dipole source term D_o due to a fluctuating force F at frequency f is:

$$D_o = \frac{F}{2\pi i f} \tag{7}$$

Maximum pressure amplitude for dipole radiation is given by

$$P = -\frac{(2\pi f)^2 D_o}{4\pi r c} = \frac{2\pi i f F}{4\pi r c} \tag{8}$$

The frequency of resonance in a circular beam is given by

$$f = \frac{(2m-1)\pi d c_b}{8\sqrt{8}L^2\sqrt{1+\rho/\rho_b}} \tag{9}$$

where c_b is sound velocity in the beam, ρ_b is beam density, and d is beam diameter (=1 m). Using a value of c_b=3000m/s, ρ_b = 4000 kg/m^3 and m=1, equation 9 results in a frequency of 40 Hz. Force F is estimated by assuming that 10% of the available pressure from fluid flow (4000 Pa from above) acts upon the inside wall of the chimney of length L and diameter 0.05 m, which results in a force of approximately 240N. Using this in equation 8 produces a fluctuating chimney pressure estimate of

$$P = \frac{3.2}{r} \text{ Pa}\cdot\text{m} \tag{10}$$

Quadrupole

Lighthill's (1952) formulation of the aeroacoustic problem showed that the mixing region of a jet could be equated to a volume of quadrupoles with strength proportional to the stress tensor in the moving fluid. Such a mathematical formulation allows radiated jet acoustic power levels to be estimated and shown to be proportional to V^8 for low Mach number flow (Lighthill, 1952; 1954).

The frequency of jet noise depends on the size of the turbulent eddies in the jet, which scale with jet diameter (Lighthill, 1963). Since the jet expands laterally and decreases speed with increasing distance from the orifice, acoustic power and frequency from a given section of jet will both decrease. The resultant far-field spectrum will have a peak frequency near 0.8V/D (Lush, 1971) with a power fall-off of 6-9 db per octave (frequency doubling) below the peak and 2-3 db per octave above the peak. In the near field, the frequency spectrum produced will be similar but depend on relative proximity to either the mixing region near the orifice, which produces high frequencies, or the fully developed turbulent region further downstream which produces lower frequencies.

The power and frequency distribution are both directional in jets, with higher frequencies being stronger at 90^{o} to the jet axis and lower frequencies dominating at low angles ($<45^{o}$) to the jet axis (Lush, 1971).

Sound production by turbulent jets is a complicated process and extensive theoretical and laboratory work has examined the exact directionality, frequency, and power of sound from low to high Mach number (M) jets (Lighthill, 1954; Ffowcs Williams, 1977; Lush, 1971;

Laufer and Yen, 1983; Goldstein, 1984; Powell, 1964; Dowling et al., 1978; Mankbadi, 1985; Cohen and Wygnanski, 1987). There are however, very few experimental results on very low Mach number jets (Jorgensen, 1961). Hydrothermal vents, with $M=10^{-3}$, fall into this category. Therefore, we can use theoretical studies of jet radiation efficiency to predict intensity of jet noise from vents. The maximum pressure field of low Mach number jets in the far-field is proportional to (Lush, 1971):

$$P \propto \frac{\rho U^4 D}{c^2 r} \tag{11}$$

at a peak frequency of

$$f \approx V/D \tag{12}$$

The absolute magnitude of the near and far pressure fields of a turbulent jet generating quadrupole radiation can be approximated by (Ross, 1976; Ffowcs Williams, personal communication):

$$p = 10^{-2}\rho V^2 = 40 \text{ Pa} \quad \text{for } r < D \text{ near-field} \tag{13}$$

$$p = 10^{-2}\rho V^2 (D/r)^3 = 5\times10^{-3}/r^3 \text{ Pa}\cdot\text{m}^3 \quad \text{for } r < \lambda \text{ near-field} \tag{14}$$

$$p = 10^{-2}\rho V^2 (D/\lambda)^2 D/r = 4\times10^{-6}/r \text{ Pa}\cdot\text{m} \quad \text{for } r > \lambda \text{ far-field} \tag{15}$$

where $\lambda=cD/V$ in equation 15 returns equation 12.

Other Effects

i) Pipe Resonance

Flow through a hydrothermal chimney can set up resonant internal pressure waves, much like an organ pipe, whose frequency depends on sound speed in the fluid and on the length of the pipe:

$$f = nc/L \tag{16}$$

where n is an integer. Power level depends on how similar the frequency of the driving pressure oscillations are to the resonant frequencies of the pipe, and is difficult to predict in hydrothermal systems since nothing is yet known about variations in fluid flow.

ii) Flow Inhomogeneities

If a turbulent flow is of non-uniform density, the most efficient source is not the velocity quadrupole term but a dipole order term whose radiated power scales as V^6 (Morfey, 1973). This is due to the fact that accelerated density differences found in heterogeneous turbulent flow are effectively force fluctuations resulting in variations of momentum, which radiate as more efficient dipoles. The radiation efficiency of this type of flow is represented by a ratio of dipole pressure field to quadrupole pressure field (Morfey, 1973):

$$P_d/P_q = c\rho\Delta/V \qquad (17)$$

where Δ is the specific volume difference between jet and ambient fluid. The amplification is inversely proportional to Mach number and as such, may be a very strong effect at hydrothermal vents. For hydrothermal fluid at 350°C, the specific volume difference is approximately 0.5×10^{-3} kg/m^3, and:

$$P_d/P_q = 4 \times 10^2 \qquad (18)$$

Using the pressure calculated above for quadrupole radiation, equation 15, yields a far-field inhomogeneous flow pressure level of:

$$P = 1.5 \times 10^{-3}/r \text{ Pa} \cdot \text{m} \qquad (19)$$

The complexities and variability of hydrothermal vent systems allow for a wide range of possible sound generating mechanisms. Sources and nominal sound frequency and power levels are tabulated in table 1 using values for vent parameters given above. Levels indicate that some vents may produce significantly more sound than others based on geometry and structure alone. In addition, the range of velocities seen at vents will give rise to an additional several orders of magnitude range in power levels as most mechanisms are heavily dependent on velocity. This theoretical analysis suggests that monitoring changes in vent fields through sound is feasible, although specific sources and power levels may vary considerably depending on vent site. On the other hand, determining exact values for velocity, diameter, length and temperature will depend so heavily on chimney dimensions and internal structure that a complete morphologic description of the vent field would be required to separate out the different source mechanisms.

LABORATORY EXPERIMENT

In order to determine whether theoretical estimates of jet noise production through quadrupole radiation and amplification by flow inhomogeneities were valid at the low Mach numbers found at vents, we conducted a simple laboratory investigation. Our measurements were made

in the near field since no experimental investigations exist in the literature on jet noise and the effects of flow inhomogeneities on near-field pressure levels in flows with velocity and spatial scales commensurate with hydrothermal vents. The aim of this study was to substantiate theoretical estimates of jet sound pressure levels and use the results to help design a field experiment to directly measure hydrothermal vent sound fields (Little, in prep.).

In the laboratory we concentrated on pure jet noise production, a process dependent on quadrupole radiation for homogeneous fluids and on dipole radiation for non-homogeneous fluids. Comparisons were made of several velocities and nozzle dimensions for cold jets (homogeneous) to determine effects of these parameters on power and frequency. Sound amplification due to inhomogeneous flow was investigated using both hot jets into cold ambient fluid, and fresh water jets into a saline solution.

Methods

The experimental tank holding ambient water was 1.2 m x 1.5 m x 2.4 m and constructed of wood with one glass face. The jet orifice was mounted on the bottom and fed through a pipe running down the side of the tank (figure B3). Flow through the jet, driven by tap pressure, was monitored to within 3×10^{-5} m^3/s by a flow meter in series with the pipe. To reduce the effects of external vibrations, the hydrophone was suspended in the tank on a long wire cable. The hydrophone itself was a deep sea hydrophone (the same one used in the field experiment (Little in prep.)), 15 cm x 5cm, and was calibrated to within 6 db by comparison to

a known receiver. Data was recorded digitally at 500 Hz and 2000 Hz after passing through an appropriate anti-aliasing filter.

Four configurations were examined: a cold (10^{o}C) jet with velocity of 3 m/s passing through an orifice of 2.7 cm diameter into cold ambient water with sound measured at a range of 49 cm (to center of hydrophone); a cold jet with a velocity of 7.5 m/s passing through a 1.05 cm diameter orifice monitored at 27 cm; a hot (55^{o}C, ρ=985kg/m^3) jet at 3 m/s and orifice diameter of 2.7 cm monitored at 49 cm, and a fresh water jet with velocity of 3 m/s passing through an orifice of 2.7 cm diameter into cold salty water with salinity 55 ppt (density: 1041 kg/m^3), monitored at a distance of 49 cm.

Results

The laboratory environment was noisier than optimal for a rigorous test of theory (figure B4) but the results achieved here agree with theoretical predictions of jet noise within the order of magnitude resolution of this experiment (summarized in table 2). Frequency was as predicted by equation 12 for jet noise in all configurations. Power measured was within an order of magnitude of that predicted by the near field quadrupole equation 14 for the two cold jet arrangements. The higher velocity jet produced somewhat less power than anticipated, which may be due to the dominant wavelength approaching the dimensions of the tank. The amplification due to convected flow inhomogeneities was less than half that predicted by theory (equation 17) for the hot jet, and ten times less than predicted for the saline solution. This is attributed to the fact that our measurements were made in the very near field where

amplification effects of flow inhomogeneities, causing dipole radiation, on the pressure field may be less dominant than in the far-field.

FIELD OBSERVATIONS

The potential difficulty in detecting hydrothermal vent acoustic signals lies not so much in the sensitivity of hydrophones and recording instruments, as in the intensity and variability of ambient ocean noise. Typical ambient ocean noise has been extensively studied (Urick, 1986; Burdick, 1984; Hodgkiss and Anderson, 1980; Wentz, 1962; Akal et al., 1986) but absolute levels depend on the exact location and time of sampling. Noise varies considerably depending on depth of water, weather, shipping, season, local topography and is punctuated by transient sources such as local ships and biological sources, making estimates for specific sites difficult.

The lowest frequency band, 0.01-5 Hz (figure B5), exhibits high power levels and is dominated by microseisms: low frequency pressure disturbances caused by non-linear interactions of ocean surface waves (Webb, 1984), and teleseismic events.

Power in the band from 5-100 Hz, produced by distant shipping, is dependent on sound that has travelled tens to hundreds of kilometers and is strongly influenced by wave guide propagation effects such as sound channelling due to a velocity minimum in the water column. Sound which travels great distances through the ocean experiences a broadening of its spectral peak.

The mid-band, 100-10,000 Hz, is a function of local sea state and wind related noise caused by spray, breaking waves and falling water droplets. Sound due to weather within a few kilometers of the

measurement site will dominate pressure levels on the seafloor in this frequency band.

Finally, the high frequency band above 10,000 Hz is dominated by thermal noise caused by agitation of water molecules.

Transient sources also contribute to noise at a given location. These include local ships and submarines, which are characterized by high energy narrow band peaks, often including harmonics of a fundamental frequency, anywhere from 5 to 200 Hz. Biological sources can also contribute to the noise field, with whales and dolphins capable of producing high amplitude, short duration sounds at frequencies from 18-100 Hz (Watkins, 1981).

Published Field Data

East Pacific Rise

The first evidence of vent sound generation came from data collected near hydrothermal vents at 21^{o}N on the EPR where an array of ocean bottom hydrophones was set out to study microearthquake activity at an active vent site (Riedesel et al., 1982). In comparing two hydrophones, located 300 m and 2 km from the vents, it was noted that the automatic gain control on the instrument nearer the vents set itself to a gain level 16-64 times less sensitive than that of the instrument far away. This indicated that the intensity of ambient sound near the vent was consistently louder than the sound further away, suggesting that the major source of ambient noise in this area was the hydrothermal vents (Riedesel et al., 1982). In addition, the month long record of gain level shows daily variations of noise level that are correlated between

the two hydrophones (figure B6). An inspection of a time series record (figure B7) reveals a major difference in amplitude at very low frequencies (.16 Hz). These frequencies are usually associated with surface generated microseisms (Webb, 1984) but it is not clear why the amplitude should be so different at a receiver separation of only 1.5 km. These data are suggestive of a low frequency vent sound source but the evidence is inconclusive.

Juan de Fuca Ridge

Recently, anomalous high ambient acoustic noise was observed in the caldera of Axial Seamount at 46^{o}N on the Juan de Fuca Ridge (Bibee and Jacobson, 1986). Noise levels from 2-30 Hz varied up to 25 db over 6 km as measured on four separate receivers (figure B8) and it was suggested that the noise source was at or near the sea floor. With the assumption of spherical spreading, the source was placed at 400m from one of the instruments, in the northern part of the caldera. This placed it within 200m of a low temperature vent field mapped on a previous expedition. Interestingly, 10 db variations in sound power level were observed over the course of the eight day record. An instrument placed several hundred meters from the known high temperature vent field Ashes, located in the southwestern part of the caldera, recorded no evidence of anomalous acoustic noise.

ARGORISE Towed Hydrophone

In December, 1985, we attached a deep-sea hydrophone to the ARGO televiewer system during the survey of the East Pacific Rise (EPR)

between latitudes 10° and 12°N (ARGORISE). Noise was recorded in real time on the ship via ARGO's conducting cable. Digital samples were taken at 1000 Hz every hour and when in the vicinity of hydrothermal areas. The vehicle was passively towed by the surface ship and flow noise was minimized by reducing the ARGO's horizontal velocity to less than 0.2 kts. Unfortunately, a heave compensator was not able to remove all the vertical motions induced by the surface swell; thus, only about 10% of the recorded data was uncontaminated by flow noise. Few vigorous black smokers were encountered during the 200+ hours of slaloming down the ridge crest, but five hydrothermally active areas, as defined by biota, were crossed. Comparison of sound recordings near (within several meters) and far (further than 1000 m) from these areas reveals consistently elevated sound levels near hydrothermal sites (figure B9) at frequencies generally between 15 and 30 Hz. Unfortunately, absolute power levels were unobtainable but noise levels near vents were up to a factor of 10 times those away from vents. Contamination from vehicle flow noise prevents more robust further analysis of the spectrum.

Ashes Vent Field, Juan de Fuca Ridge, Acoustic Monitor Experiment

In September, 1987, high quality recordings of noise within a few tens of meters of an active vent were made using two hydrophones emplaced by the submersible Alvin in Ashes Vent Field, Axial Seamount, on the Juan de Fuca Ridge (45°55'N, 130°02'W) (Little, in prep). The hydrophones were suspended 38m apart on a vertical cable with the lower one placed 2-3m from the vent orifice. No continuous vent signals were deemed significant based on a criterion of 90% probability of detection and 5%

probability of false alarm. However, a small signal near 40 Hz, with a power level of $1x10^{-4}$ Pa^2/Hz was noticed on two records taken near Inferno vent (figure B10). This vent had an exit diameter of 4 cm and velocity of 2 $\pm$ 0.5 m/s and, using equation 12 above, the expected peak frequency for jet noise is 40$\pm$10 Hz, which is consistent with the measurements. Predicted power level for the near-field of such a jet is, from equation 14 with r=2.3m, $1.7x10^{-7}$ Pa^2/Hz. The power level suggests the occurrence of jet noise amplification of about 10^3 due to convected density inhomogeneities. Theoretically, amplification due to convected flow inhomogeneities for a density difference of $0.5x10^{-3}$ kg/m^3 (corresponding to the measured exit temperature of 329°C) can be a factor of up to $1.6x10^5$ above homogeneous quadrupole radiation, or a power level of $3x10^{-2}$ Pa^2/Hz. Measured power is less than predicted for near-field radiation with such amplification and we attribute the difference to the fact that measurements were made in the near-field where, as seen in the laboratory, amplification effects are reduced.

Summary of Field Observations

The high amplitude, low frequency noise observed at 21°N, if it is of hydrothermal origin, would have to be produced by pulsations of flow or large cavity resonance (or an unidentified mechanism) since sound source processes associated with turbulent flows would generate much higher frequencies than observed.

The ARGORISE data is consistent with black smoker inhomogeneous jet sound production in that the frequencies were within the expected range and signals were above ambient only within a few meters of vents. The

fact that no anomalous signals were detected by Bibee and Jacobson (1986) near the Ashes vent field is consistent with Little's Ashes experiment in which the hydrophone had to be within several meters of the black smoker to detect a signal. Even at that distance the probability of detecting a signal was lower than 90%. The anomalous sound recorded in the northern part of the caldera is, in light of these results, not due to a high temperature, high velocity black smoker. It may be more related to subsurface hydrothermal/tectonic interactions where the cracking of rocks would be able to produce higher power at lower frequencies than the simple movement of water.

CONCLUSIONS

The need to determine long-term variations in hydrothermal fluid flow prompted this study of sound generation at hydrothermal vents. Theoretical examination of hot, turbulent, buoyant jets exiting from hydrothermal chimneys illuminated several acoustic source mechanisms capable of producing sound at levels higher than ambient ocean noise. Among these were fluctuating flow, pipe resonance, cavitation, chimney vibrations and jet noise with amplification due to convected density inhomogeneities. Pressure levels and frequency generated by these mechanisms are dependent on chimney dimensions, fluid velocity and temperature and therefore can be used to monitor changes in these parameters over time.

A laboratory study of low Mach number jet noise and amplification by flow inhomogeneities confirmed theoretical predictions for homogeneous

jet noise power and frequency. The increase in power due to convected flow inhomogeneities, however, was lower in the near field than expected.

Indirect evidence of hydrothermal sound fields (Reidesel et al., 1984; Bibee and Jacobson, 1986) showing anomalous high power and low frequency noise associated with vents (21^{o}N, northern Axial caldera), is due to processes other than jet noise. Possible hydrothermally induced processes include low frequency fluid source pumping, cavity resonance, and flow/rock interactions in the form of fracturing.

Direct measurements of hydrothermal vent sound fields (ARGORISE, Ashes vent field) show that frequency and power levels are consistent with jet quadrupole near-field sound which has been amplified by the dipole behavior of convected flow inhomogeneities. This near-field amplification is not as great as predicted for the far-field but is consistent with theoretical considerations for near-field dipole and quadrupole behavior.

Hydrothermal vents generate sound but source mechanisms at vents will be site specific, depending on vent geometry and velocity. This coupled with great variability in ambient ocean noise means that some vents will generate sound which is more easily detectable than others. The nominal vent, however, produces sound at a level close to ambient ocean noise and as such, needs a complex hydrophone array for quantitative flow monitoring.

Table 1

Source Mechanism	Frequency Hz	Pressure Level Pa	Power at 3m Pa^2/Hz
Monopole			
Pulsation	< 3000	12.0/r	16
Cavity Res.	< 1000	?	<O(1)*
Pipe Res.	n*250	?	<O(1)
Cavitation	> 1000	?	<O(1)
Boiling	?	?	?
Dipole			
Chimney Vibr.	40	3.2/r	>1
Flow Inhomog.			
far field	40	$2x10^{-3}/r$	$>5x10^{-7}$
near field	40	$2/r^3$	$>6x10^{-3}$
Quadrupole			
far field	40	$4x10^{-6}/r$	$>2x10^{-12}$
near field	40	$5x10^{-3}/r^3$	$>4x10^{-8}$

* O()= Of order of magnitude ()

Table 2

				Theoretical			Measured		
Jet	Tank	Vel. m/s	Dia. cm	Freq. Hz	Power Pa^2/Hz	Amp.	Freq. Hz	Power Pa^2/Hz	Amp.
Cold	Cold	3.0	2.80	88	$2\text{-}8x10^{-4}$	-	70-90	$5.0x10^{-4}$	-
Cold	Cold	7.5	1.05	550	$5\text{-}50x10^{-4}$	-	450-650	$1.0x10^{-6}$	-
Hot	Cold	3.0	2.80	88	$2\text{-}8x10^{-4}$	x 55	70-90	$1.2x10^{-3}$	2.5
Cold	Salt	3.0	2.80	88	$2\text{-}8x10^{-4}$	x 380	70-90	$1.0x10^{-3}$	2.0

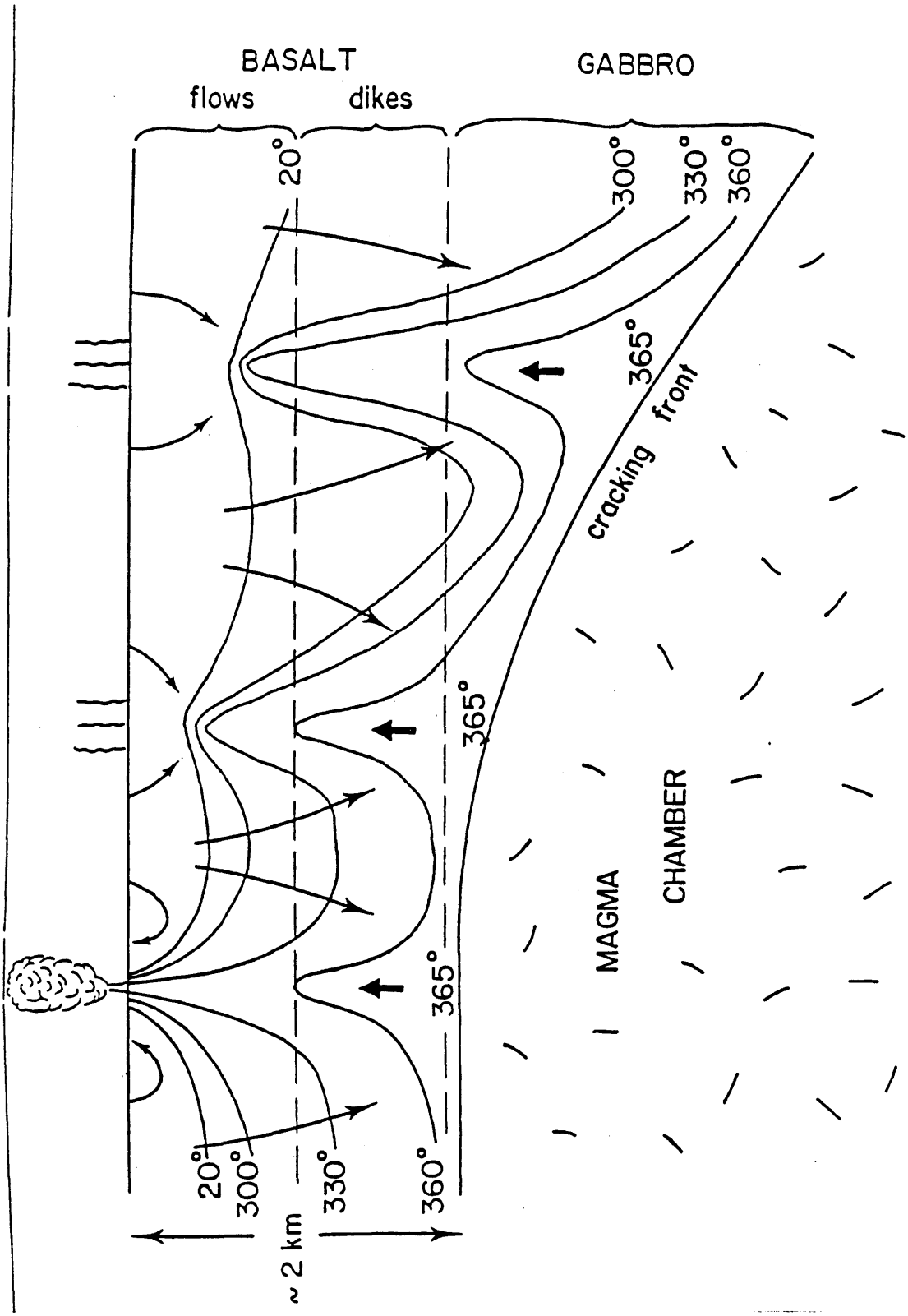

Figure B1

Schematic of hydrothermal circulation in oceanic lithosphere above a magma chamber showing isotherms caused by convection.

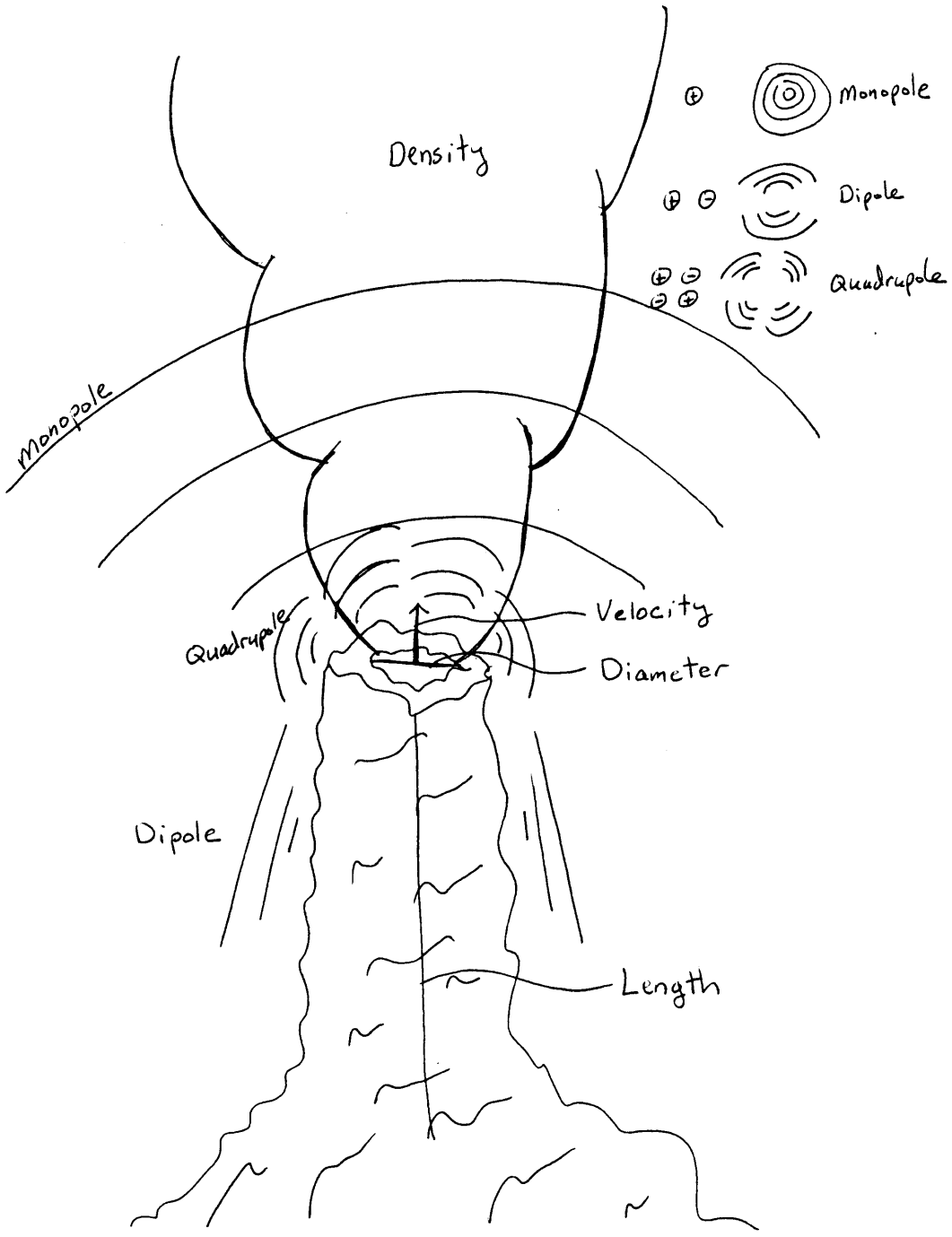

Figure B2
Important jet sound generating parameters, including chimney length L diameter D, exit velocity V_j, density ρ_j, and ambient density ρ_a, and monopole, dipole, and quadrupole source mechanisms.

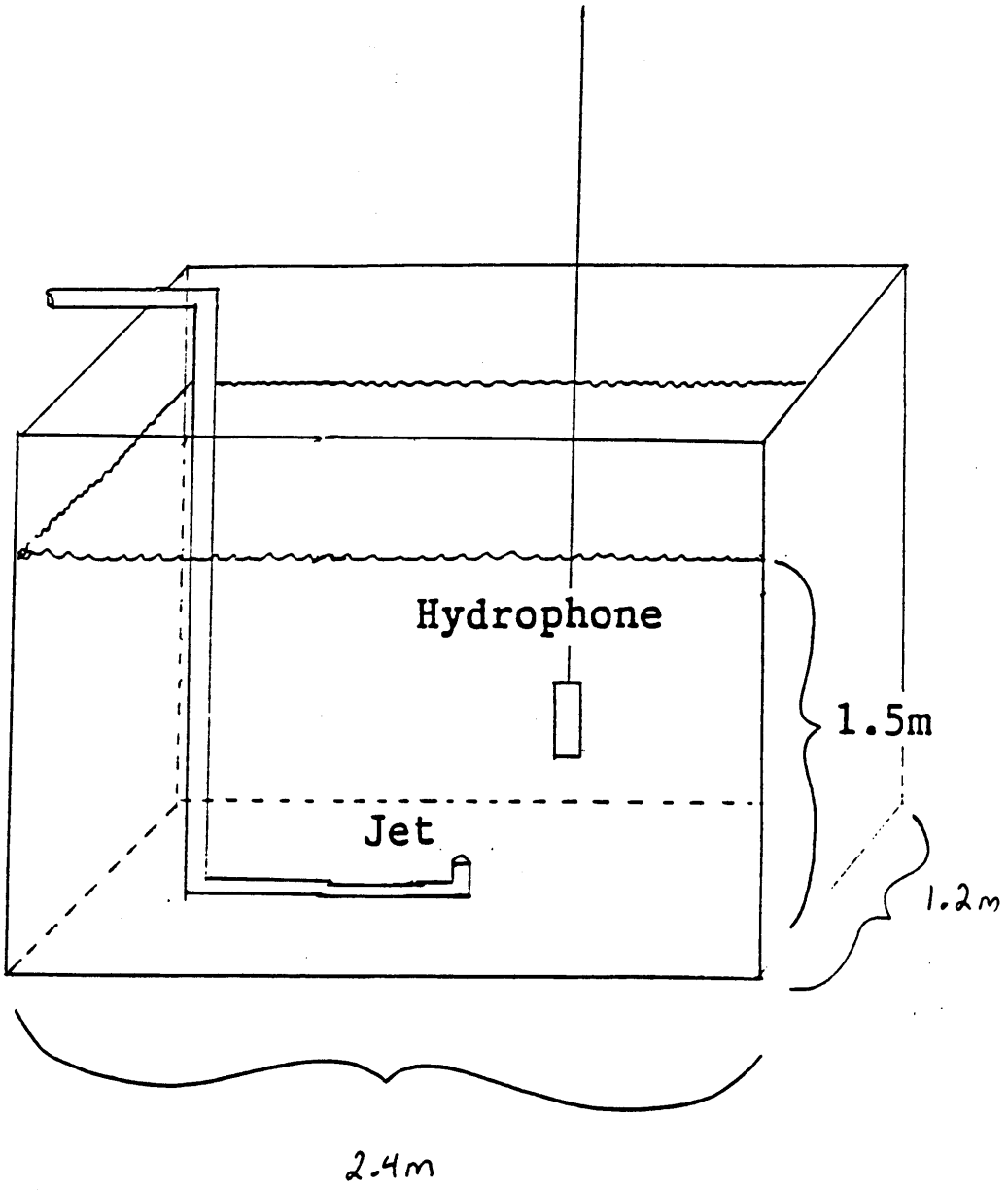

Figure B3
Laboratory configuration with bottom mounted jet and cable mounted hydrophone.

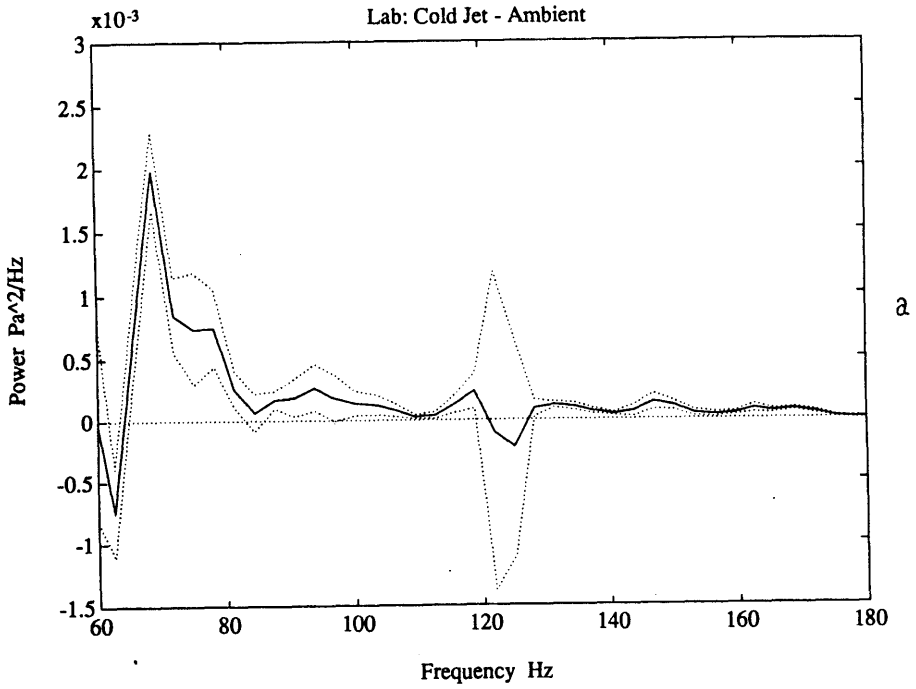

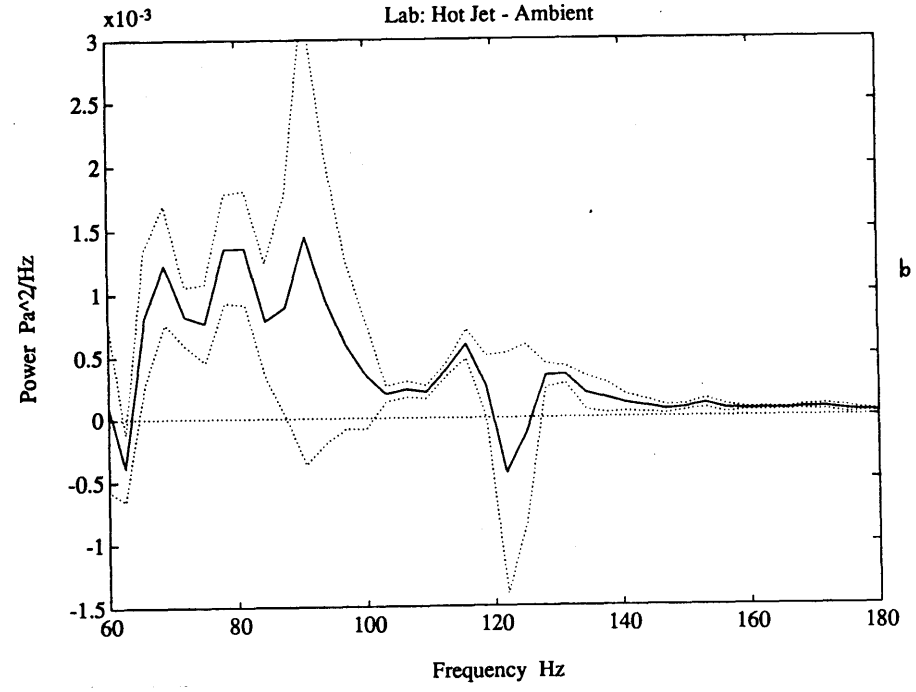

Figure B4a
Mean and 95% confidence limits for difference in sound power between ambient and a laboratory jet of cold water at 3 m/s through a 2.7 cm diameter nozzle. Expected peak frequency is about 85 Hz. Variation near 60 and 120 Hz is electronic noise.

Figure B4b
Mean and 95% confidence limits for difference in sound power between ambient and a laboratory jet of hot (130° F) water into a cold tank at 3 m/s through a 2.7 cm nozzle. Expected peak frequency is about 85 Hz. Variation near 60 and 120 Hz is electronic noise. Hot jet sound is elevated above cold jet sound.

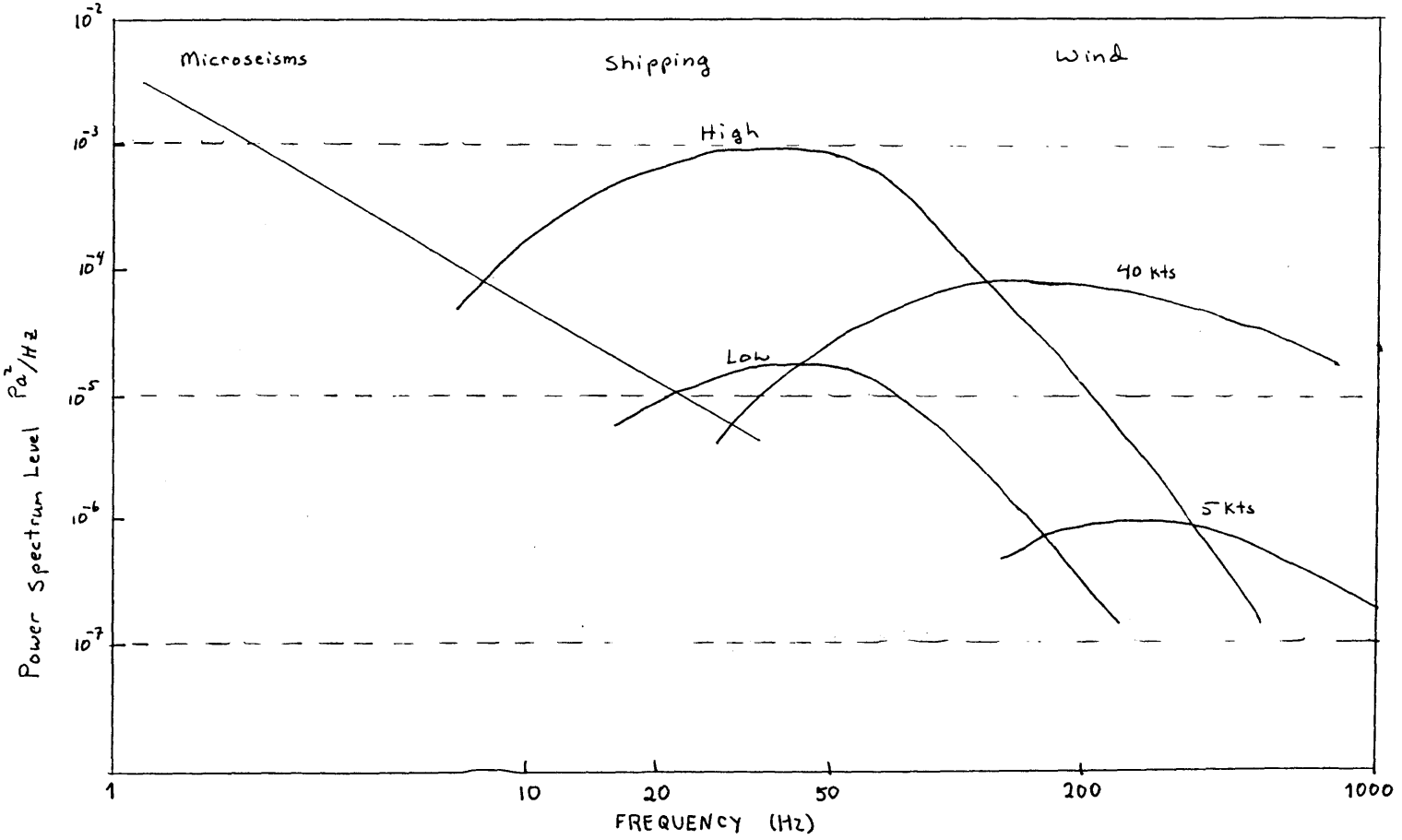

Figure B5
Ambient ocean noise levels (after Burdick, 1986) showing three primary noise sources: microseims, distant shipping, and weather.

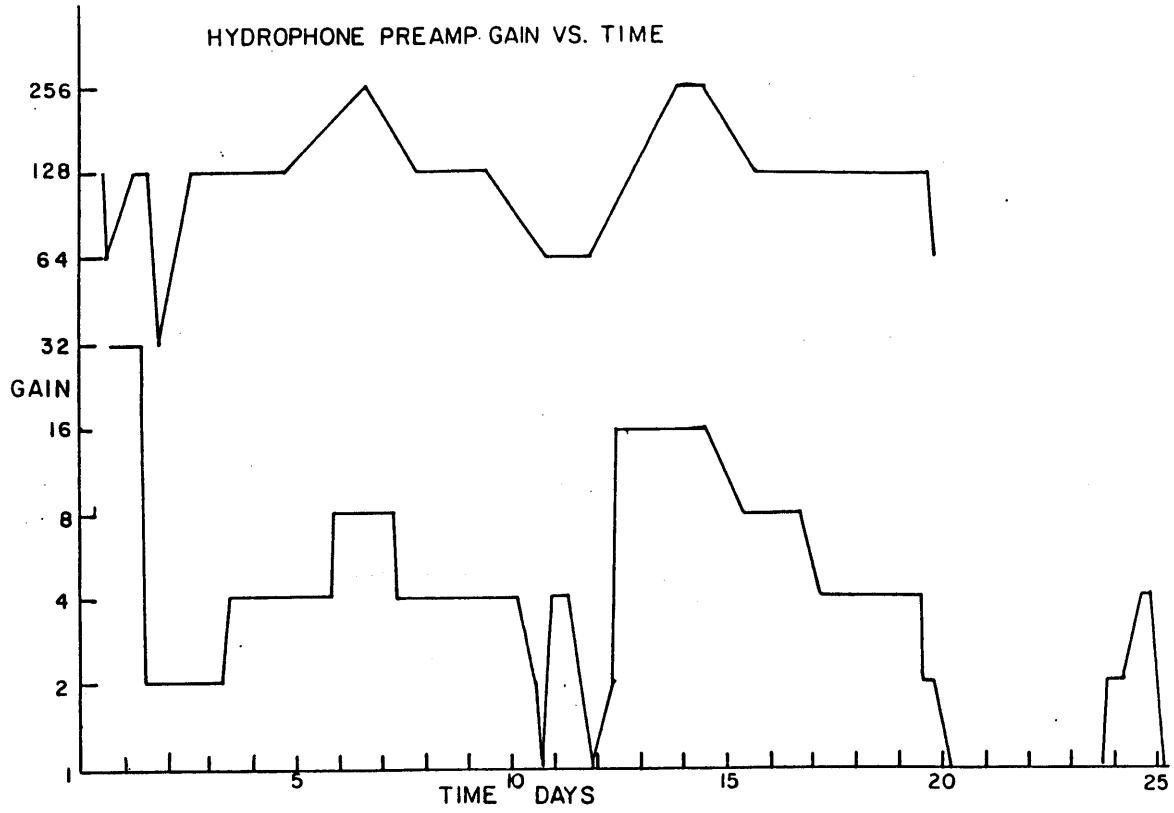

Figure B6

Plot of gain in hydrophone preamps vs. days on station for two hydrophones near the black smoker vent field at 21°N on the East Pacific Rise. The upper curve is from the hydrophone 2km from the vents and the lower from the hydrophone 300m from the vents. The signals are correlated and indicate louder sound near the vents than far away.

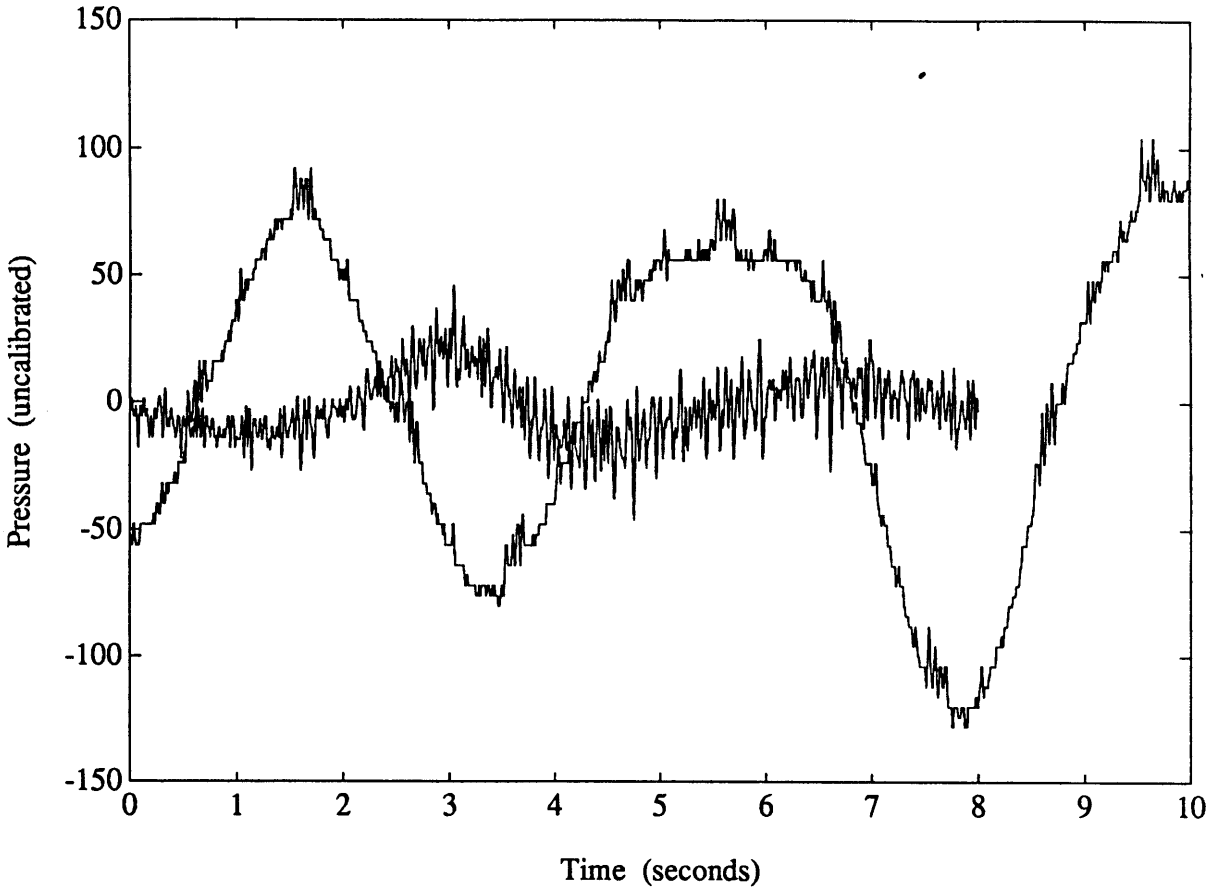

Figure B7

Time series of data from two hydrophones near 21°N on the EPR. Larger amplitude low frequency record is from the hydrophone 300m from the vents and the other from the hydrophone 2km away.

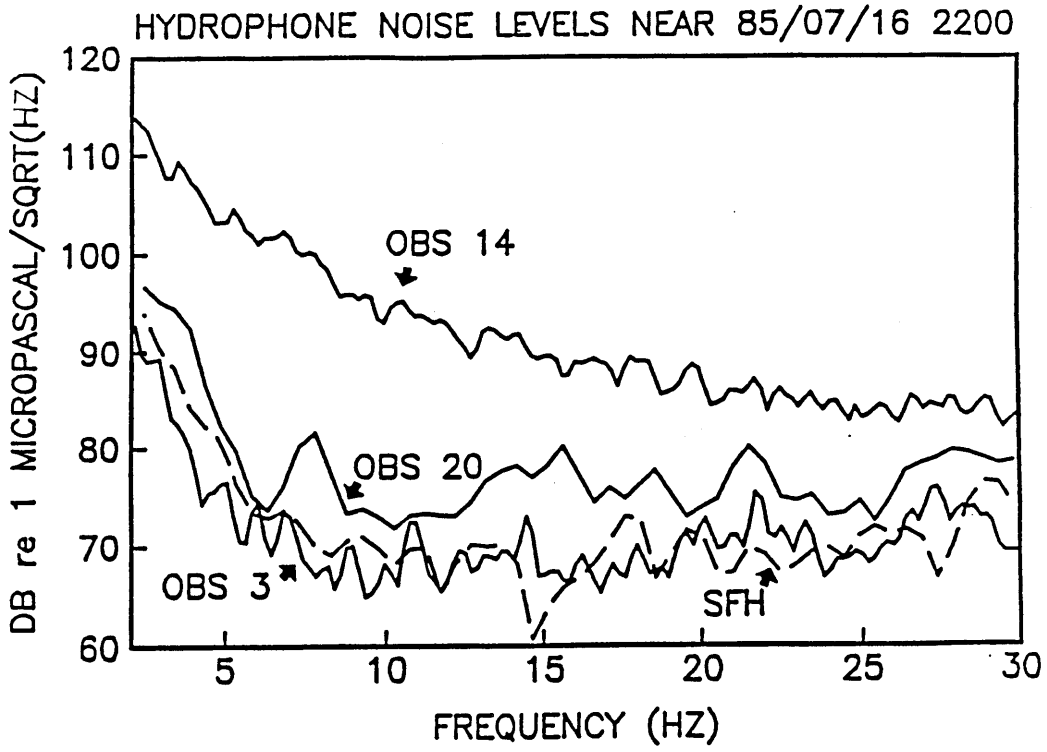

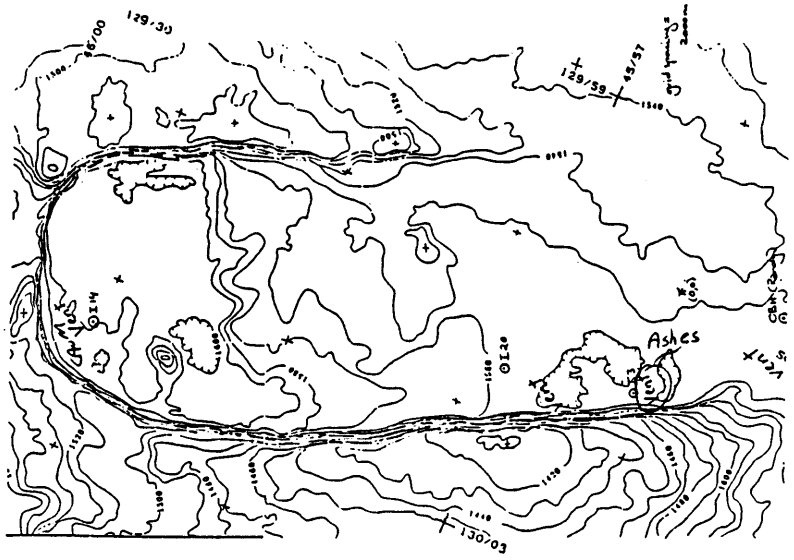

Figure B8a
Noise levels in Axial Volcano from Bibee and Jacobson's 1985 experiment. OBS 14 was in the northern part near a low temperature vent field. OBS 3 was near Ashes vent field.

Figure B8b
Site map of above experiment with Ashes vent field in south-western part of caldera and CASM low temperature field in northern part.

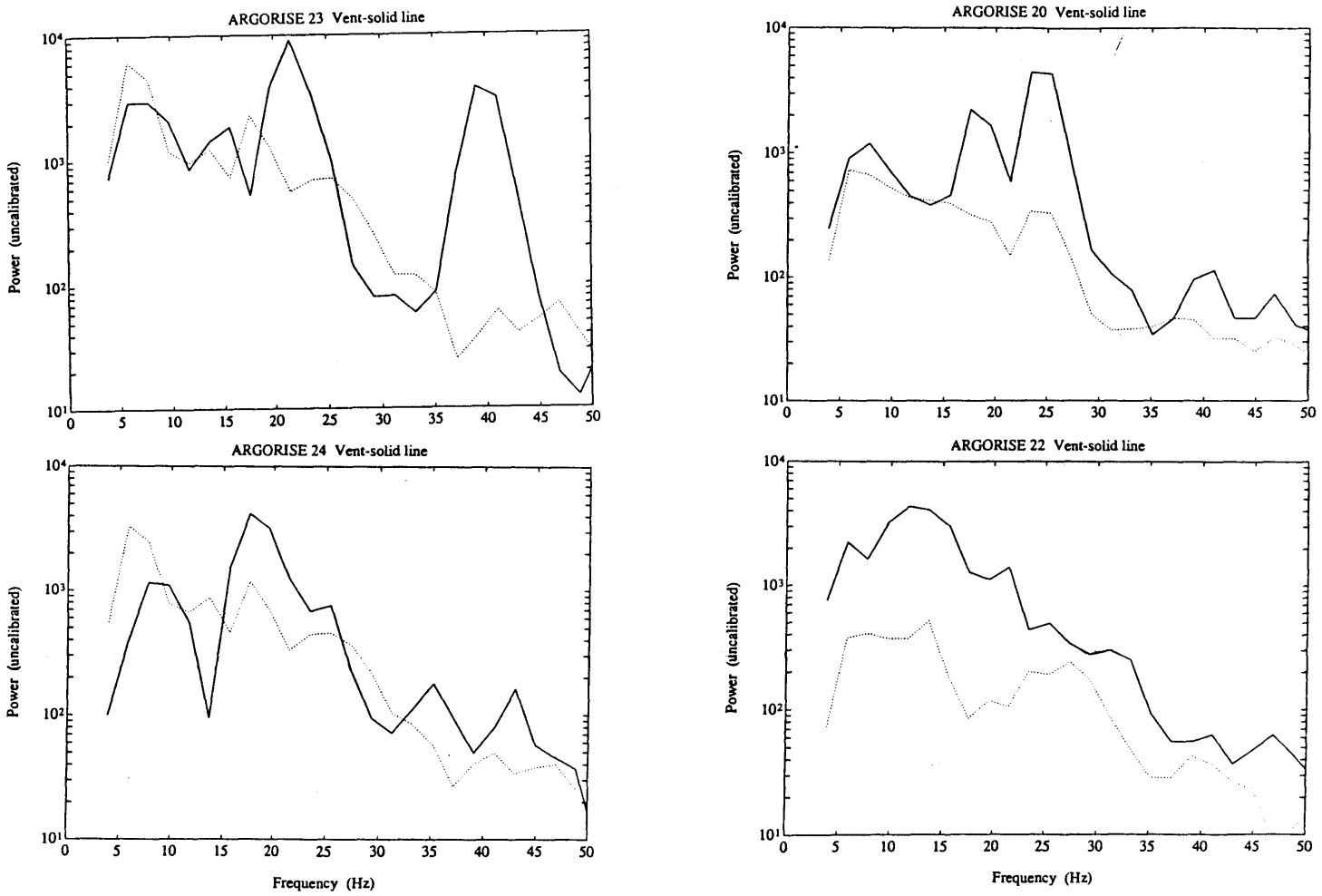

Figure B9

ARGORISE towed hydrophone power spectra from four different deployments. Records taken within several meters of vents are in solid lines; those taken greater than 1km are in dashed lines. Power levels near vents are up to 10 times those away from vents in frequencies from 15-30 Hz.

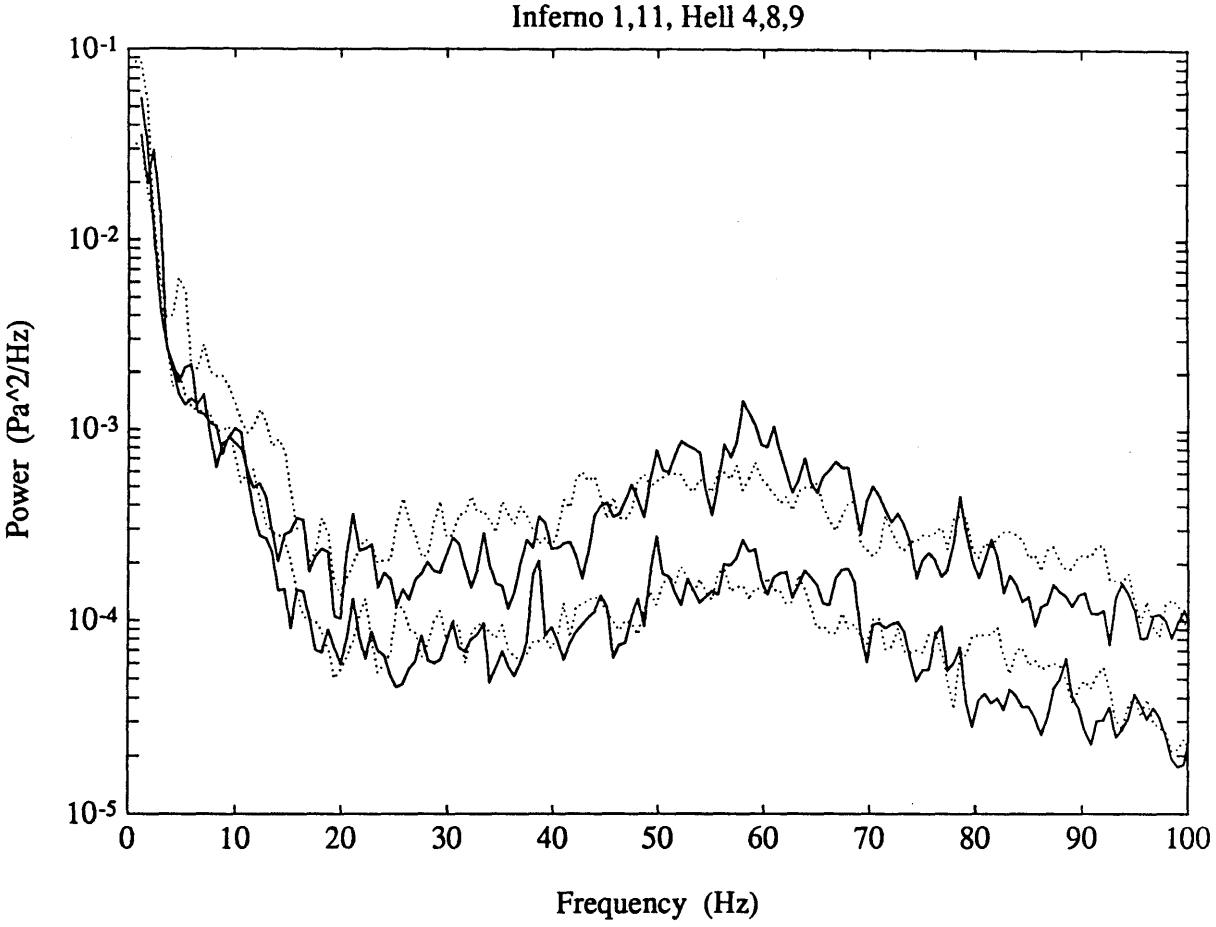

Figure B10

Low noise period from two hydrophone deployment on Ashes vent field, Axial volcano (Little, in prep). Upper solid curve is from upper hydrophone on first deployment, upper dotted is from upper hydrophone on second deployment. Lower solid curve is from the lower hydrophone on the first deployment, lower dotted curve is from lower hydrophone on the second deployment. Notice in particular the peak on the lower, first deployment at 39 Hz, due to jet noise at Inferno vent.

SOUND ASSOCIATED WITH HYDROTHERMAL VENTS: JUAN DE FUCA RIDGE FIELD EXPERIMENT

ABSTRACT

High quality acoustic noise measurements were obtained by two hydrophones located 3 m and 40 m from an active hydrothermal vent on Axial Seamount, Juan de Fuca Ridge, in an effort to determine the feasibility of monitoring hydrothermal vent activity through flow noise generation. Most of the noise field could be attributed to ambient ocean noise sources of microseisms, distant shipping and weather, punctuated by local ships and biological sources. Water/rock interface waves were detected which showed high pressure amplitudes near the seafloor and, decaying with vertical distance, produced low pressures at 40 m above the bottom. The rapidity of pressure fall off with height implies a local source.

Detection of vent signals was hampered by unexpected spatial non-stationarity due to shadowing effects of the caldera wall. No continuous vent signals were deemed significant based on a criterion of 90% probability of detection and 5% probability of false alarm. However, a small signal near 40 Hz, with a power level of $1x10^{-4}$ Pa^2/Hz was noticed on two records taken near the Inferno black smoker. The frequency of this signal is consistent with predictions and the power level suggests the occurrence of jet noise amplification due to convected density inhomogeneities.

INTRODUCTION

At mid-ocean ridges the circulation of seawater brings heat and chemicals up from the depths of oceanic lithosphere, releases part of this load onto the seafloor and injects the rest into the water column. The full impact of hydrothermal circulation on ocean composition, global heat flux and the generation of economic ore deposits has not been assessed because neither the full spatial nor temporal distributions of venting are known. Thirty or so vent sites of varying size have been identified both in the Pacific and Atlantic oceans since their first discovery in 1977 (Corliss et al., 1979; Hoagland and Broadus, 1987). Although instantaneous measurements of hydrothermal characteristics such as morphology, temperature, salinity, chemistry, heat flux, and biological composition have been taken at many of them (Converse et al., 1982; Hekinian et al., 1983; Hessler and Smithey, 1983; Ballard et al., 1984; Hammond et al., 1984; Normark et al., 1986; Rona et al., 1986; McConachy et al., 1986; Tivey and Delaney, 1986; Little et al., 1987; Craig et al., 1987), long-term measurements of any type greater than a few days are extremely rare (Johnson and Tunnicliffe, 1985; Little et al., submitted). This deficiency is due to the inaccessibility and severe environmental conditions found at vents eg. high temperatures, high pressures and reactive chemicals. An understanding of the local scale fluid flow characteristics and changes in these over time is required to develop models of hydrothermal processes ranging from subsurface water-rock interactions (Cann and Strens, 1986) to biological dispersion and growth (Hessler et al., 1985; Van Dover, 1986). The current scientific need to remotely monitor long-term changes in flow

velocity has justified a feasibility test of a passive acoustic monitor at a high temperature vent field. This method utilizes the sound generated by moving fluid at hydrothermal chimneys, the frequency and amplitude of which depend upon the fluid velocity and density, orifice diameter and chimney structure (Lighthill, 1952; Dowling et al., 1977; Ffowcs Williams, 1969; Morfey, 1973).

In theory an exact description of vent sound could be used to determine flow velocity, orifice diameter and possibly fluid density (Little and Stolzenbach, submitted). In practice, however, no unequivocal proof exists that vents generate sound at levels that are detectable in the deep ocean, although some data is available that suggests this is so (see review in Little and Stolzenbach). No measurements of vent sound have been made of adequate quality to determine source mechanisms and permit estimation of vent parameters. In this paper an experiment is described that was designed to determine the feasibility of detecting hydrothermally generated sound in the ocean. In September, 1987, high quality recordings of noise within a few tens of meters of an active vent were made using two hydrophones emplaced by the submersible Alvin in Ashes Vent Field, Axial Seamount, on the Juan de Fuca Ridge (45°55'N, 130°02'W). The results of this experiment are presented in this paper.

REVIEW OF AMBIENT OCEAN NOISE

The potential difficulty in detecting hydrothermal vent acoustic signals lies not so much in the sensitivity of hydrophones and recording instruments, as in the intensity and variability of ambient ocean noise.

Typical, ubiquitous, deep-water ambient ocean noise spectra can be separated into four frequency bands caused by four different source mechanisms, figure C1, (Urick, 1975; Burdick, 1984; Wentz, 1962).

The lowest frequency band, 0.01-5 Hz, exhibits high power levels and is dominated by microseisms: low frequency pressure disturbances caused by non-linear interactions of ocean surface waves (Webb, 1984), and teleseismic events. Temporal variations are as rapid as a few minutes for interface waves travelling near the sea floor, and as long as a few hours for variations in sea state and swell.

Power in the band from 5-100 Hz, produced by distant shipping, is dependent on sound that has travelled tens to hundreds of kilometers and is strongly influenced by wave guide propagation effects such as sound channelling due to a velocity minimum. Travelling great distances through the ocean broadens the spectral peak and eliminates waves travelling outside a few degrees of horizontal. Time variations in this band are slow, on the order of hours to days and depend on changes in ship traffic and large scale temperature and salinity structure (in the sound channel).

The mid-band, 100-10,000 Hz, is a function of local sea state and wind related noise caused by spray, breaking waves and falling water droplets. Sound due to weather within a few kilometers of the measurement site will dominate pressure levels on the seafloor in this frequency band. Changes with time in power level are on the order of hours to days and are dependent on weather patterns.
Finally, the high frequency band above 10,000 Hz is dominated by noise caused by thermal agitation of water molecules.

Transient sources also contribute to noise at a given location. These include local ships and submarines, which are characterized by high energy narrow band peaks, often including harmonics of a fundamental frequency, anywhere from 5 to 200 Hz. Biological sources can also contribute to the noise field, with whales and dolphins capable of producing high amplitude, short duration sounds at frequencies from 18-100 Hz (Watkins, 1981).

Noise in the ocean is typically non-stationary both in time and space (Burdick, 1984; Hodgkiss and Anderson, 1980). The noise field varies considerably over time due to the rich variety of sources (Akal et al., 1986) and measurements made hours apart can show striking dissimilarity (as will be seen below). Sound recorded at near bottom hydrophones is subject to additional propagation effects of local topography, seafloor heterogeneity, and the interface of the ocean-seafloor boundary. These effects can produce severe spatial variability in the sound field over short distances through diffraction, scattering and exponential decay of interface waves with distance from a boundary. In the face of these difficulties, and to make the study of noise in the ocean tractable, the necessary assumption of stationarity is often validated by making comparisons over closely spaced times and distances.

SITE DESCRIPTION

Ashes Vent Field (Hannington and Scott, 1985; Hammond et al, 1986) is located 75 m from the south-western wall of Axial Seamount on the Juan de Fuca Ridge at $45^{o}55'N$, $130^{o}02'W$ (CASM, 1983; CASM, 1985; Embley et al., 1988), figure C2. The site is noted for its smooth floor and

absence of cracks and fissures, which makes it an ideal spot in which to work with the submersible and emplace a vertical instrumented cable. The caldera floor, approximately 4 km from east to west and 10 km north to south, is 1540 m below the sea surface which nominally places it in the deep sound channel for this latitude (Burdick, 1984). In the Ashes Vent Field, there are two main black smokers with accompanying sulfide and anhydrite chimneys, "Hell" and "Inferno", separated by 35 m (figure C3). In addition to these there are several lower temperature and velocity white smokers and many patches of diffuse flow within the 60x60 m area of hydrothermal activity. At the time of acoustic sampling, the chimney of Inferno was 3 m high, topped by one site of black smoke efflux sampled at a temperature of 326^{o}C with visually determined velocity of 1-2 m/s and diameter of 4 cm. There were, in addition, several other sites of clear fluid discharge, one located 20 cm from the black smoker, with a temperature of 126^{o}C, velocity of less than 1 m/s, and diameter of 1 cm. The others were located near the bottom of the edifice. The chimney of Hell was 2 m high and hosted a single black smoker at its top with an orifice diameter of 5 cm and a visually estimated velocity of 0.5-1.5 m/s.

INSTRUMENTATION AND DEPLOYMENT

The hydrothermal acoustic monitoring instrument consisted of two hydrophones suspended on a cable beneath a float (figure C4) and attached to a microprocessor controlled digitally recording system (Mellinger et al., 1986). Designed for detecting an unknown vent acoustic signature, the system had a 16 bit analog to digital converter and a programmable 1-

10-100-1000 gain amplifier resulting in a dynamic range of 156db. One tunable 8-pole Butterworth filter for each channel provided anti-aliasing for sampling rates of 300 and 2400 Hz. Calibration to absolute sound power levels was obtained by comparison to a known receiver and is accurate to within 6 db for the bandwidth 15-1200 Hz and 15db for the bandwidth 1-15 Hz. Calibration of relative response between the two channels revealed less than a 4 db difference for all frequencies of interest (1-1200Hz) in this experiment.

The deployment scheme was designed to accommodate three major constraints: minimizing the use of the submersible, recording without ships or submarines in the vicinity, and limited memory storage capability. To this end, the procedure was to drop the instrument from the ship onto the vent site using an acoustic navigation net, dive on the mooring with a submersible, pick it up, and move it to within 5 m of an active chimney. The instrument then turned on that evening at a preset time and recorded through the night after the submarine and ship had left the area. The following day, the instrument was acoustically released and recovered by the surface ship. The data was then transferred to a portable computer and the instrument readied for further deployments.

DATA DESCRIPTION

Two fully successful hydrothermal acoustic monitor deployments were obtained on Atlantis II/Alvin voyage 118, leg 21. For the first deployment, Alvin dive #1917, the lower hydrophone was placed 2 m horizontally and 1 m vertically from the north-east side of black smoker Inferno. The upper hydrophone was 39.5 m above the lower one. The

instrument turned on at 23:00 on 9/23/87 local time and recorded two consecutive sets of data every hour until 03:00 on 9/24/87. The first set was 9216 points long taken at 2400 Hz with anti-alias filter at 800 Hz. The second set was 8192 points long recorded at 300 Hz with anti-alias filter at 100 Hz. A total of 14 sets were obtained, 7 at each of the two frequencies.

On the second deployment the lower hydrophone was positioned 2 m horizontally and 2 m vertically above black smoker Hell, 35 m from Inferno, on dive #1923. The upper hydrophone was 38.9 m above the lower. The instrument began recording at 18:00 on 9/29/87 local time and sampled once an hour until 06:00 on 9/30/87. Each sample was 8192 points long taken at 300 Hz with anti-alias filter at 100 Hz, for a total yield of 13 sets.

GENERAL DATA REDUCTION

The output of a hydrophone placed in the ocean results from a combination of system noise and pressure fluctuations in the ocean. Due to the fact that all the sources of fluctuations are not completely known, only a statistical description is permitted, based on observations over an extended time period. In producing our statistical description of the hydrophone output and in analyzing the sound we will use several assumptions. First, we will assume that the noise is temporally stationary over our individual sample periods. This enables interpretation of fourier transforms of the time series as representative of the distribution of power over frequency. To help validate this assumption, examinations of the time series will be used to eliminate

impulsive signals and gross differences with time. The second assumption is that the signal from the vent is constant over the duration of the experiment. Visual observations of the smokers support this assumption as the flow velocity appeared to remain constant from dive to dive.

Power spectra are calculated for this analysis using the Welsh method (Oppenheim, 1975). The 8192 point records were divided into 16, 512 point sets, each set multiplied by a Hanning window, and used with an FFT algorithm to compute the power spectral densities which are subsequently averaged together. This gives a power estimation accuracy of $1/\sqrt{N}$ P = 1/4 P where N is the number of sets and P is the power level at a given frequency. The mathematical spectral estimates are thus accurate to $\pm$ 0.125xP. The calibration between the two hydrophones is better than a factor of 1.3xP, since the measured differences (for which corrections have been made in the plotted spectra) were about 4 db or a factor of 1.5 for the frequencies in the bandwidth of this system. The frequency resolution of 1/T, where T is the time length of a set, is 0.6 Hz for the 300 Hz samples, and 4.7 Hz for the 2400 Hz samples.

In addition to comparisons of simple power spectra, the coherence (coherence squared) and phase between the two channels will be examined. The coherence level reveals the amount of signal common to both receivers while the phase differences at a given frequency provides information on the angle of incidence of the incoming wave. The direction of wave travel can be obtained by looking at linear trends in phase as a function of frequency. Phase is calculated here such that if a broadband signal impinges on the array at an angle θ from above, the phase will be a linearly increasing trend in frequency whose slope is

dependent on θ and receiver separation. If the waves arrive from below, phase will decrease with increasing frequency.

ANALYSIS OF NOISE FIELD

Two power spectra encompassing bandwidths of 1-800 Hz from the first deployment (Inferno) and 1-100 Hz for the second (Hell), presented in figure C5 and C6, represent two of the lower noise periods of the experiment. The most obvious feature in these spectra is the difference in power levels between the two hydrophones in the bandwidth 10-200 Hz, with the upper hydrophone receiving more power than the lower. Further, a comparison with ambient ocean noise curves (figure C1, from Urick) reveals a marked similarity in power levels and spectral shape. We hypothesize that most of the noise recorded in the caldera is due to the ambient ocean noise sources described above and that the major difference in signal level is due to a shadowing and reflecting effect by the nearby caldera wall. The following analysis examines this hypothesis in detail.

High frequency: 100-800 Hz

Sound in this frequency band is dominated by sea state and wind force and will experience changes on a time scale of several hours to days. An examination of the time history for the Inferno deployment, figure C7, reveals power variations of about a factor of three for the bandwidth 200-800 Hz over the course of the deployment. The ship's log records a constant sea state of 3-5 feet and wind increasing from 11 to 21 knots over the deployment. This is consistent with the general trend of increasing power seen in figure C7.

Weather related sound propagates downward from the sea surface with sea conditions directly overhead exerting the most influence on sound at the seafloor below. Since sound waves are travelling to the receiver array from above, one would expect little or no caldera wall effects on this bandwidth if the sources are indeed weather related. Figure C8 supports this as there is very little difference in power between the two receivers above about 250Hz. Although the coherence is generally weak (figure C9), it is to be expected for wavelengths short as compared to receiver separation. A look at the cross-correlation reveals the highest correlation for a lag corresponding to an end-on wave approach from above (figure C10), suggesting sources at the sea surface.

Medium Frequency Band: 5-100 Hz

Sound from distant shipping, travelling horizontally large distances (hundreds to thousands of kilometers), often in the sound channel, will depend on both traffic density and speed, and propagation path characteristics. Time variations are expected to be on the order of hours but may be punctuated by local sources such as ships overhead (figure C11). It is because these waves from long distant sources travel very close to horizontal that the caldera wall can influence the sound at the vent field. All the sound arriving from the west must diffract around the edge of the wall to reach the lower receiver as it is in the geometric shadow of eastward travelling acoustic waves (figure C3). In addition, westward travelling waves can reflect off the wall and increase the power levels at the upper receiver, while the lower receiver, being so close to the bottom, will intercept fewer reflected

waves. Several effects are seen in the power spectra which support this hypothesis. First, the upper hydrophone has up to four times as much power in the affected bandwidth as the lower (figure C12a,b,c). Second, the effect should drop off at low frequencies as the wavelength of sound approaches the dimensions of the wall. Wavelengths near 75 m and longer, 20 Hz and below, will be less influenced by the wall and hence reach both receivers more equally, as can be seen in figure C12a,b. Power differences should also be reduced at higher frequencies, above 200 Hz, because the predominant sound at these frequencies is not travelling horizontally, as was seen above (figure C12c). Third, the second deployment should show slightly greater differences since Hell vent is 15 m closer to the caldera wall than Inferno; this is seen in figure C12a, and C12b. Finally, the phase difference of the waves at the two receivers should be roughly zero and constant as the sound hits the array broadside from westward travelling waves. Figure C13 presents coherence and phase for a record taken during Hell deployment. The generally low coherence is expected if one receiver samples part of a sound field not sampled by the other. However, the coherence is markedly above random, and the phase significant as can be seen by comparing them to coherence and phase calculated between two totally uncorrelated samples taken hours apart (figure C14). The phase between 20-100 Hz on Hell 8 is quite constant and near zero (compare to uncorrelated phases in figure C14), implying that the sound impinges at right angles to the vertical array and is thus travelling horizontally.

Low Frequency Band: 0.25-10 Hz

There appear to be two major types of sound in this band, one, microseisms caused by local sea surface waves, and the other of unknown origin which produces evanescent interface waves travelling along the seafloor boundary whose amplitudes decay exponentially with distance from the boundary (Dowling and Ffowcs Williams, 1983). The power falls off rapidly with height, implying short wavelengths and therefore a local source generating these interface waves. The power levels in this band for the interface waves is quite variable and intermittent. On the other hand, microseism power changes more slowly as it is tied to changing sea state. The upper hydrophone, being less influenced by interface waves, should have slower and lower amplitude variability than the lower hydrophone. Figures C15-C17 depict this effect and show the striking difference between microseism and interface waveforms. A record from Inferno, figure C15, and one from Hell, figure C16, show nearly identical low frequency waves, in phase, as expected from long-wavelength microseisms. The second record from Hell (figure C17), taken four hours earlier, shows high amplitude interface waves on the lower hydrophone and typical microseismic amplitude waves on the upper, exemplifying the effect that interface wave amplitude dies away exponentially from the seafloor. The power, coherence and phase confirm the conclusions of the visual examination of the time series. In figures C18a and C18b can be seen the high coherence and constant phase for microseisms. In figures C19a and C19b are shown the low coherence and variable phase for the interface waves.

In summary, the general power spectral level, time variability, power differences and wave phase relationships suggest that the bulk of

recorded sound is attributable to the identifiable ocean noise sources of microseisms, distant shipping, and ocean surface weather. In addition, several records present striking evidence of evanescent interface waves generated by a local source.

Isolated Events

Several individual noise events were recorded during the course of this experiment. One record taken during Inferno deployment captured a monochromatic 19 Hz sound signal which we attribute to a whale (figure C20). The signal has high power (figure C21), coherence (figure C22a) and the phase shows that the signal is coming in end-on from above (figure C22b). The separation, d, of the receivers is such that for this frequency, $d=\frac{1}{2}\lambda$, so sound arriving from above will have a phase delay between the two receivers of 180^{o}, as is seen in figure C22b. Curiously, the amplitude is higher on the lower hydrophone than on the upper. This may be due to the reflected wave from the hard bottom causing constructive interference on the lower hydrophone and destructive interference on the upper hydrophone ½ wavelength away.

Similar power and phase phenomena are seen on a record taken when the Atlantis II is the sound source. Figure C23 shows the power spectra of noise with the ship overhead and slightly eastward of the vent site. There is very high coherence in the signals and a linear phase with slope describing waves coming in end-on (figure C24). At 20 Hz the 180^{o} phase shift is evident, similar to that of the whale.

Hydrothermal Noise Detection

Neither Hell nor Inferno vents produce enough sound to isolate unambiguously their entire spectrum levels from ambient ocean noise. In fact, as seen above, overall noise levels are higher far from the vents than they are close to them. This unexpected result makes direct comparisons of simultaneous but spatially separated noise spectra difficult. In order to identify regions of the spectra which may have vent signal, we must identify a background noise level for this site. It had been hoped that the far receiver would provide this information, but geometrical influences, ie the caldera wall, proved to be too significant and complex. As an alternative, we have chosen to represent background ambient ocean noise with the lowest recorded noise spectra. Anything recorded significantly above this, as defined below, will be considered a signal which we will attempt to attribute to known sources.

Since all analyses are within a statistical framework, it is useful to assign significance by examining the probability that a given signal is real and not a chance fluctuation. The effective signal to noise level will be described here using a value called the detection index (Burdick, 1984; Bangs and Schultheiss, 1973; Owsley and Swope, 1981). This is an array output signal to noise ratio which depends on the number of receivers, the sample length, and the signal field and noise field. It describes both the probability of detection and the probability of false alarm (mistakenly detecting a signal when its not present) for a given signal and noise input to the hydrophones (see appendix). A high detection index provides simultaneously high confidence in correctly detecting a signal when it is present and in not falsely detecting one when it is absent. We will calculate this detection index by assigning

the lowest power level record to be noise, comparing the other records to these values and designating as signal anything above the noise. The magnitude of the resulting detection indices will represent our confidence in a given signal. We will deem as significant any detection index over 10 - this value represents a probability of detection of 90% and probability of false alarm of 5%.

The average of the lowest noise spectra, one set from Hell and the other from Inferno, assigned to represent ambient ocean noise (figure C25), are remarkably similar considering they were recorded several days apart. The lower hydrophone near Hell will be used for comparison to Inferno and vice versa, based on the logic that the vents are not exactly identical and any differences in sound level due to venting should be apparent given the 35 m separation between vents.

When we compare the quietest record at Hell with background Inferno noise we find that the detection indices at all frequencies are less than ten, as shown in figure C26. Also, when the quietest record from Inferno is compared to background at Hell, the indices are all less than ten (figure C26. We must conclude that the sound produced by the vents are below the 90% confidence detection limit of this array in this noise field, a detection limit that is equivalent to a SNR of about 10 in a 5 Hz band, or about 10^{-4} Pa^2/Hz.

We will note here, however, that Inferno appears to be generating a small sound signal at about 40 Hz, as seen in figure C25, of approximately $1x10^{-4}Pa^2/Hz$. This signal is evident on the two lowest noise 300 Hz bandwidth records. The other five contain high noise on both channels at this frequency as well as others, probably due to an

undocumented ship or submarine in the area, and no conclusions can be drawn from these. The frequency and power level of Inferno vent are consistent with theoretical estimates of noise from a jet (Little and Stolzenbach, in prep.). A velocity of 2 m/s from the 0.04 m orifice would generate sound with a peak frequency of 40 Hz. Sound pressure level at 2.3 m in the near field region of a cold turbulent jet is predicted to be $2x10^{-4}$Pa at peak frequency, (a power level of about $5x10^{-8}$ Pa^2/Hz). A hot, 350°C jet exiting into cold seawater can produce up to a factor of 10^6 higher power levels, through the amplification of sound by convecting flow inhomogeneities (Morfey, 1973). The data from the Inferno deployment show a factor of about 10^3 elevation in power levels over expected cold, jet sound, which we attribute to the high temperature and consequently low density of the exiting hydrothermal fluid.

Comparison with other Data

Noise measurements made in Axial Caldera two years earlier (Bibee and Jacobson, 1986) are comparable to the data from this experiment. The 1985 instrument placed closest to the vents detected sound about a factor of 10 in power lower than our lowest noise record. Anomalously high noise from the northern part of the caldera measured on the 1985 experiment remains unexplained but, in light of our experiment, it is not from a typical black smoker vent field like Ashes.

CONCLUSIONS

High quality data collected on this experiment were used to characterize the noise field associated with Ashes Vent Field on Axial

Seamount. Narrow band temporal variability was dominated by local ship traffic, submarines and whales. Broadband variability is attributed to changes in distant shipping or propagation paths thereof, and to changes in local weather.

The very low frequency signals (0.5-2Hz) appear to be from two distinct sources, one continuous microseisms and the other intermittent local events. Microseisms which are equal in amplitude on both receivers appear in almost all records. Sporadically appearing interface waves show high pressure amplitudes near the seafloor and, decaying rapidly with vertical distance, produce very low signal levels at 40 m above the bottom.

No continuous vent signals were deemed significant based on a criterion of 90% probability of detection and 5% probability of false alarm. However, a small signal near 40 Hz, with a power level of $1x10^{-4}$ Pa^2/Hz was noticed on two records from the Inferno deployment. This frequency of this signal is consistent with predictions and the power level suggests the occurrence of jet noise amplification due to convected density inhomogeneities.

Detection of vent signals was hampered by the unexpected spatial non-stationarity where receivers 38 m apart had about a factor 4 ambient noise level difference due to effects of local topography. This made absolute power level comparisons impossible and the resulting low signal coherences reduced confidence in phase and directionality results.

Future experiments will need to include more receivers to improve the effective SNR. Several hydrophones should be located close enough to the vent (~5 m) to allow beamforming through coherence and phase

calculations. In addition, to improve SNR, a more active vent site should be chosen since acoustic power output increases rapidly with increasing fluid exit velocity.

To generalize from one vent site, it appears that the method of monitoring hydrothermal vent fluxes through passive acoustics will require more than a simple surface ship deployment of a two-element hydrophone array. It may be most useful on high output vent sites rather than on low to moderate hydrothermal areas.

APPENDIX

The signal detection ability of a hydrophone array in a noise field is calculated by determining the raw input signal level required to achieve a given probability of detection while maintaining an acceptable probability of false alarm. The probability of detecting a signal within a gaussian noise distribution depends on the amplitude of the signal, amplitude and coherence length of noise, number of observations, and number of receivers. A matrix description, P_f, of the signal waveform for a receiver array with a point source located at the hydrothermal chimney orifice, can be generated from a description of the waveform at each receiver (from Owsley and Swope, 1981), V_f:

$$V_f = [a_1 e^{-j2\pi fr1/c} , a_2 e^{-j2\pi fr2/c}] \quad (1a)$$

Here f is frequency, j is $\sqrt{(-1)}$, r1 and r2 are receiver-source separation distances (figure C27), c is sound speed and a is an amplitude factor accounting for spherical spreading loss:

$$a_i = 1/r_i \quad \text{and,} \quad (2a)$$

$$P_f = V_f V_f^{+} \quad (3a)$$

The correlation length of the ambient noise field in the ocean will determine how difficult noise removal will be given a fixed receiver separation. We will assume that the noise field is isotropic both for simplicity and since the results are not significantly different from either surface generated or azimuthally distributed noise fields. For isotropic noise, the correlation function q is (Burdick, 1984):

$$q = \sin(2\pi d/\lambda)/(2\pi d/\lambda) \quad (4a)$$

where d is receiver separation and λ is wavelength. The array noise correlation function for two receivers will then be:

$$Q_f = \begin{bmatrix} 1 & q \\ q & 1 \end{bmatrix} + \epsilon \begin{bmatrix} 1 & 0 \\ 0 & 1 \end{bmatrix} \tag{5a}$$

where ϵ is zero for perfectly bandlimited, perfectly predictable, noise but for real, ocean systems with a random uncorrelated noise component, ϵ must be non-zero. For isotropic noise, ϵ is approximated by 0.1 (J. Krolik, personal communication).

The effective signal to noise ratio output (SNR_o) of a system in a coherent noise field is (from Bangs and Schultheiss, 1973):

$$SNR_o = N\{\sum_{f=1}^{f} (S_f/N_f)^2 \text{ trace}[(P_f Q_f^{-1})^2]\} \tag{6a}$$

where N is number of sample sets and S_f/N_f is the SNR as a function of frequency input to each receiver. Equation 6a is used to calculate the output SNR_o given an input S_f/N_f. For the 100Hz bandwidth, S_f/N_f is calculated using an average of the quietest records from the lower hydrophone of the opposite deployment as the value of ambient noise N_f. This must be done because the upper hydrophone of both deployments had such high noise levels. The assumption inherent in this procedure is that the two vents are not producing exactly the same signal. The SNR_o is then calculated in 5.3Hz frequency bands. The SNR_o equals Burdick's (1984) detectability index d_o. We have chosen as significant a d_o greater than 10, which is equivalent to a probability of detection of 90% and a probability of false alarm of 5% (Burdick, 1984).

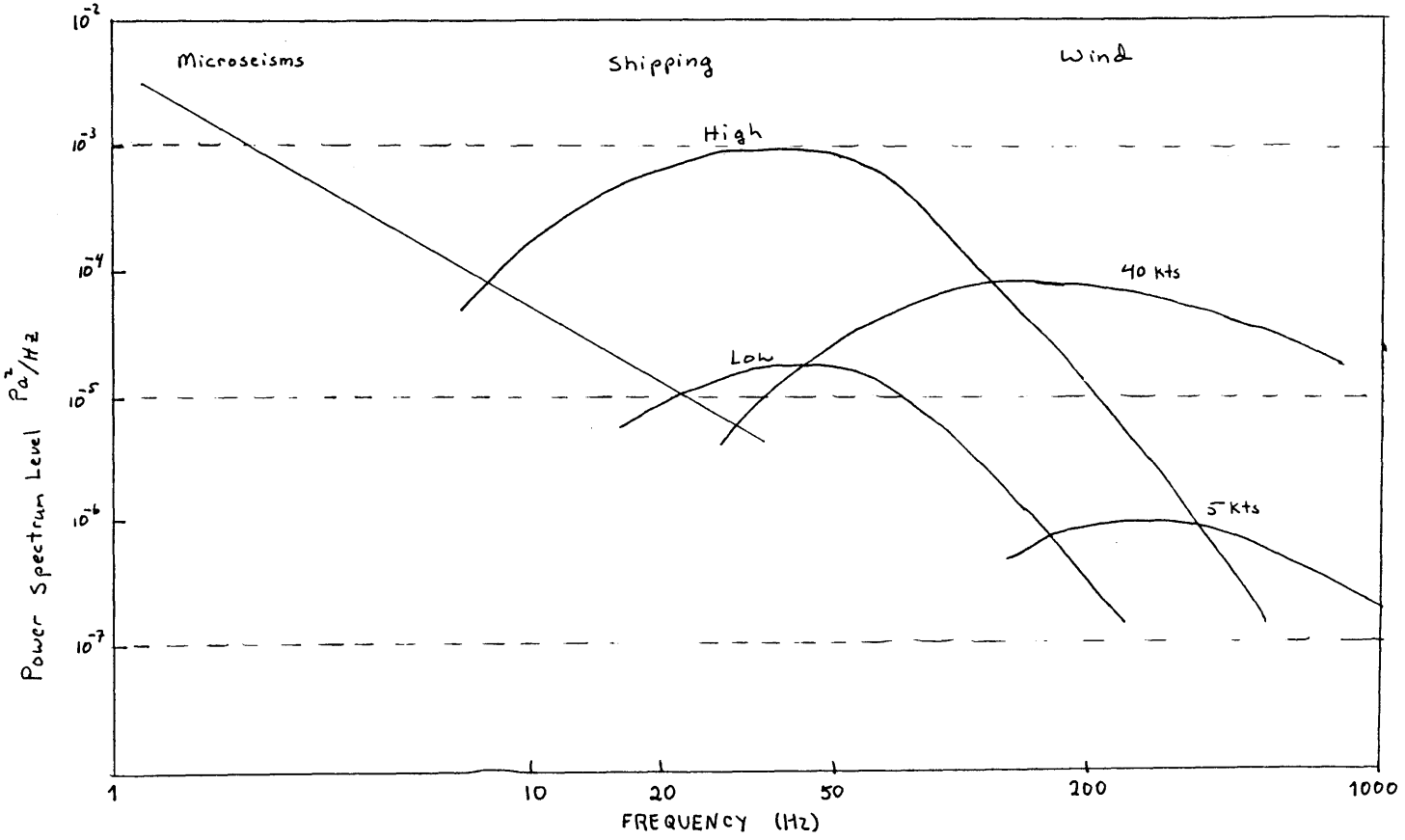

Figure C1
Typical ambient ocean noise spectra (Urick, 1986). Noise below 10 Hz is dominated by microseisms, between 10 and 200 by shipping, and between 200 and 1000 by weather.

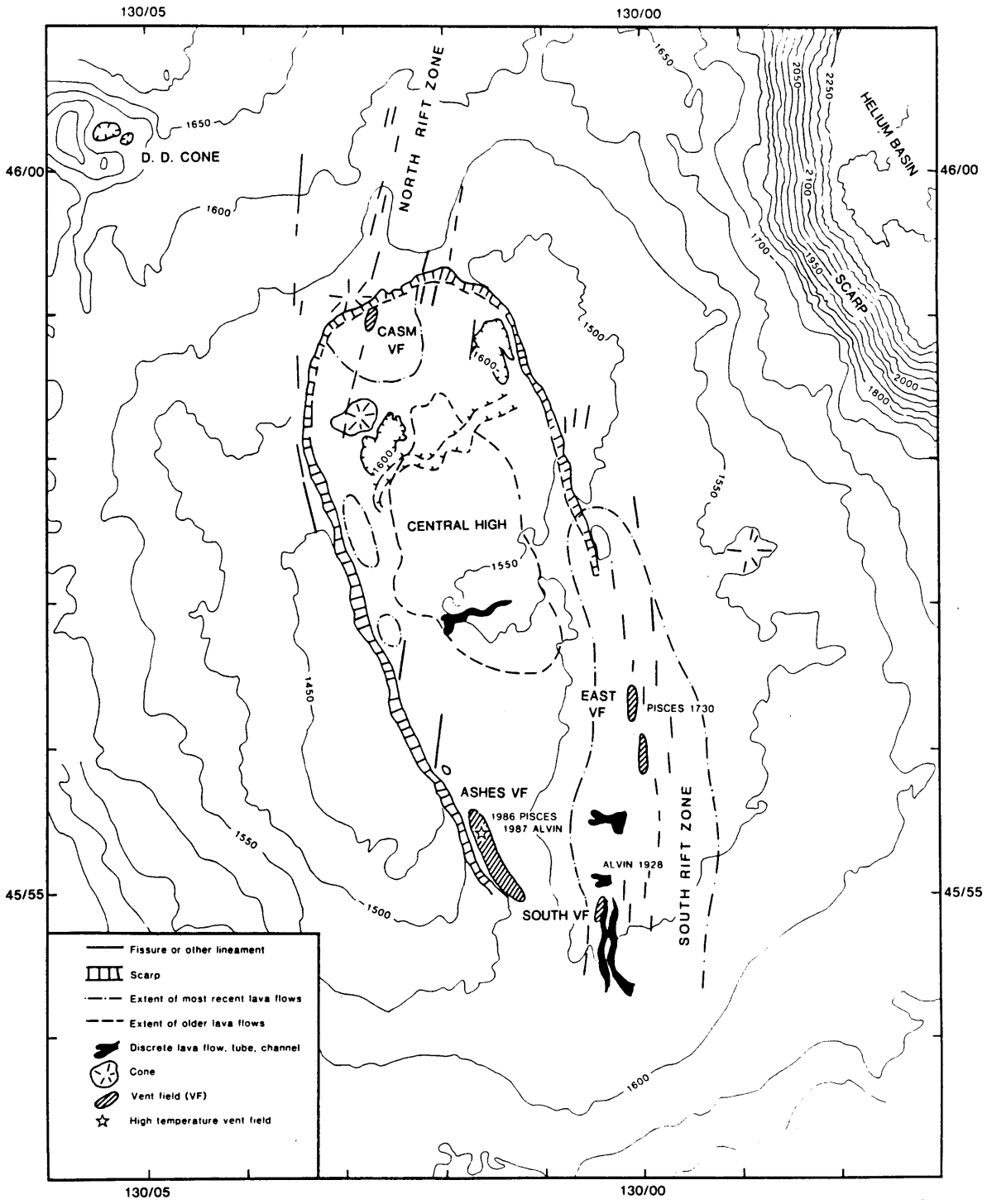

Figure C2

Location of Ashes Vent Field in Axial Seamount, on the Juan de Fuca Ridge. The field is just east of the 50-100 m high scarp defining the caldera wall (Embley et al., 1988). An earlier seismic experiment had a hydrophone near CASM vent field in the northern part of the caldera.

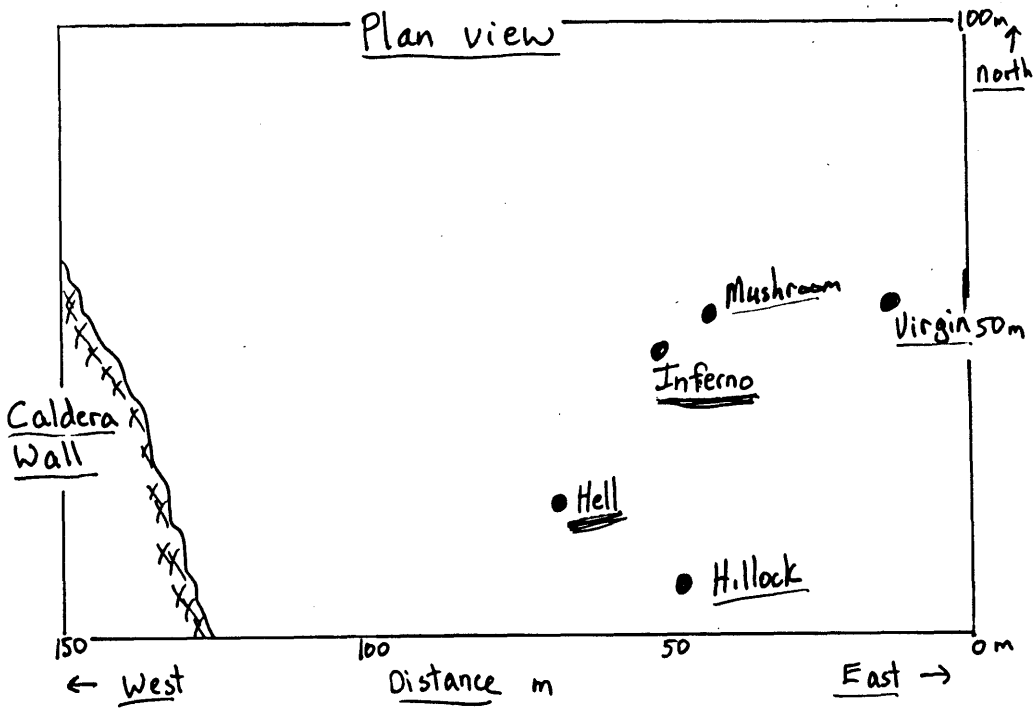

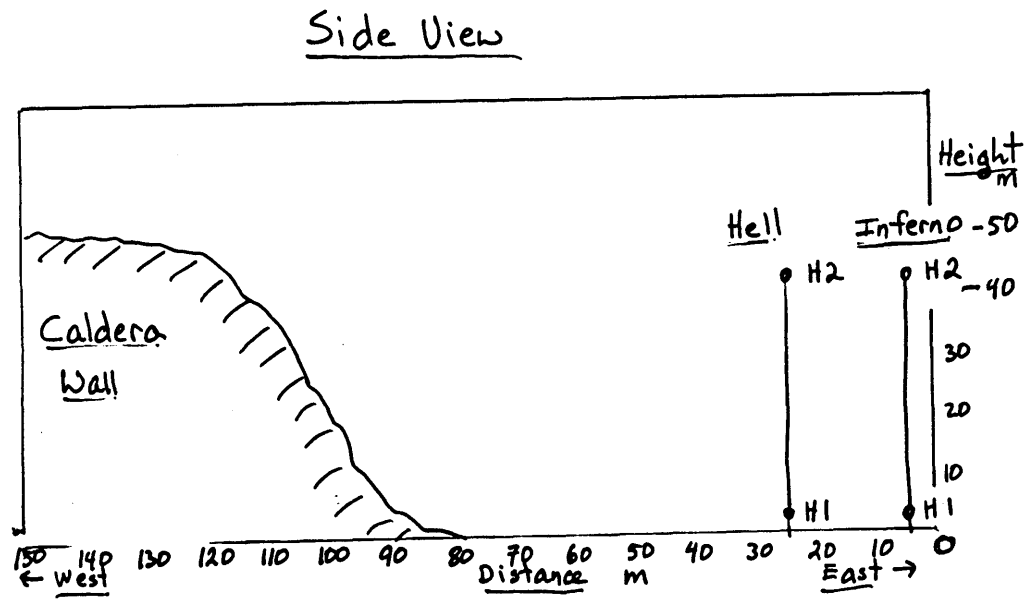

Figure C3

a) Plan view of Ashes Vent Field showing black smokers Hell and Inferno, and white smokers Mushroom, Hillock, and Virgin Mound, with caldera wall 60-80 m to the west of deployment sites.

b) Side view of deployment showing relationship between wall, vents and hydrophone array. Eastward travelling waves are prevented from reaching lower hydrophones by the shadowing effect of this wall.

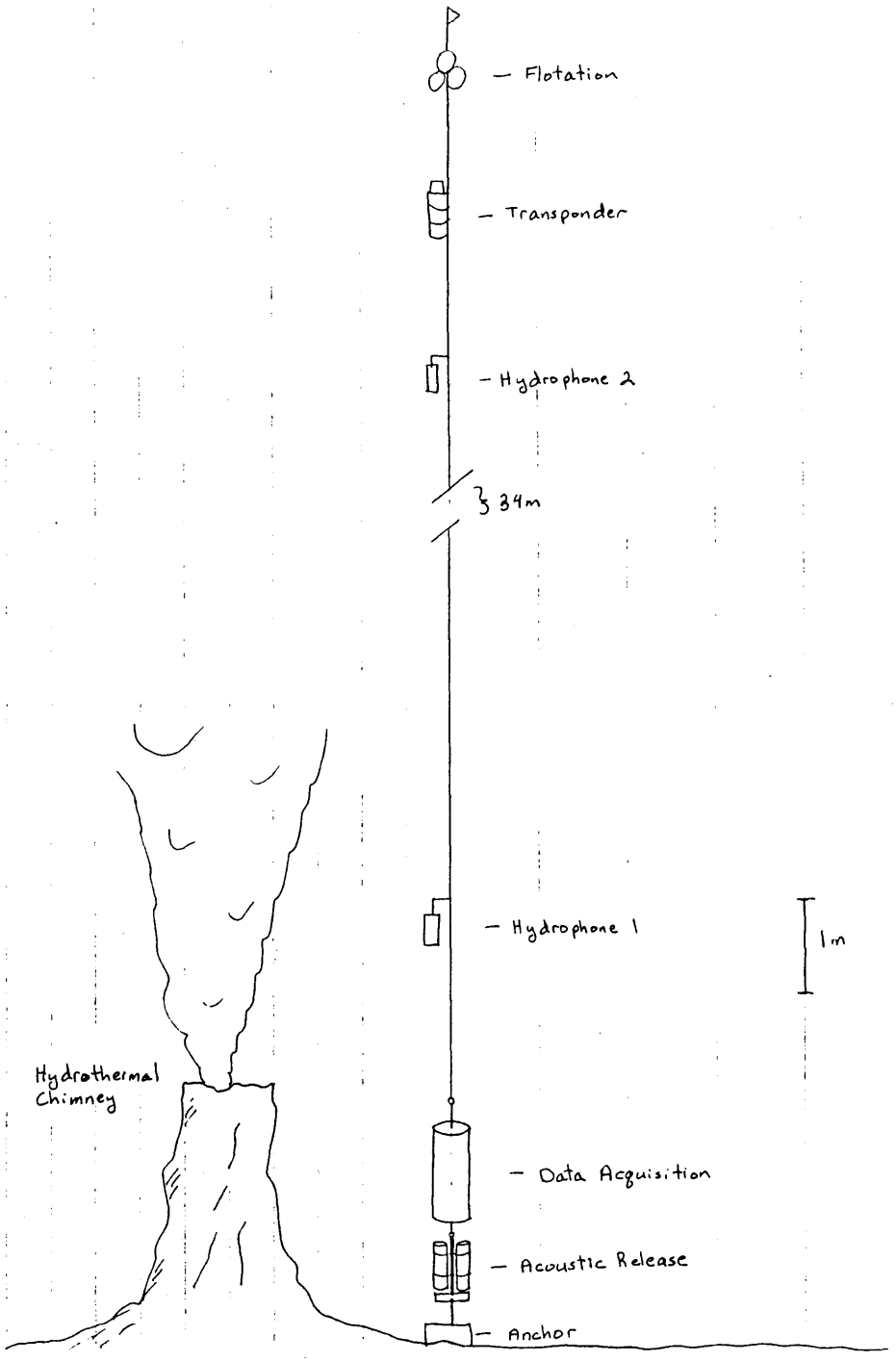

Figure C4
Detail of instrumented cable and deployment scheme. Lower hydrophone was 2-3 m from vent orifice, upper hydrophone was 38-40 m above lower.

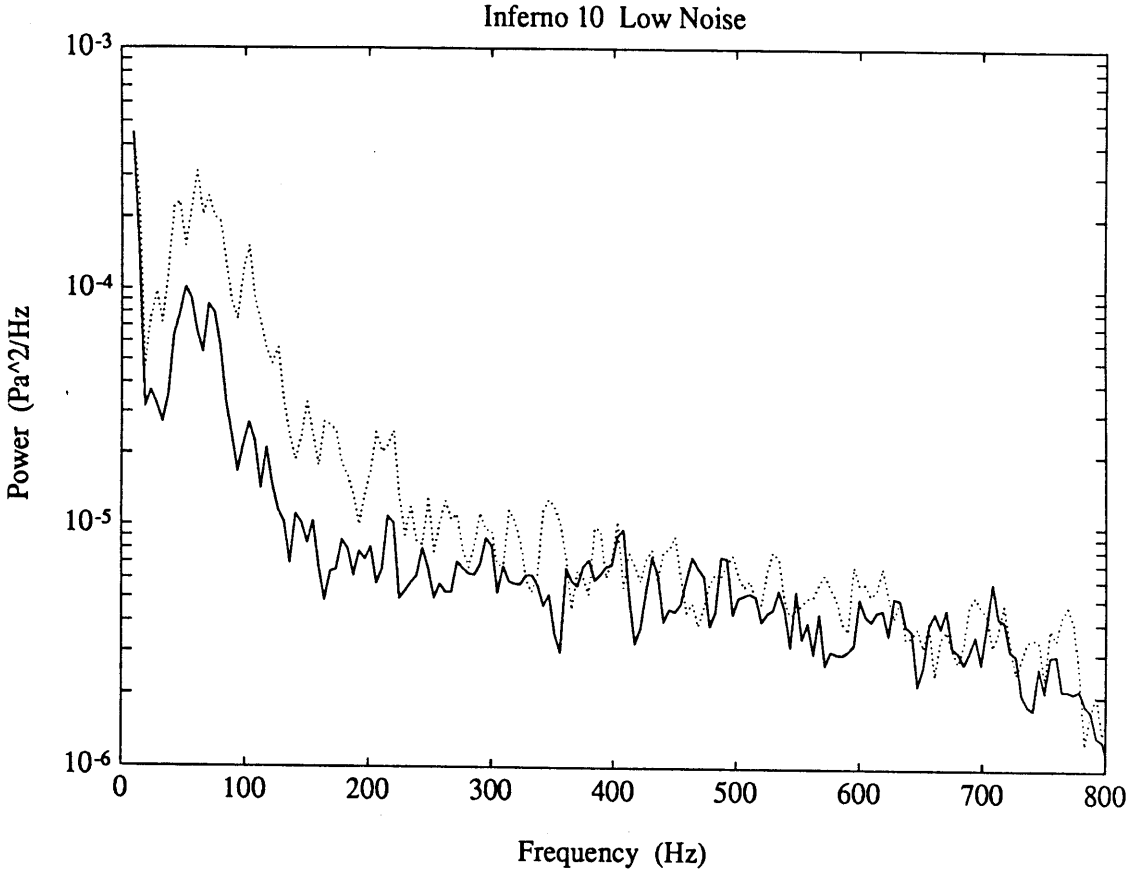

Figure C5

Low noise period power spectral density from Inferno deployment (record 10) of bandwidth 1-800Hz. Solid line is for lower hydrophone (close to the vent) and dotted line is for upper hydrophone. Differences in the bandwidth 30-250 Hz are attributed to effects of the caldera wall on ambient ocean noise. The mathematical spectrum estimation for all spectra shown in this paper is accurate to ± 0.13 x power level. In addition, the spectra shown include the calibration between upper and lower hydrophones, a difference which was less than a factor of 1.6 for the frequencies presented here.

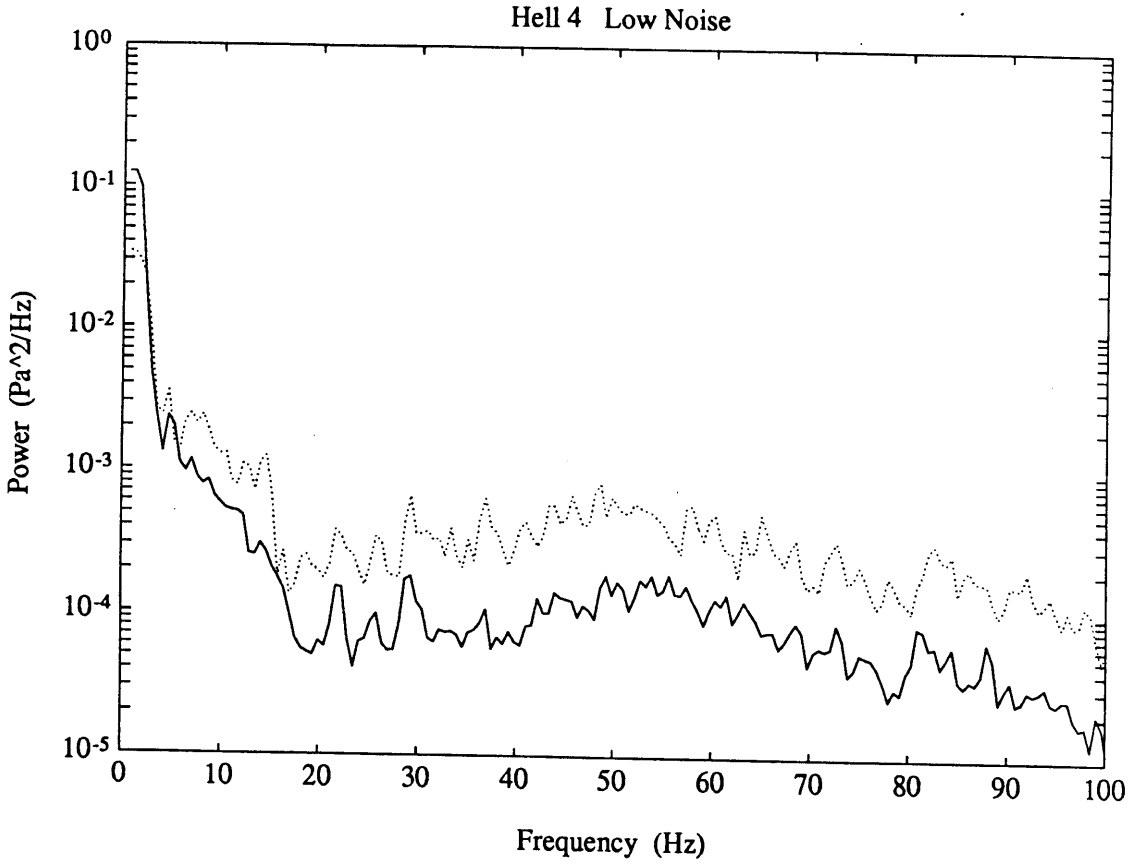

Figure C6

Low noise period power spectral density from Hell deployment (record 4) of bandwidth 1-100Hz. Solid line is for lower hydrophone (close to vent) and dotted line is for upper hydrophone. This details differences in sound level caused by the wall in the bandwidth 0.5-100 Hz.

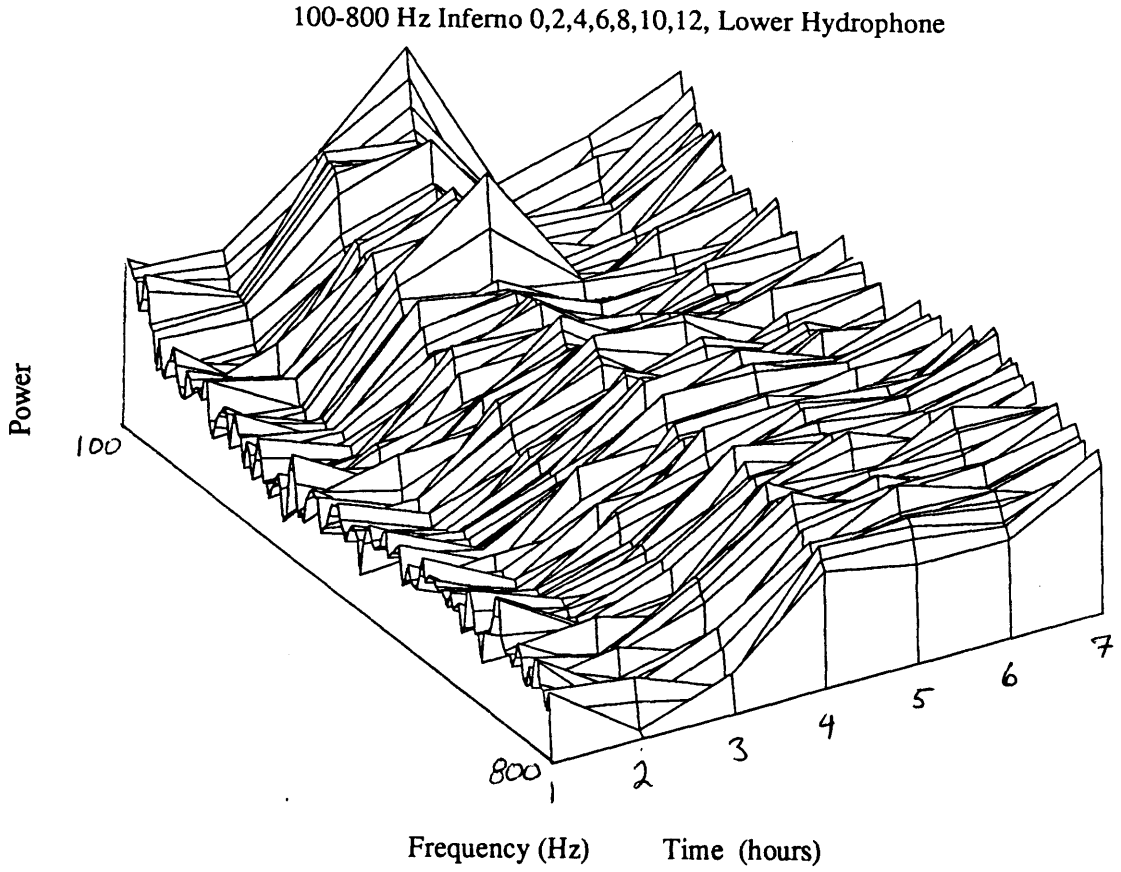

Figure C7
Hourly time history of spectra from Inferno deployment (lower hydrophone) of bandwidth 100-800Hz showing increasing energy toward end of deployment which corresponds to increasing wind velocity.

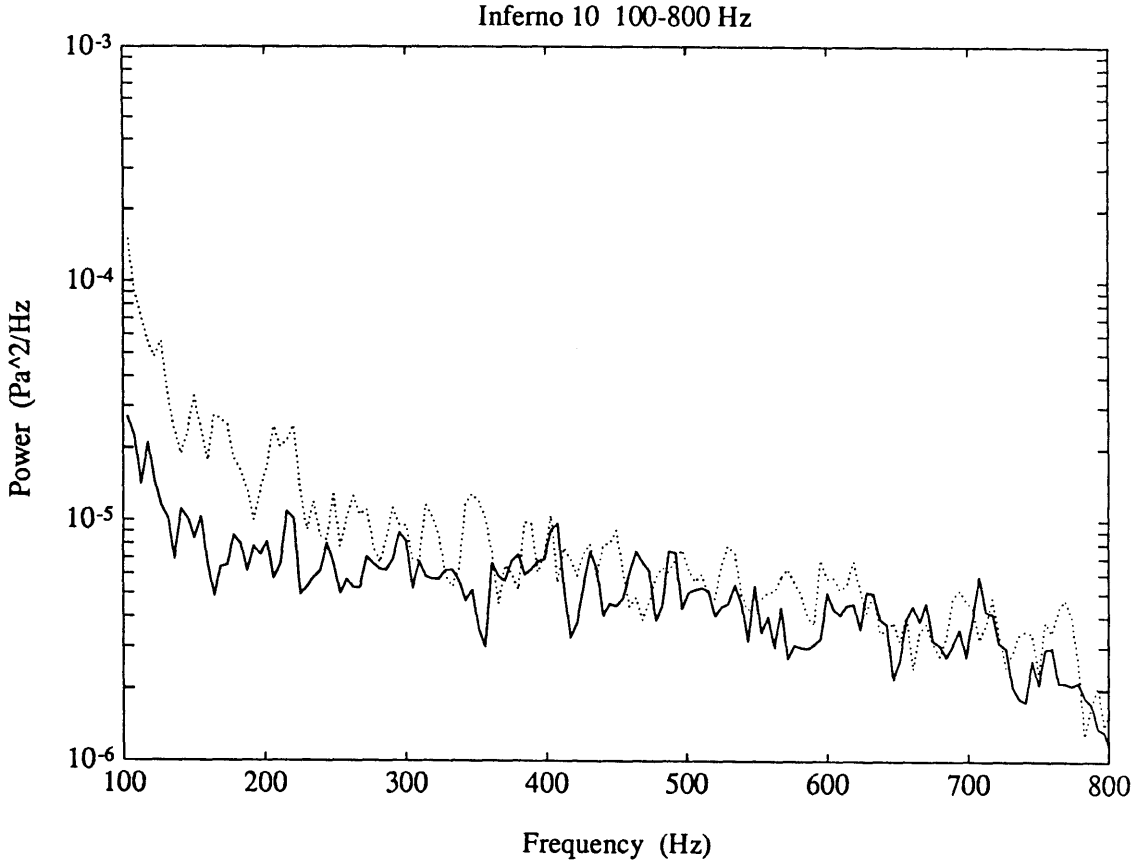

Figure C8

Low noise period power spectral density from Inferno deployment (record 10) showing difference in upper (dotted line) and lower (solid line) hydrophone power levels out to 250 Hz, followed by similar levels. This due to the caldera wall affecting horizontally travelling 20-250 Hz waves and not influencing 250-800 Hz vertically travelling waves.

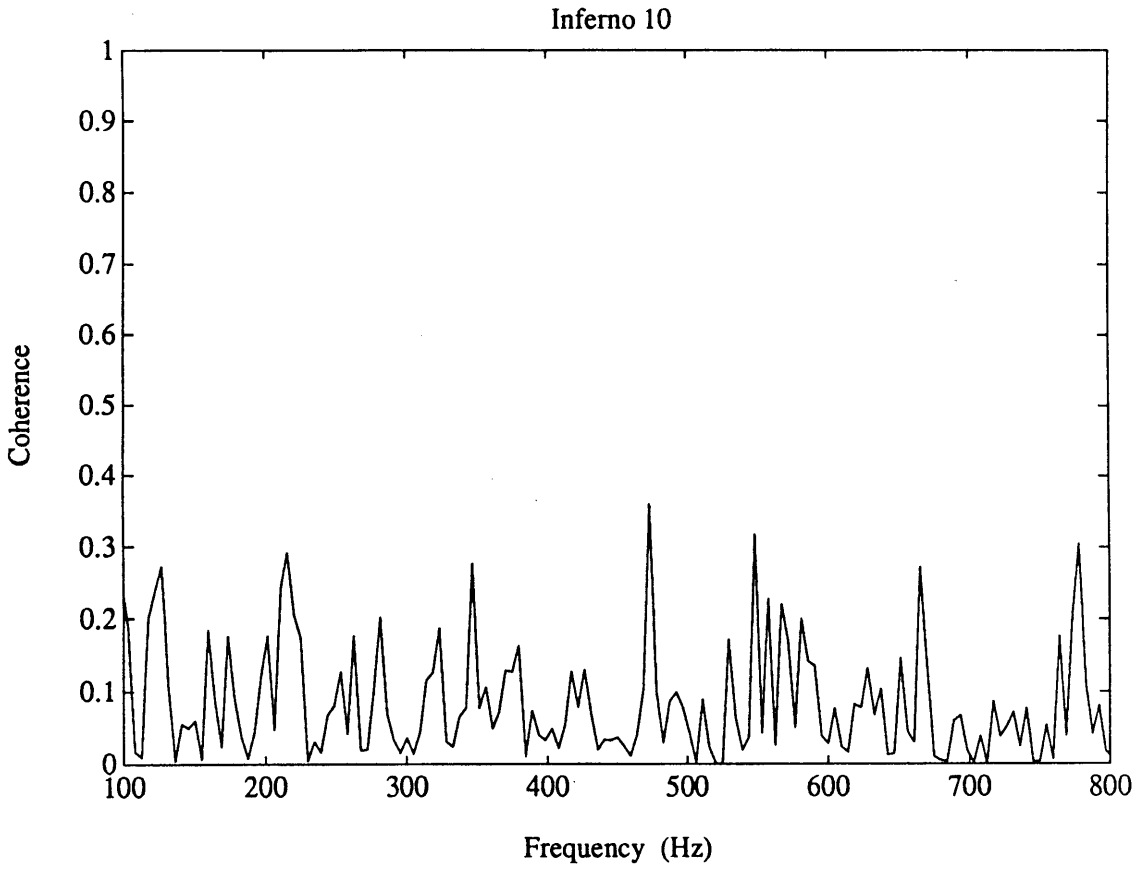

Figure C9
Coherence between upper and lower hydrophones for bandwidth 100-800 Hz for Inferno (record 10).

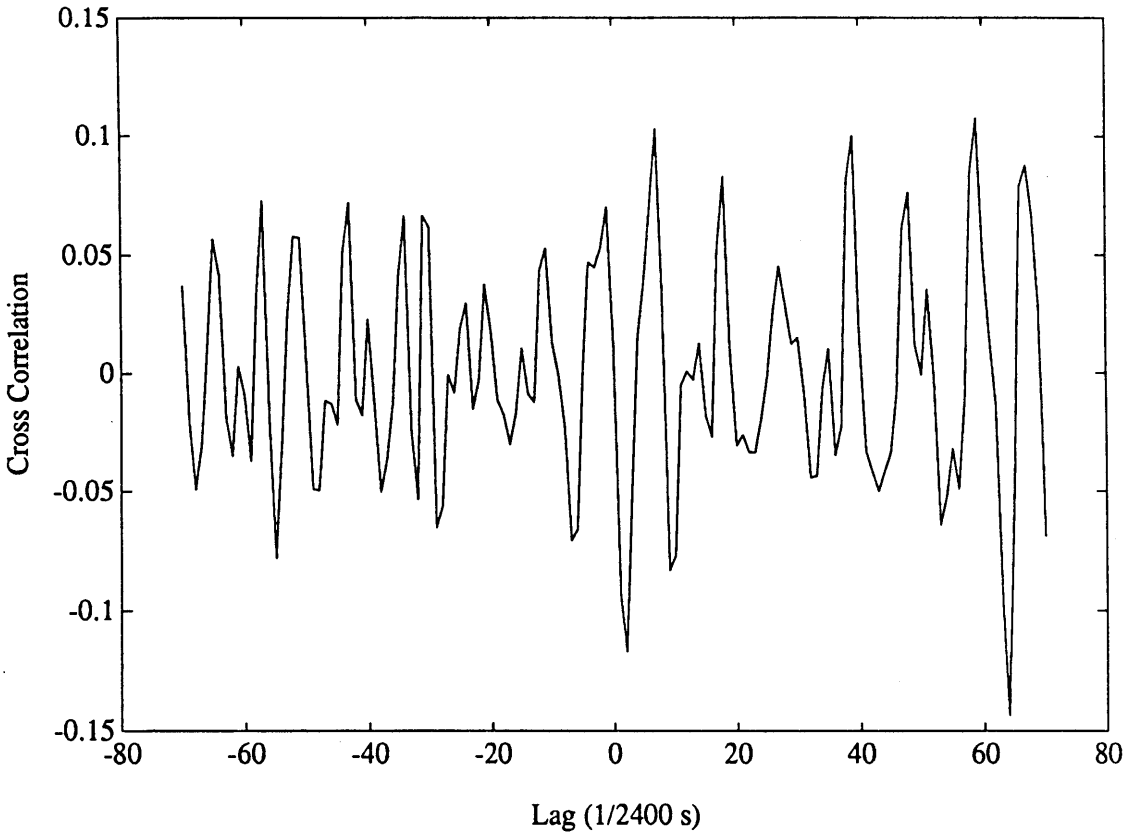

Figure C10

Cross correlation between upper and lower hydrophone for high pass filtered (above 200 Hz) Inferno low noise period (record 10). Greatest magnitude of correlation occurs at a lag of 64 points, which corresponds to the receiver separation, implying that the waves are impinging on the array from end-on (from above).

Inferno 5-100 Hz 1,3,5,7,9,11,13 Lower Hydrophone

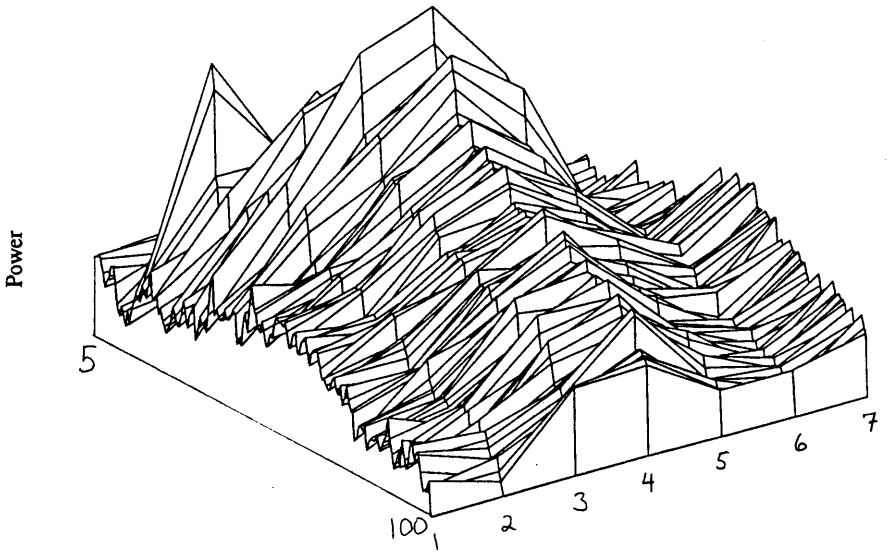

Hell 5-100 Hz 3,4,5,6,7,8,9,10,11,12 Lower Hydrophone

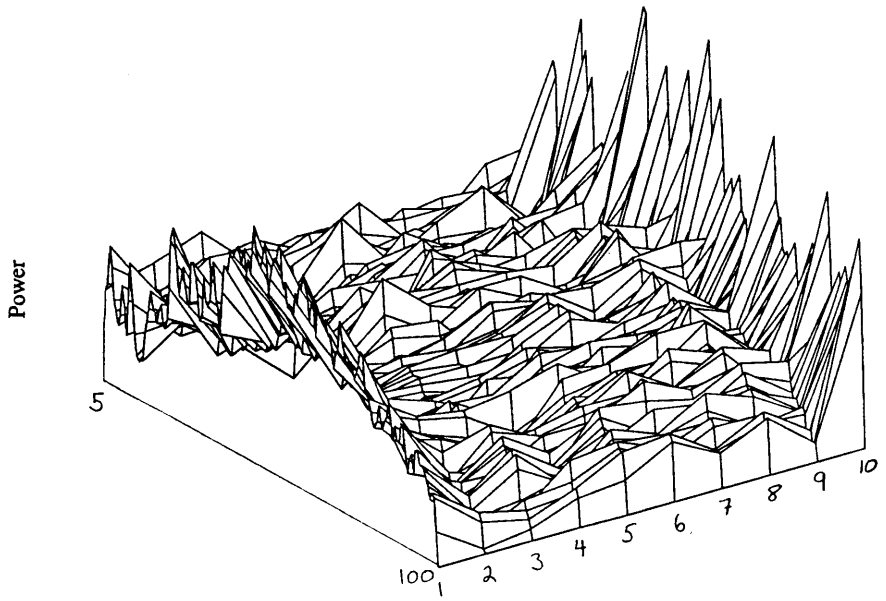

Figure C11

a) Hourly time history of spectra from Inferno deployment for bandwidth 5-100 Hz, showing a general increase during the middle of the deployment, probably in response to an increase in ship activity.
b) Hourly time history of spectra from Hell deployment for bandwidth 5-100 Hz, showing relatively constant levels except for the first and last hour during which time the Atlantis II was in close proximity to the vent site.

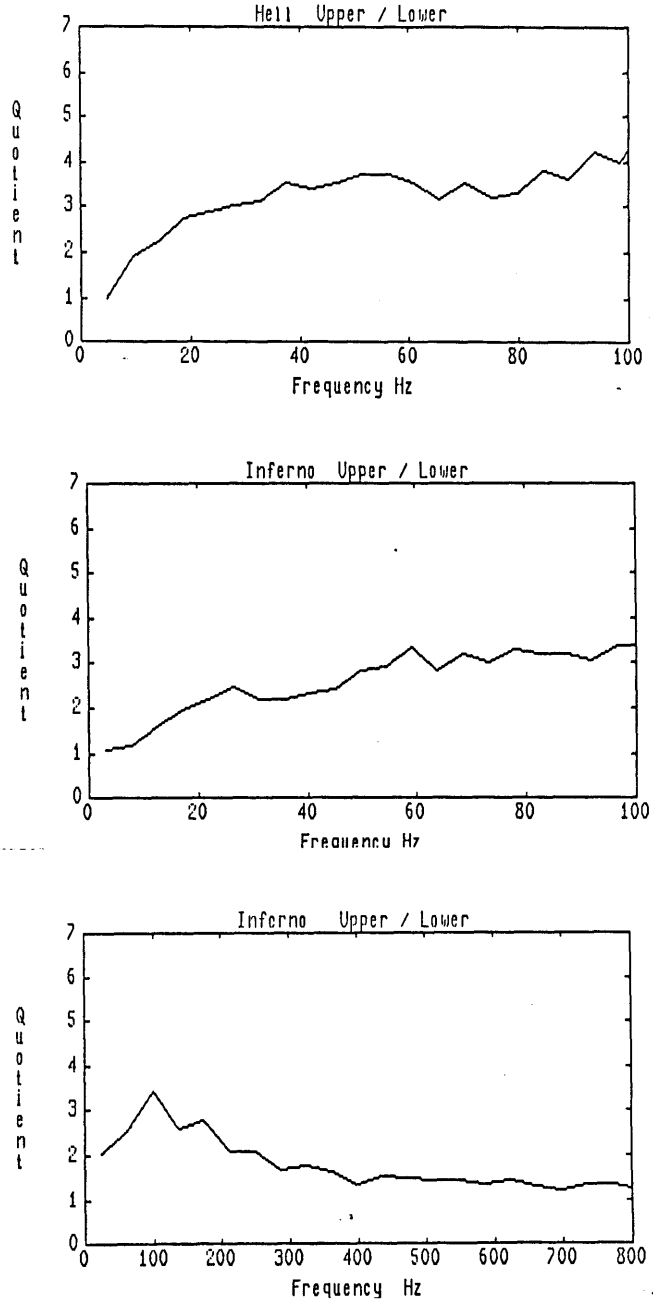

Figure C12

Ratios of upper and lower hydrophone power levels for all records from a) Hell deployment, b) Inferno deployment: 1-10 Hz and, c) Inferno deployment: 1:800 Hz. Notice that the quotient decreases with both decreasing and increasing frequency, centered around typical distant shipping frequencies of 30-200 Hz. This difference is due to effects of the caldera wall.

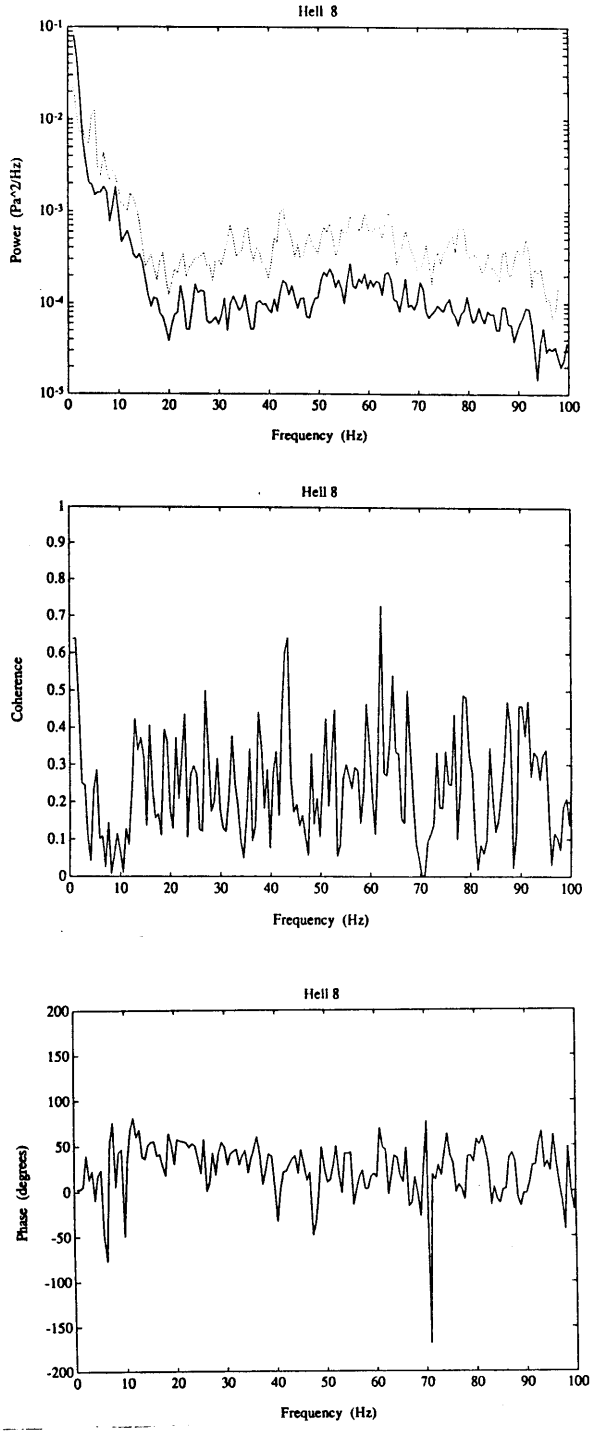

Figure C13

a) Power spectral density for low noise period of Hell deployment (record 8). Solid line is lower hydrophone, dotted line is upper hydrophone.

b) Coherence between upper and lower hydrophones for low noise period of Hell deployment (record 8). Coherence, although low, is significant (compare to figure 14).

c) Phase for same period showing relatively constant and zero phase produced by waves impinging on the array broadside because they were travelling horizontally.

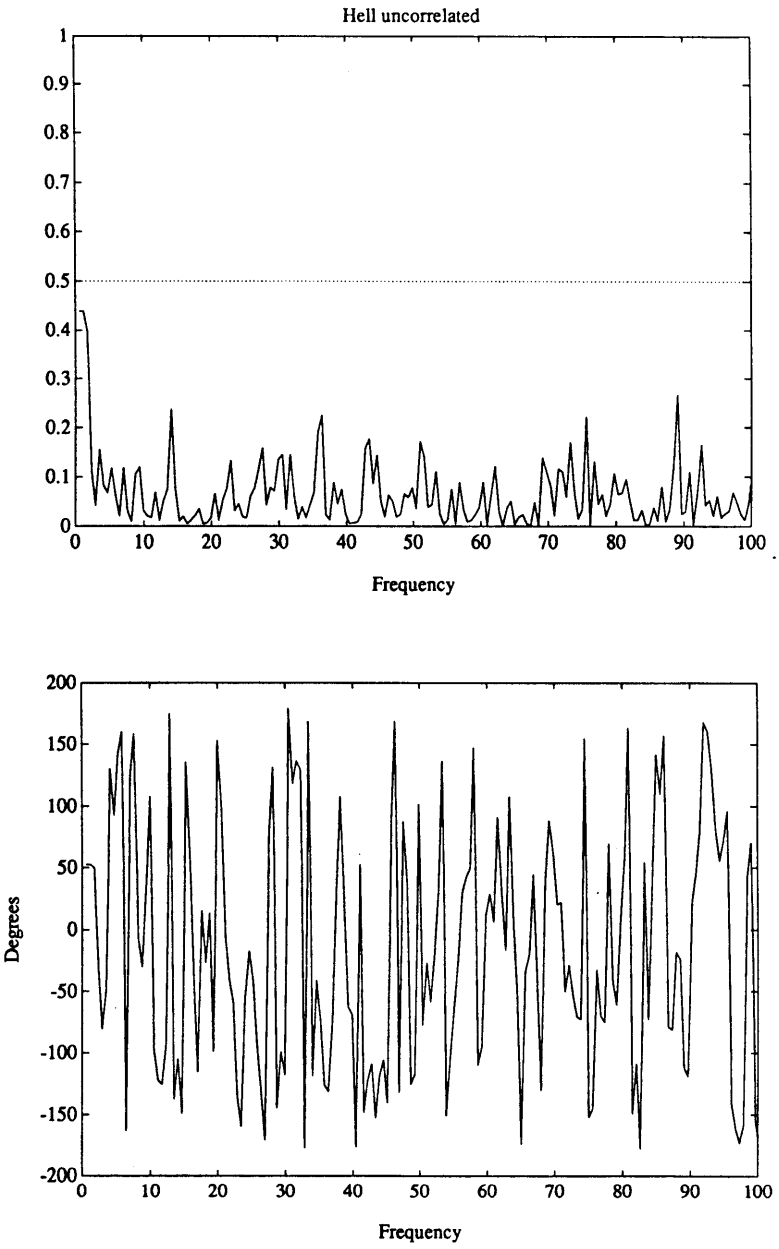

Figure C14
a) Coherence calculated between records taken from upper and lower hydrophones at two different times (totally uncorrelated). Note the low level of this random coherence.
b) Phase for same records. Note the completely random phase (especially as compared to figure 13b).

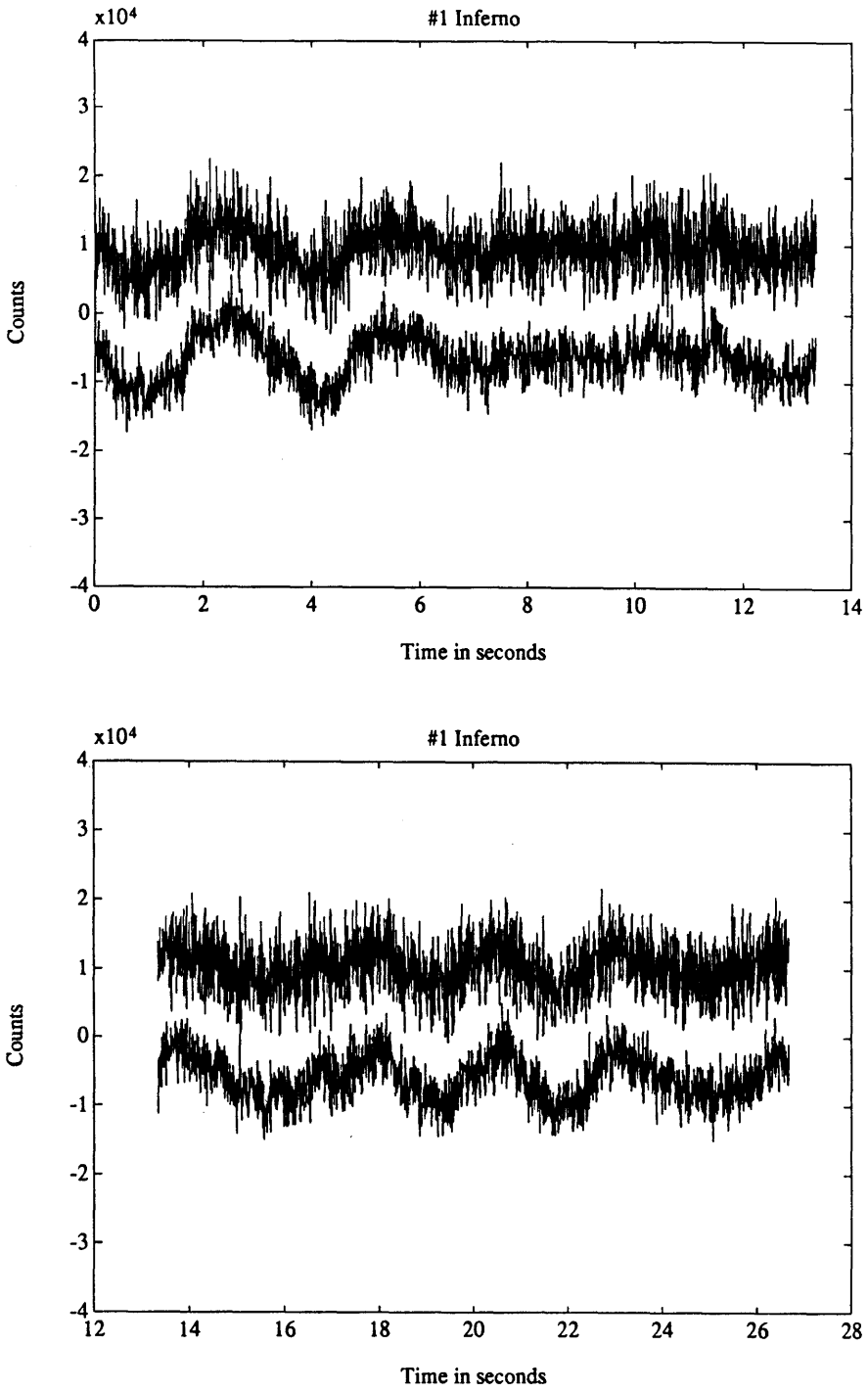

Figure C15
Time series pressure level from Inferno deployment (record 1), upper trace is from upper hydrophone and vice versa. Note similarity in phase and pressure level for low frequency oscillations on both hydrophones due to microseisms.

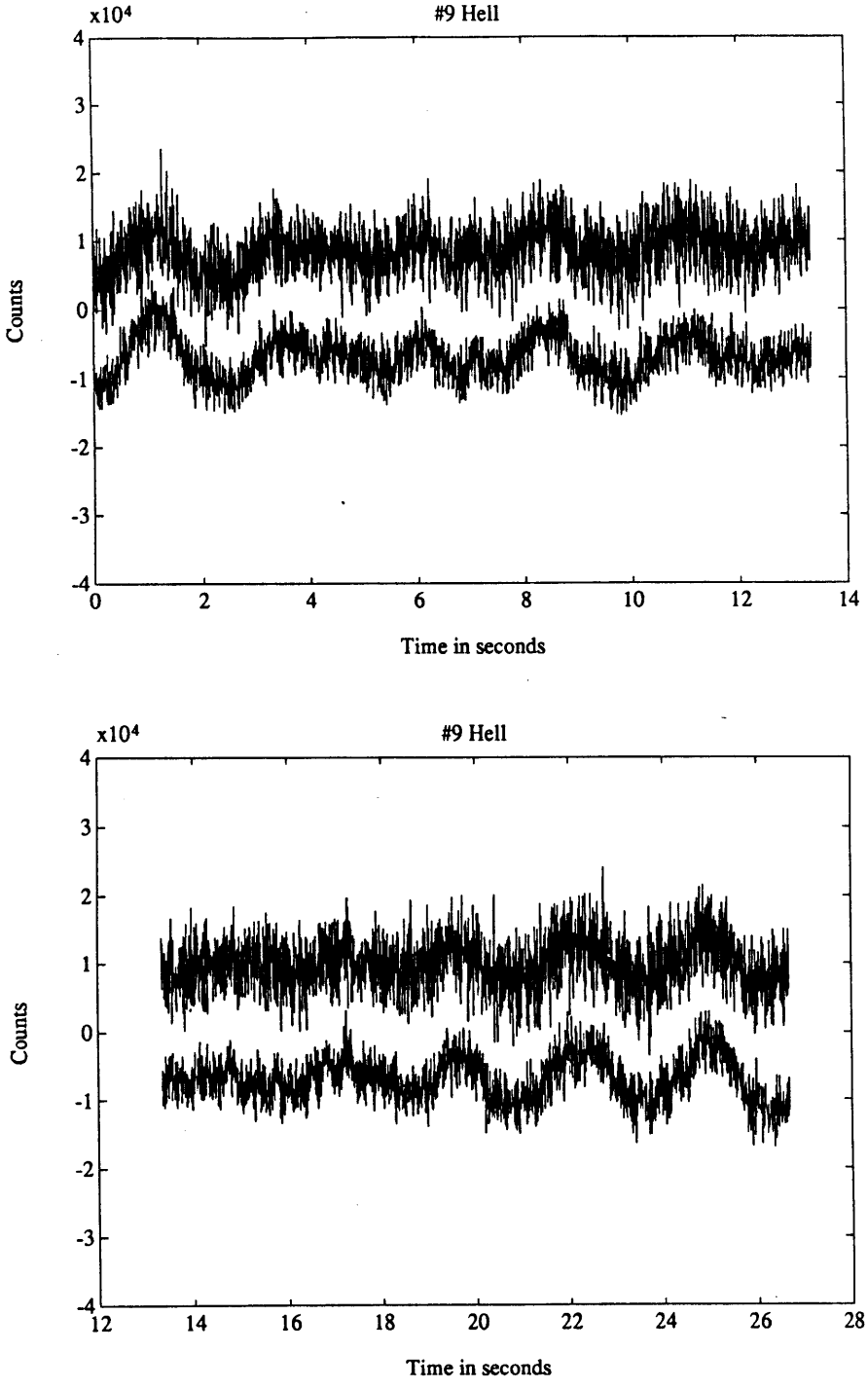

Figure C16
Time series pressure level from Hell deployment (record 9), upper trace is from upper hydrophone and vice versa. Note similarity in phase and pressure level for low frequency oscillations on both hydrophones due to microseisms.

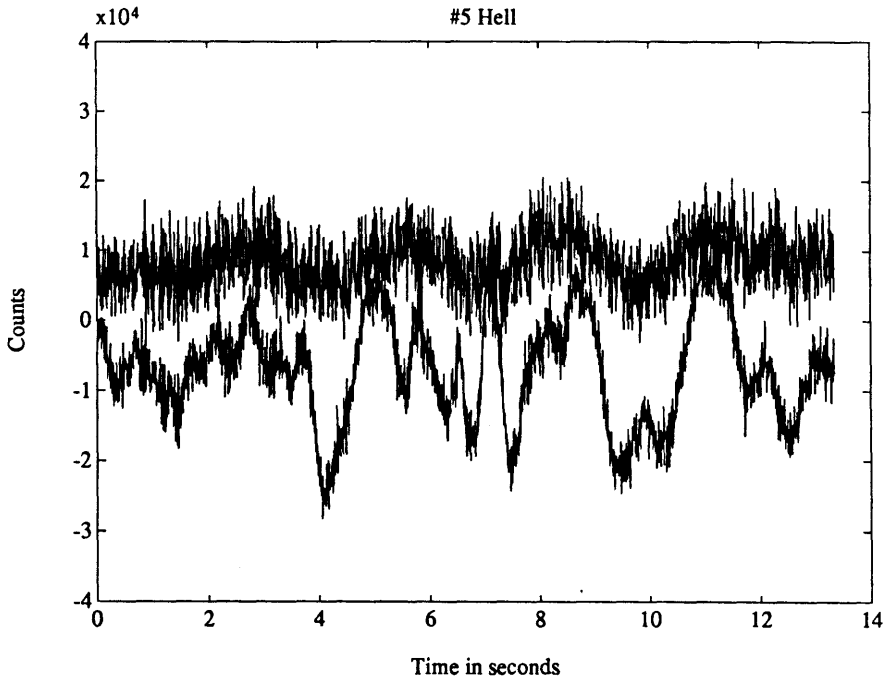

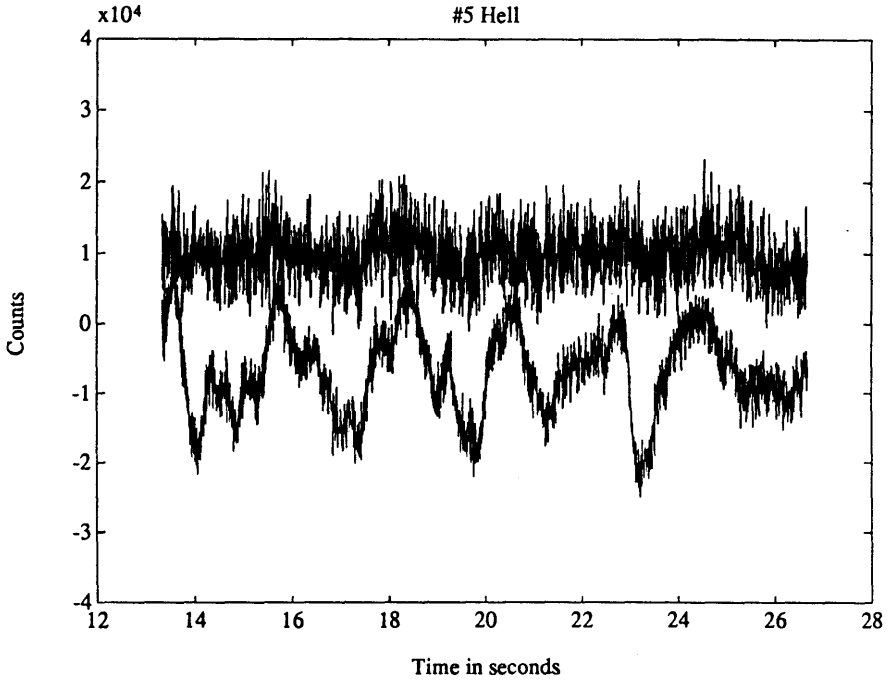

Figure C17
Time series pressure level from Hell deployment (record 5), upper trace is from upper hydrophone and vice versa. Note large amplitude erratic oscillations on lower hydrophone not seen on upper hydrophone. Upper hydrophone shows typical microseism oscillations while lower records passage of interface waves which poorly penetrate water column.

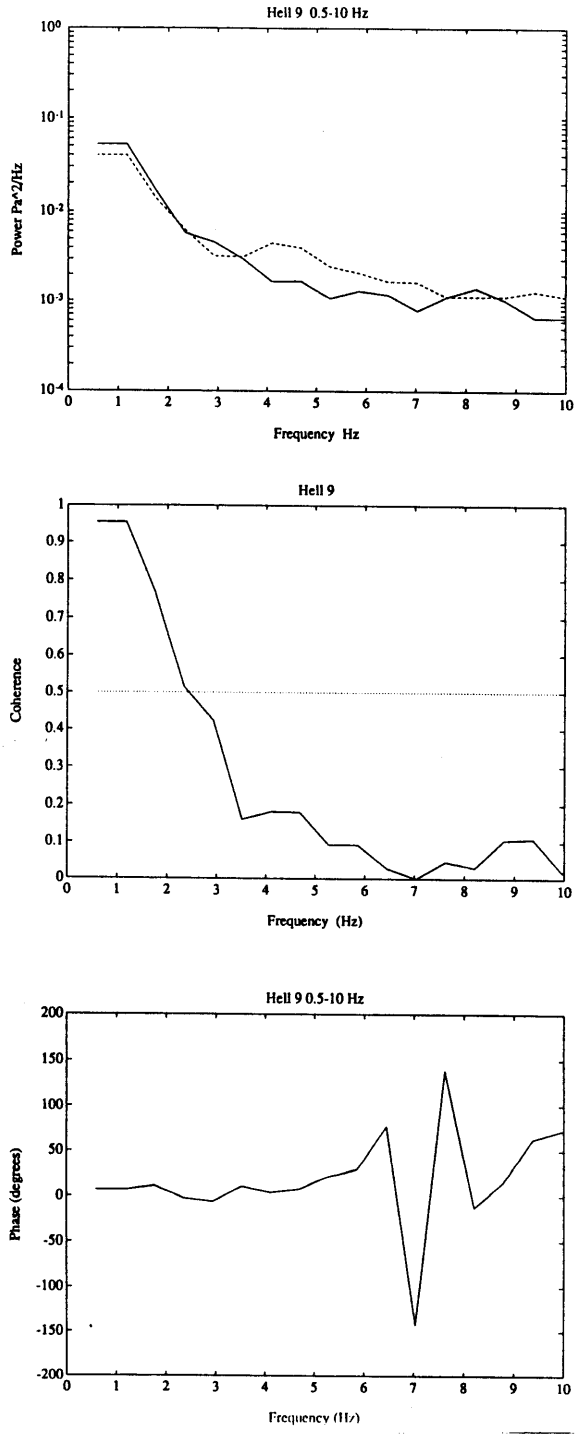

Figure C18

a) Upper part shows power levels from Hell (record 9) in 0.5-10 Hz bandwidth. Note similarity in power between upper hydrophone (dotted line) and lower hydrophone (solid line) due to microseism energy.
b) Lower part shows high coherence between the two hydrophones from 0.5-3 Hz characteristic of microseisms.
c) This shows the constant and zero phase between upper and lower hydrophone.

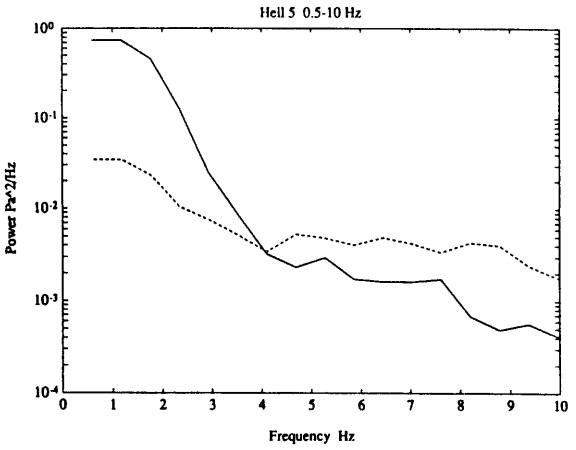

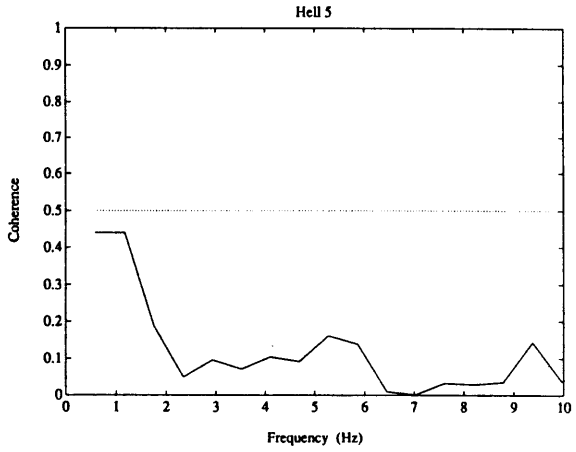

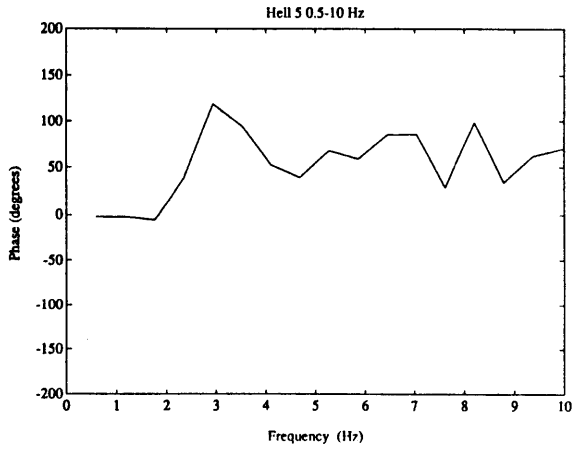

Figure C19

a) Upper part shows high power level on lower hydrophone (solid line) and lower power on upper hydrophone (dotted line) for Hell deployment (record 5).

a) Low coherence between the two hydrophones is seen since pressure levels at lower hydrophone are due to interface waves not seen on upper hydrophone.

b) This shows non-constant and non-zero phase as is expected between the upper and lower hydrophones since they are receiving different signals.

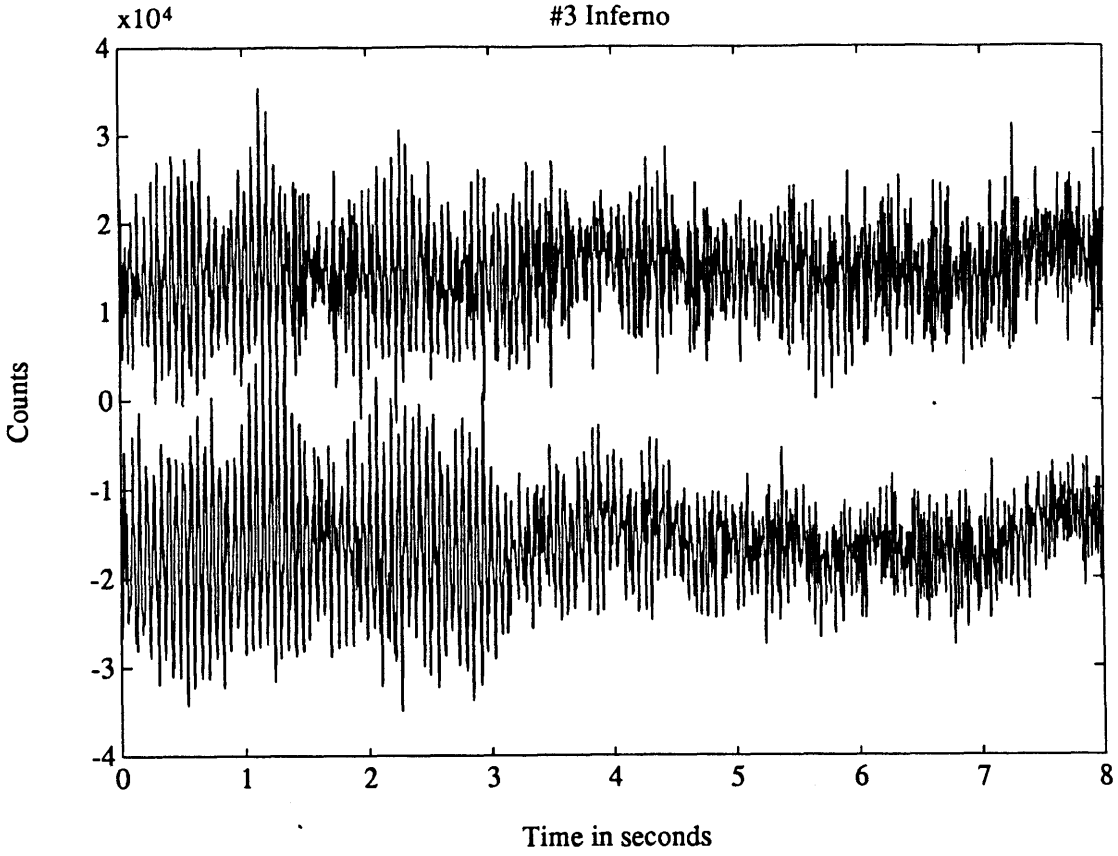

Figure C20

Upper trace is pressure level from upper hydrophone, lower trace is pressure level at lower hydrophone. The beginning of this period from Inferno (record 3) a monochromatic, 19 Hz signal is detected, which we attribute to a whale.

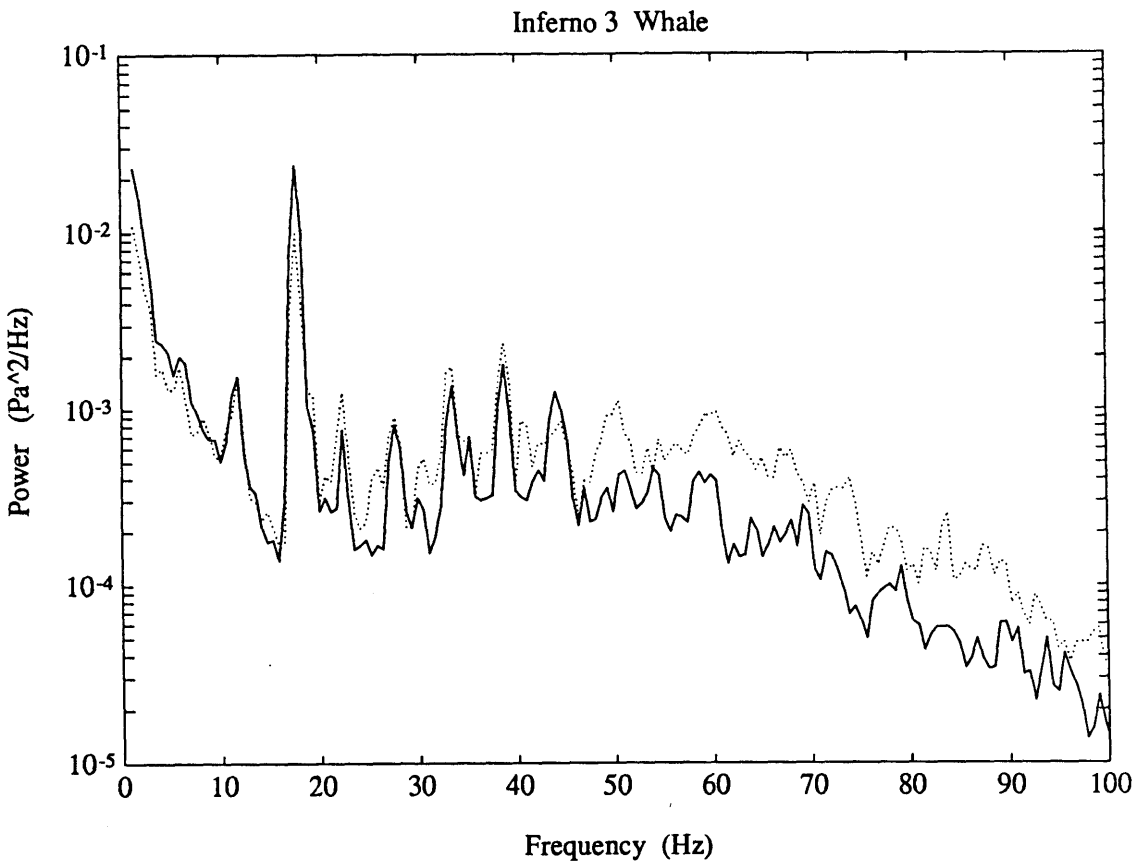

Figure C21

Power spectral density for Inferno (record 3), solid line is from lower hydrophone, dotted line is from upper hydrophone, showing peak at 19 Hz attributed to a whale. The amplitude is higher on lower hydrophone due to reflections off the hard bottom causing constructive interference on the lower phone and destructive on the upper.

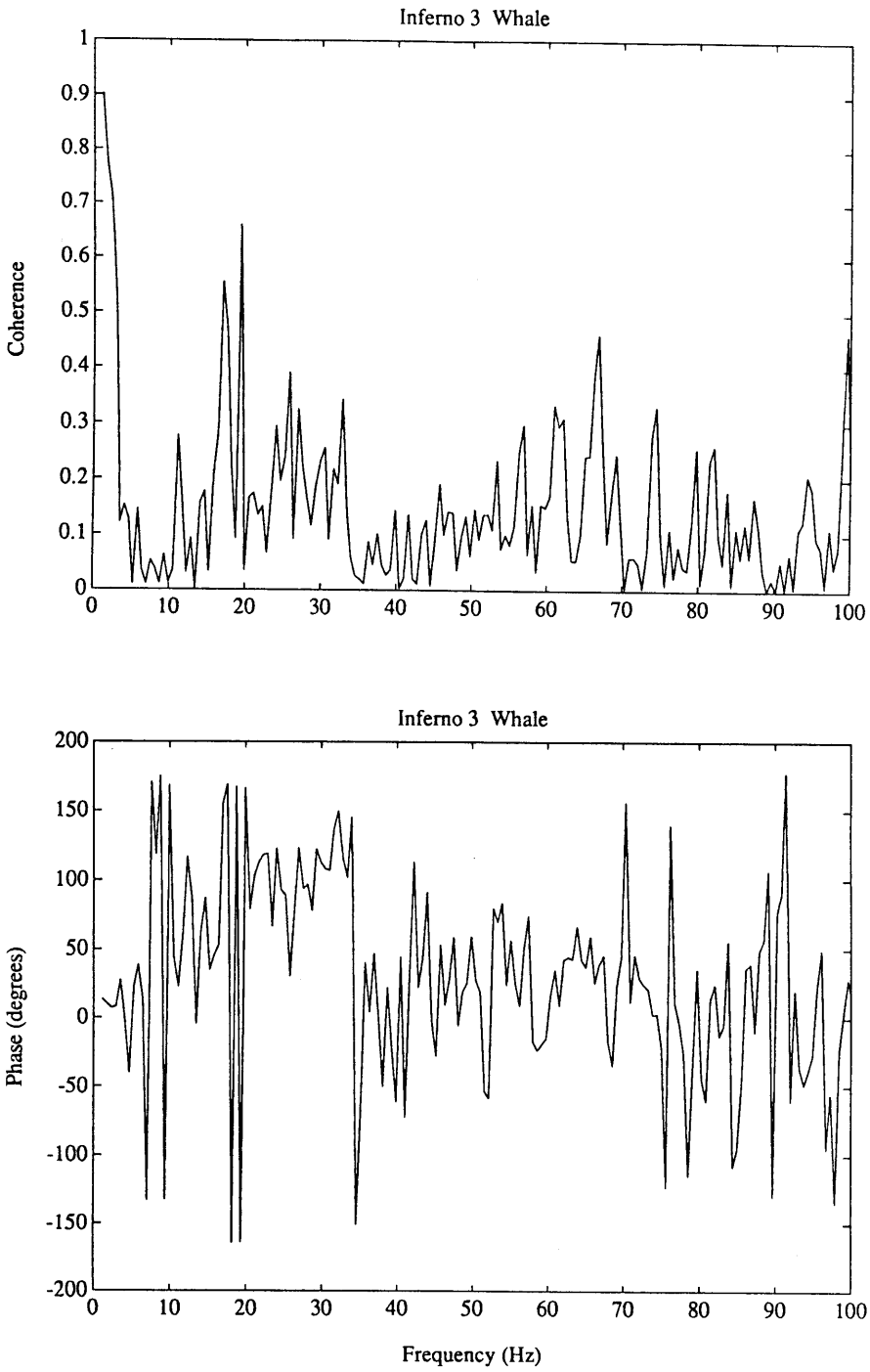

Figure C22

a) Coherence between upper hydrophone and lower for Inferno (record 3) which detected 19 Hz signal.

b) Phase between upper and lower hydrophone (Inferno record 3) showing 180^{o} phase shift near 20 Hz. This is due to the fact that the receiver separation is approximately twice the wavelength at this frequency, and hence waves coming into the array end-on will see a 180^{o} phase delay between the two receivers.

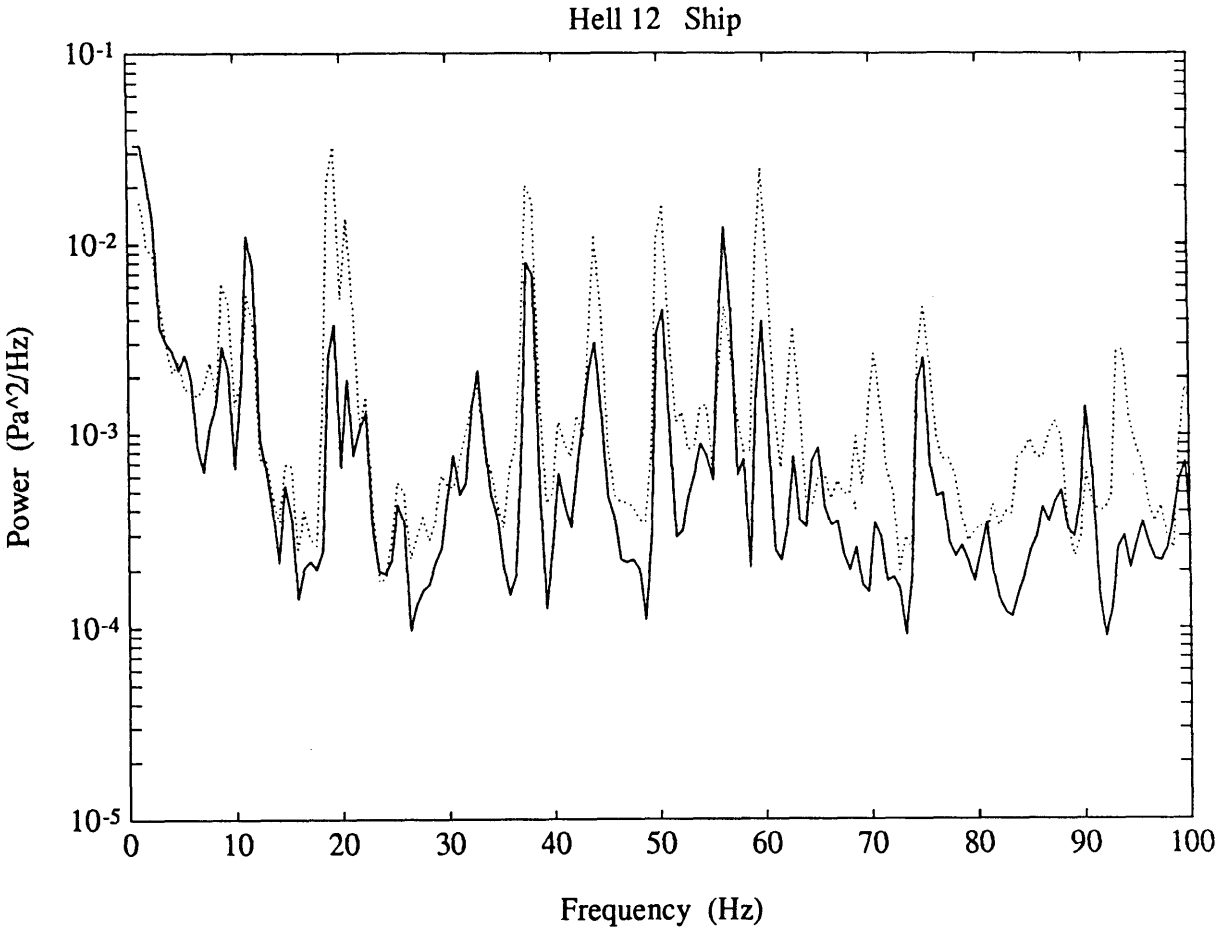

Figure C23

Power spectral density from Hell deployment (record 12) when the Atlantis II is overhead and slightly to the north east of the vent site. Peaks and harmonics are typical of near ship noise.

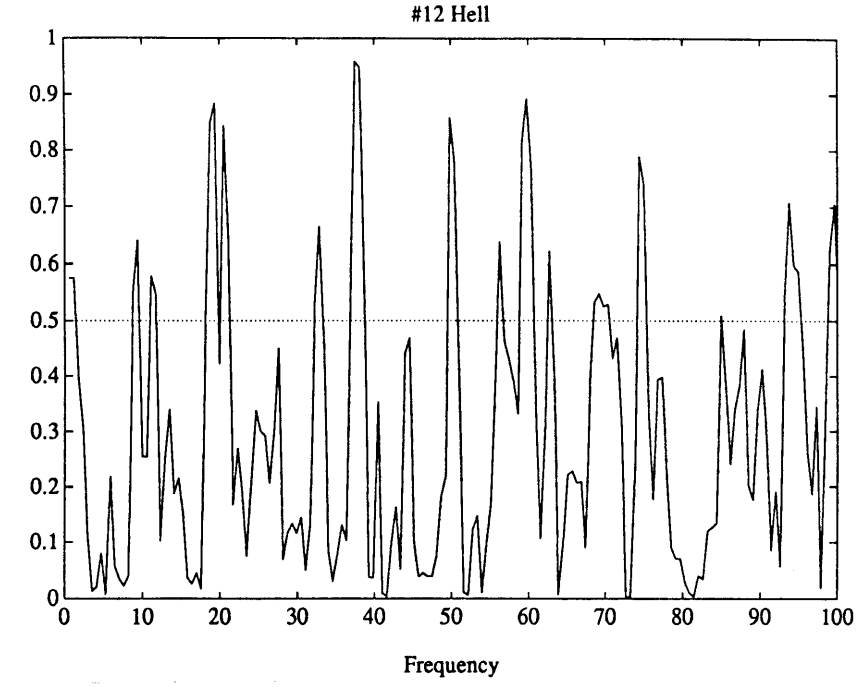

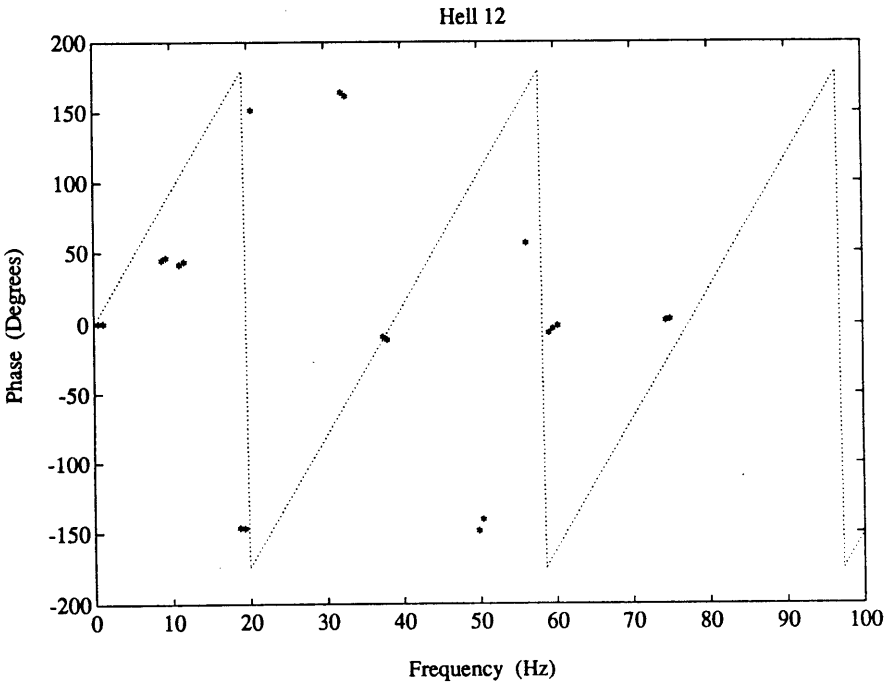

Figure C24

a) Coherence between two receivers for Hell (12) when ship is near. Notice extremely high coherence at ship's frequencies.

b) Transfer phase between the two receivers for this record at high power and coherence frequencies. Linear trend shown by dotted line would be produced by waves arriving from nearly vertical. Phase from ship noise falls mainly on this line, or $\pm$ 180^{o} from it due to reflections.

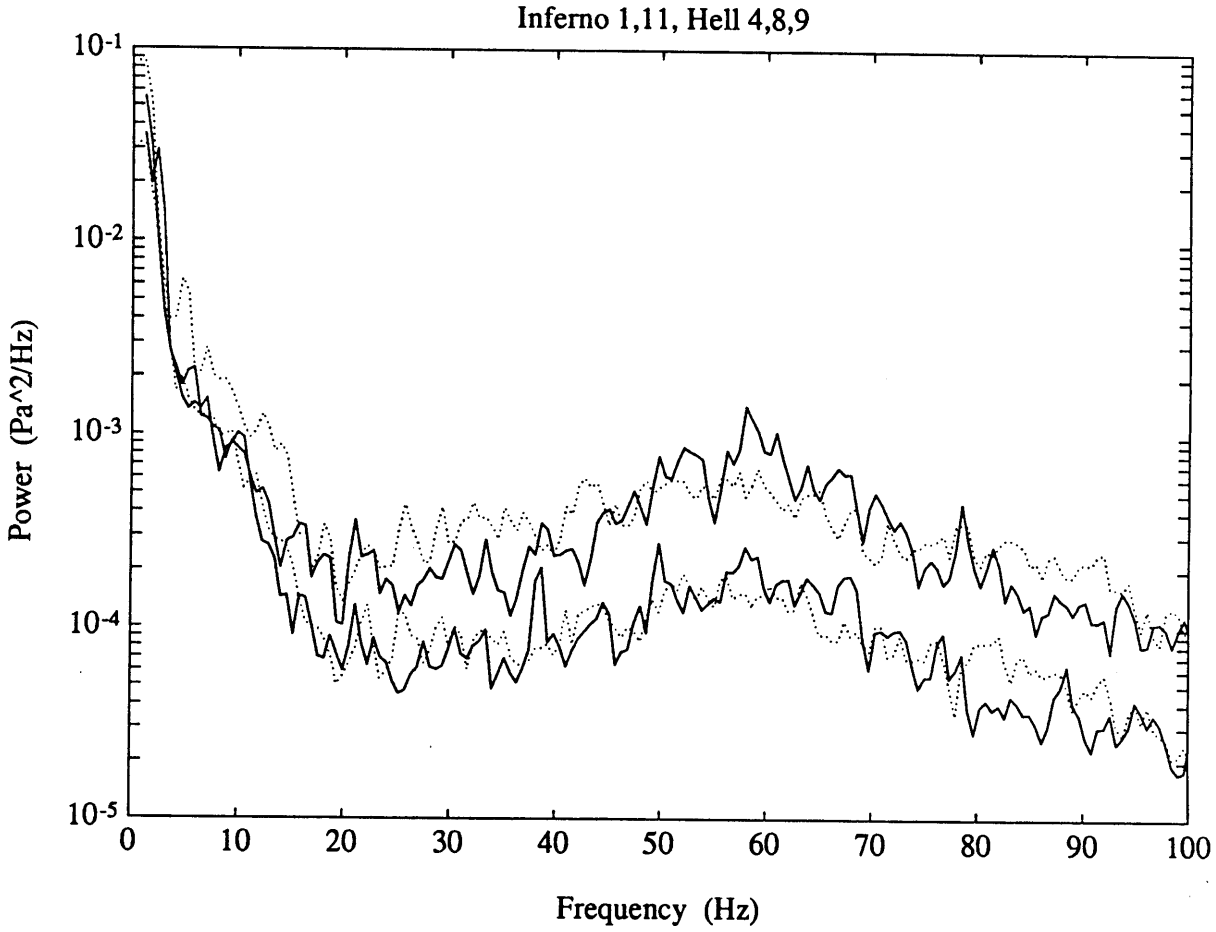

Figure C25

Low noise records used for calculation of signal detection index, average of Inferno records 1 and 11, (upper solid line from upper hydrophone, lower solid line from lower hydrophone) and Hell records 4, 8, and 9 (upper dotted line from upper hydrophone, lower dotted line from lower hydrophone). Note small peak in lower Inferno power spectral density near 38 Hz; this is attributed to jet noise from Inferno vent.

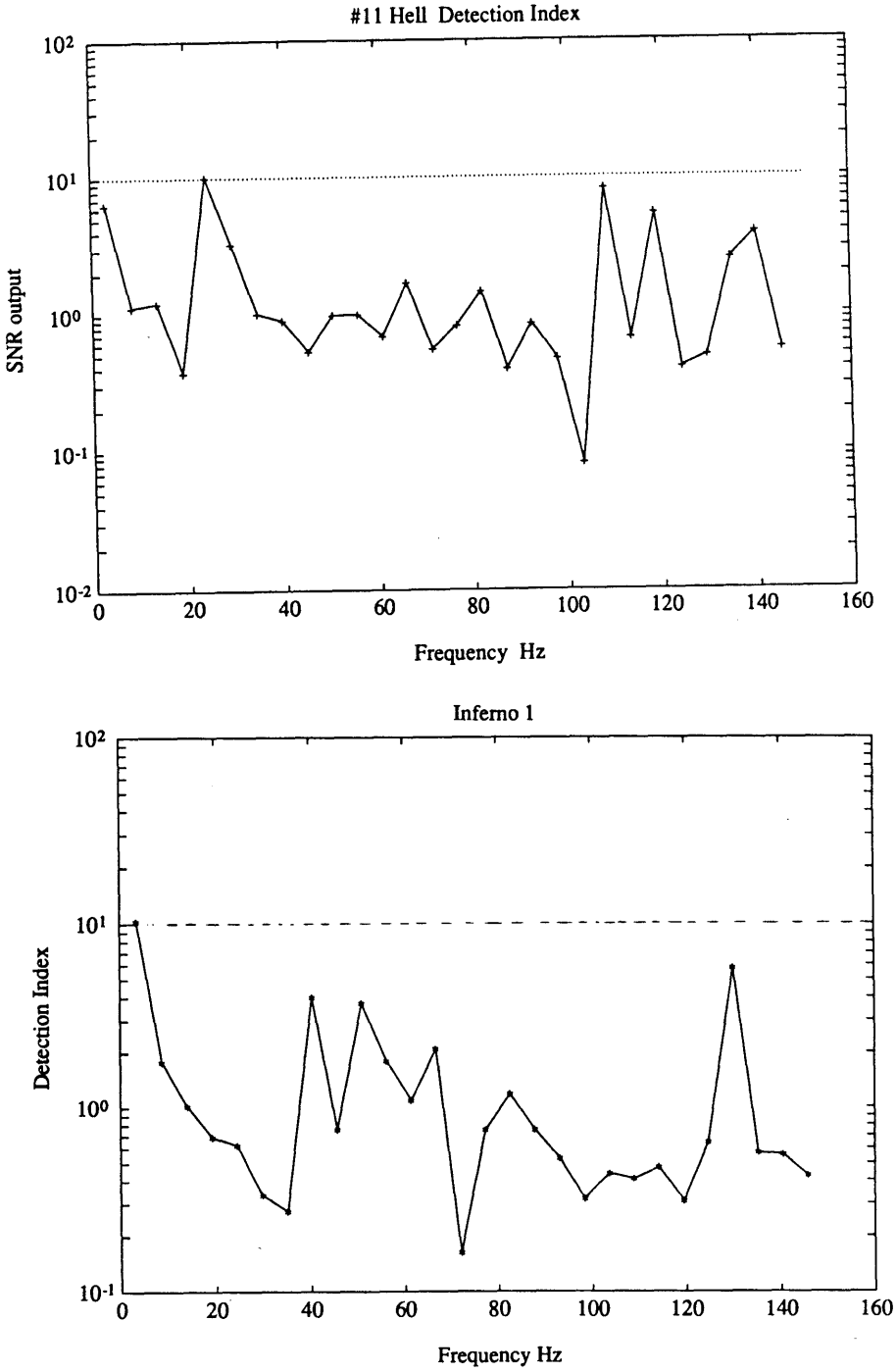

Figure C26

a) Signal detection index for low noise Hell deployment (record 11), note that nowhere is the SNR greater than 10, the value which corresponds to a 90% confidence in signal detection with a 5% false alarm rate.

b) Detection index for low noise Inferno deployment (record 1), note that nowhere is the SNR greater than 10, the value which corresponds to a 90% confidence in signal detection with a 5% false alarm rate.

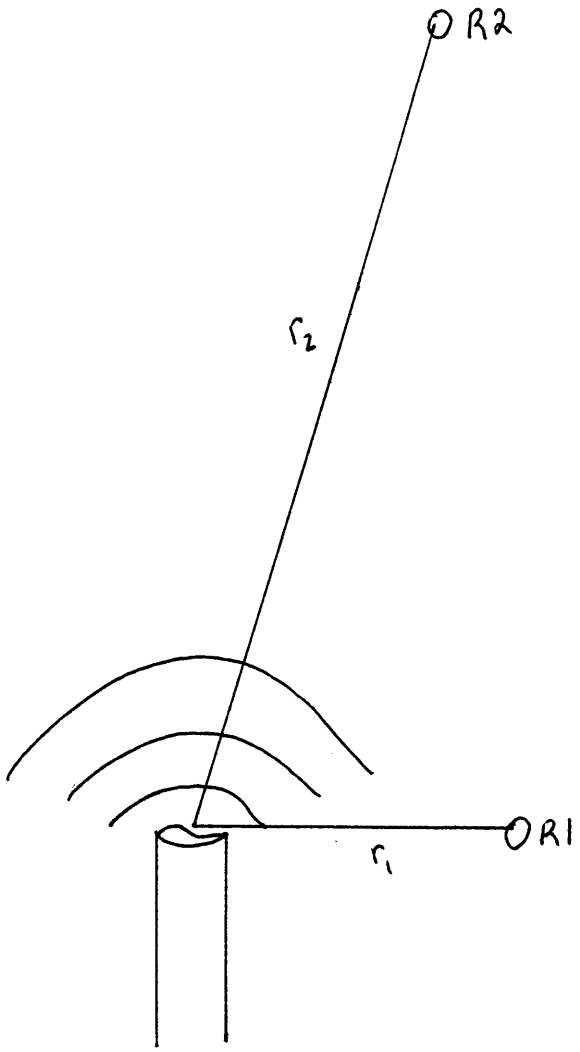

Figure C27
Diagram showing geometry for wave paths in detection index calculation.

OCEAN NOISE MEASUREMENTS NEAR THE TAG HYDROTHERMAL AREA, MID-ATLANTIC RIDGE, LATITUDE 26°N

ABSTRACT

In light of the potential utility of a remote, passive acoustic technique for monitoring variations in hydrothermal vent fluxes, we have examined ambient noise in the frequency band 1-30 Hz at a range of 0.75-14 km from the TAG (Trans-Atlantic Geotraverse) hydrothermal area on the Mid-Atlantic Ridge near 26°N, the site of an extremely active high temperature hydrothermal vent field (Rona, 1986). The ambient noise field exhibits great temporal and spatial variations attributed in part to typical ocean noise sources such as distant shipping and microseisms. Power spectral levels as measured at each of six ocean bottom hydrophones (OBH) were used to estimate the location of point sources of sound in the area, if any.

The hydrothermal vent did not produce enough sound to be located as a point source using data from the OBH array. The only consistently identifiable point source found with the data set was generating sound in a 0.8-3.5 Hz bandwidth and located outside the median valley. It appears to be harmonic tremor associated with the tip of a ridge on the western side of the spreading axis and may be volcanic in origin.

INTRODUCTION

High temperature hydrothermal fluid travels through fractured oceanic crust in narrow upflow zones to exit at the seafloor in flows ranging from high velocity buoyant jets emerging from tall chimneys to diffuse seepage from local cracks and fissures. This diversity of flow makes detailed characterization of vent fields over space and time extremely difficult. Without this information, precision modelling of hydrothermal systems from chemical, geological, fluid dynamical and biological standpoints is nearly impossible. The lack of long-term flow information motivated a study of the use of passive acoustics for monitoring flow characteristics (Little and Stolzenbach, in prep). The sound field produced by a turbulent jet is theoretically heavily dependent on fluid velocity and exit geometry (Lighthill, 1952). Such a sound field could be used to monitor changes in these jet parameters over time. A technique to monitor and understand changes in sound output as they relate to fluid flow would give researchers a much needed tool for studying long-term temporal variations in hydrothermal activity. The feasibility of this method will depend on an ability to detect and identify hydrothermally generated sound in a background of ambient ocean noise. Recently published papers have reported anomalous sound fields, in the bandwidth 1-30 Hz, associated with hydrothermal centers, one at 21^{o}N on the East Pacific Rise (EPR) (Reidesel et al., 1982) and one on the Juan de Fuca Ridge (Bibee and Jacobson, 1986). The mechanism responsible for sound generation in these two cases has not been identified. In light of these results and the potential utility of a

passive acoustic monitoring technique for hydrothermal vents, we have examined ambient noise collected near the TAG (Trans-Atlantic Geotraverse) hydrothermal area on the Mid-Atlantic Ridge near 26°N, the site of an extremely active high temperature hydrothermal vent field (Rona, 1986). A microearthquake study of the TAG area (Kong et al, 1986), conducted prior to the discovery of the high temperature vent field, conveniently provided a data set with which to examine the ambient sound field in the frequency band 1-30 Hz at a range of 0.75 to 14 km from the vent site. The purpose of examining this data set was first, to determine whether the hydrothermal vent could be identified as a source of sound, and second, whether any other point sources of sound could be located within the study area.

AMBIENT OCEAN NOISE

The level of ambient ocean noise in a given frequency band determines the degree of difficulty associated with identifying and detecting an unknown sound source. Noise in the ocean is typically non-stationary both in time and space (Burdick, 1984; Hodgkiss and Anderson, 1980). The noise field varies considerably over time due to the rich variety of sources (Akal et al., 1986) and measurements made hours apart can show striking dissimilarity. Spatially, the noise field power levels can be orders of magnitude different depending on topography, water sound velocity structure, and proximity of receiver to the seafloor or sea surface (Urick, 1986; Burdick, 1984; Wentz, 1962). On average, typical, ubiquitous, deep-water ambient ocean noise spectra in the frequency range covered by this experiment are caused by two different source mechanisms.

The lowest frequency band, 0.01-5 Hz, figure D1, exhibits high power levels and is dominated by microseisms: low frequency pressure disturbances caused by non-linear interactions of ocean surface waves (Webb, 1984), and teleseismic events. Temporal variations are as rapid as a few minutes for interface waves travelling near the sea floor from teleseismic and local sources, and as long as a few hours for variations in sea state and swell.

Power in the higher frequency band from 5-100 Hz, produced by distant shipping, is dependent on sound that has travelled tens to hundreds of kilometers and is strongly influenced by wave guide propagation effects such as sound channelling due to a velocity minimum in the water column. Travelling great distances through the ocean broadens the spectral peak and removes waves travelling outside a few degrees of horizontal. Receivers placed in a depression or valley are likely to be screened off somewhat from such distant sources and have lower noise levels (Urick, 1986). Variations in this band are slow, on the order of hours to days and depend on changes in ship traffic and large scale temperature and salinity structure (in the sound channel).

Transient sources also contribute to noise at a given location. These include local ships, which are characterized by high energy narrow band peaks, often including harmonics of a fundamental frequency, anywhere from 5 to 200 Hz. Biological sources can also contribute to the noise field, with whales and dolphins capable of producing high amplitude, short duration sounds at frequencies from 18-100 Hz (Watkins, 1981).

HYDROTHERMAL SOUND GENERATION

No unambiguous field data exists characterizing vent sound, but theoretical estimates on power and frequency, as well as laboratory results (Little and Stolzenbach, in prep) give a range of values to help delimit the frequency bands of possible energy. Sound produced by turbulent mixing, as is found at the jet orifice, will be generated at a frequency close to V/D where V is exit velocity and D is orifice diameter (Morfey, 1973). For typical vent velocities and geometries, this frequency range is 10-100Hz. Other source mechanisms, such as fluid pumping or cavity resonance, may generate lower frequencies, depending on the distribution and geometry of subsurface fluid pathways as well as hydrodynamic flow characteristics deep within the hydrothermal system. Higher frequencies can be produced by pipe resonance, and are proportional to c/L where c is sound speed and L pipe length. In this paper we are confined to examining frequencies of 1-30 Hz by the bandwidth set for the microearthquake study.

HYDROTHERMAL SITE DESCRIPTION

The TAG hydrothermal area (Rona et al., 1986; Thompson, et al., 1988) is located at 26°08.28'N, 44°49.63'W, on a wall 1.5 kilometers east of the spreading axis of the Mid-Atlantic Ridge (figure D2). This east wall rises from the valley floor at 4000 m to a height of 2000m through a series of block faults. The hydrothermal site is composed of an inner mound of sulfides 250m wide and 55m tall which sits atop an outer mound 580 m wide and 25m high. The base of this structure is situated at a maximum depth of 3700 m. White smokers and shimmering water, with

temperatures up to 226°C, were found around the periphery of the inner mound. Tall chimneys, at least 10 m high, and black smokers were predominantly located at the very top of the inner mound, emitting fluid at temperatures of 350°C at velocities of about 1-2 m/s. A zone of low temperature hydrothermal activity is located between 2400 and 3100 m depth on the east wall, 3.7 km upslope to the east of the main field (Rona, 1980). Water column anomalies suggest a heat flux from this 10 km section of ridge of $5x10^8$ W (Klinkhammer, et al., 1986).

DATA DESCRIPTION

During the summer of 1985, a successful three week deployment of a network of six continuously recording ocean bottom hydrophones (OBH), (Koelsch and Purdy, 1979; Kong et al., 1986) was carried out within an area of 19x10 km on the crest of the Mid-Atlantic Ridge. This network provided coverage of the known low-temperature hydrothermal field on the eastern wall (Rona, 1976; Kong et al., 1986) and, coincidentally, surrounded the subsequently discovered high temperature vent field (figure D2). The instruments were deployed within the median valley (OBH 1,2,3,6) and on the valley walls (OBH 5,8). The six instruments were located around the vent at ranges of approximately 0.75, 3.5, 5.5, 6.5, 12.0, and 14.0 km. Data for this paper were obtained from a small subset of the earthquakes and shots which were recorded on all six instruments. The data set included thirteen separate time periods consisting of approximately 8-13 seconds of digitized (at 100 Hz) ambient noise preceding each event. These thirteen sets of simultaneously recorded

ambient noise, each 12.8 s long, spanned a period of 15 days. The reliable bandwidth of the system was 1-30 Hz. Power spectra were calculated using the Welsh method, dividing each record into 256 point length sets, multiplying by a Hanning window and averaging the results.

Temporal variations are evident in the raw time series data as seen in figure D3 which depicts two records taken 11 days apart by the same instrument. The second record shows high amplitude low frequency components not seen in the first. An examination in the frequency domain reveals power variations over time of three orders of magnitude on the instrument nearest the vent (figure D4a) and almost four orders of magnitude at the instrument 12 km away (figure D4b). Spectra from the lower noise periods resemble typical ambient ocean noise with high power at low frequencies (0.8-5 Hz), a minimum near 15 Hz, and increasing levels out to 30 Hz (the bandwidth of this system) as the effects of distant shipping become important. Spectral peaks at 22 Hz were seen when the R.V. Knorr was within the array and not at other times.

Spatial variability is exemplified by two time series taken at 0.75 and 6.5 km from the vent (figure D5). A look at the power spectra reveals several orders of magnitude difference over the array for a number of the events, figure D6a, D6b, D7a, D7b. Plotting power versus proximity to vent does not reveal any frequency at which power decreases monotonically with distance for typical events (figures D8a, D8b, D9a, D9b).

SOURCE LOCATIONS

In order to determine whether the hydrothermal vent site is generating detectable sound, and if there are any other point sources of sound near the array, we use the power spectral measured at each instrument. Our use of power levels to locate point sources is based on the assumption that such sources radiate acoustic waves whose power decays inversely with the square of distance. To minimize contamination from different sources we have divided the frequency into 3.2 Hz bandwidths. Of these, only ones with relatively high power levels are chosen (0.8-3.5, 3.5-6.6, 6.6-9.7, 12.9-16.0, 19.1-22.3, and 28.5-31.6 Hz) in order to reduce errors caused by the superposition of the isotropic noise field in this area and any point source noise fields. Power in each bandwidth is calculated for each of the six instruments. These levels are then compared to power that would be expected if a point source of amplitude A, call this a predictive source, was located at point x,y in a 40 km x 40 km grid surrounding the study area where:

$$P = \frac{A}{(x^2+y^2)}$$

To limit the number of free parameters to A, x and y, and improve the estimate of location, source depth was fixed at 3750, the depth of the high temperature vent field. Next, the root-mean-square difference between actual and predicted power is calculated using the six instruments. This value, the misfit in units of Pa^2/Hz for at 3.1 Hz bandwidth, is then plotted (figure D10a and D10b) for each grid point (spacing x: 2 km, y: 2 km). The minimum misfit is then the best estimate for point source location for the given measured power levels at the specified bandwidth and event. Perfect data from a point source would yield a misfit of 0 at the source location. The misfit value approaches

the rms value of the six instrument power levels as the predictive source is placed further and further away from the array. High misfits occur near the instruments (provided the actual source is not there) because the calculated power becomes very high for predictive sources placed near the receivers. Sources were sought for each of the six bandwidths and 13 events. Some events and bandwidths do not result in isolatable misfit minima and hence have not point source solutions. This would be the case for sound recorded from an isotropic noise field. Figure D10a shows a contour plot of the misfit for an event. The low in the north-west corner is the best source location for an event in bandwidth 0.8-3.5 Hz. A similar example is seen in figure D10b for an event one day earlier. Events in the next bandwidth, 3.5-6.6 Hz, have more poorly defined minima located in between the receivers for all events. High misfits occur near the receivers since as range = (x^2+y^2) decreases, P increases rapidly. Sources of error in calculating these locations include errors in instrument calibration, non-spherically spreading waves, or the existence of multiple sources.

The only bandwidth with consistent source locations from event to event was 0.8-3.5 Hz (figure D2). This bandwidth also exhibits the highest overall power level and hence may be less affected by superposed isotropic noise. The other bandwidths with relatively high power levels, show great scatter in source location over time and hence it is impossible to attribute them to a stationary geophysical process. The bandwidth 0.8-3.5Hz sources cluster near the tip of a small ridge on the western part of the Mid-Atlantic Ridge (figure D2).

Harmonic tremor characterized by narrow band frequencies in the range of 1-10 Hz has been associated with eruptive activity and magma movement in volcanoes (Aki et al., 1981; Koyanagi et al., 1987). Persistent, long tremor events which last for hours and recur for days probably result from magmatic activity beneath the volcano. In Hawaii, this shallow (<5 km) activity is confined to areas as small as 5 km in diameter centered on the summits of the volcanoes. We postulate that the high 0.8-3.5 Hz signal seen in the TAG area, with a peak at 2.5 Hz, is produced by volcanic processes, such as magma flow, on the western wall of the rift valley.

CONCLUSIONS

The ambient sound field in the bandwidth 1-30 Hz recorded within 13 km of the TAG hydrothermal area shows considerable spatial and temporal variation over the course of fifteen days. The hydrothermal vent did not produce enough sound to be detected by the ocean bottom hydrophone array located from 0.75 to 14 km away.

Using a model to find a point source given actual power levels at each of six OBH instruments, under the assumption of spherical spreading, the only stationary source uncovered was generating sound in a 0.8-3.5 Hz bandwidth and located outside the median valley. It appears to be harmonic tremor associated with the tip of a ridge on the western side of the spreading axis and may be volcanic in origin.

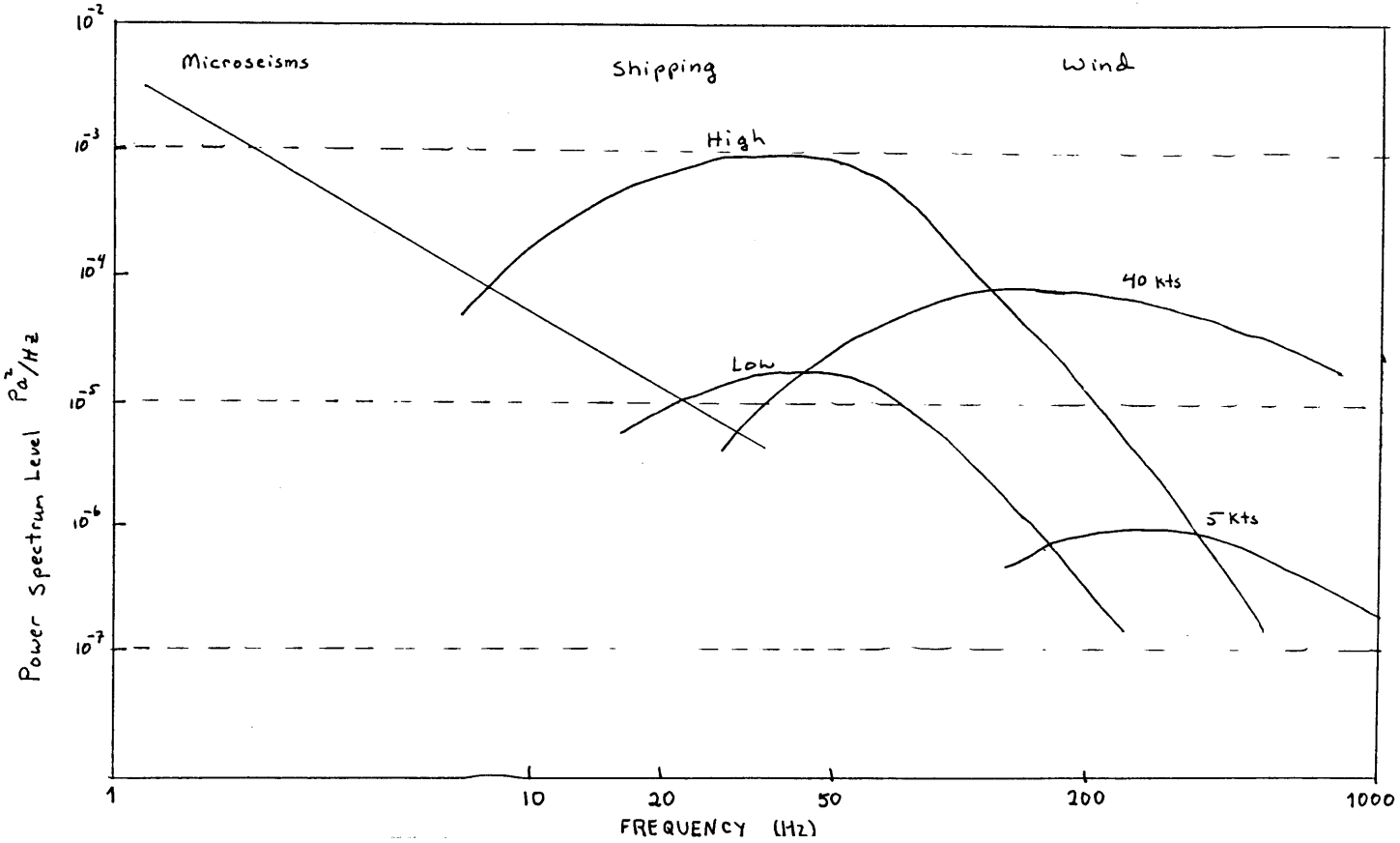

Figure D1
Spectra of ambient noise in the band 1 to 1000 Hz, based upon measurements in the literature and present models for noise spectra in various frequencies ranges. (From Urick, 1986).

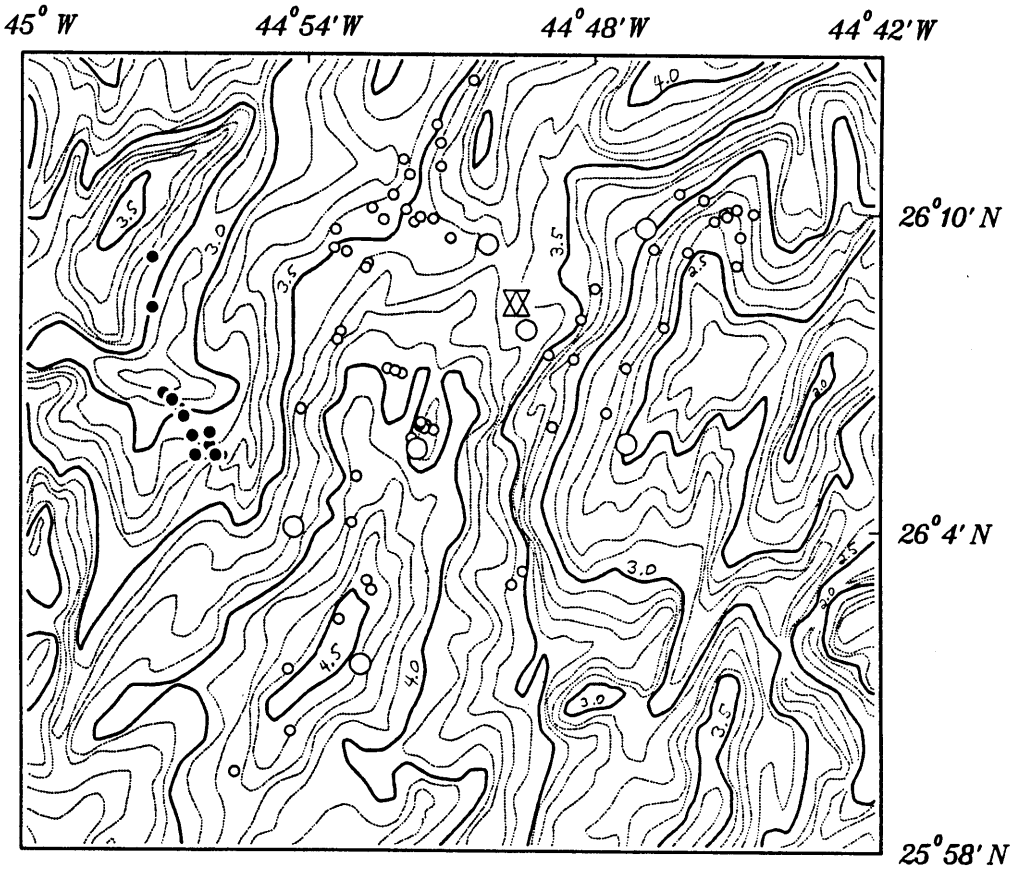

Figure D2

Topographic map of TAG study area in the Mid-Atlantic Ridge (Rona, et al., 1986), showing hydrophone locations (large open circles), earthquake locations (small open circles) from Kong et al., 1986, high temperature vent location (double cross), and 0.8-3.2 Hz source locations for events used in this study (solid circles). Contours are in 100 m intervals, median valley runs from north-east to south-west.

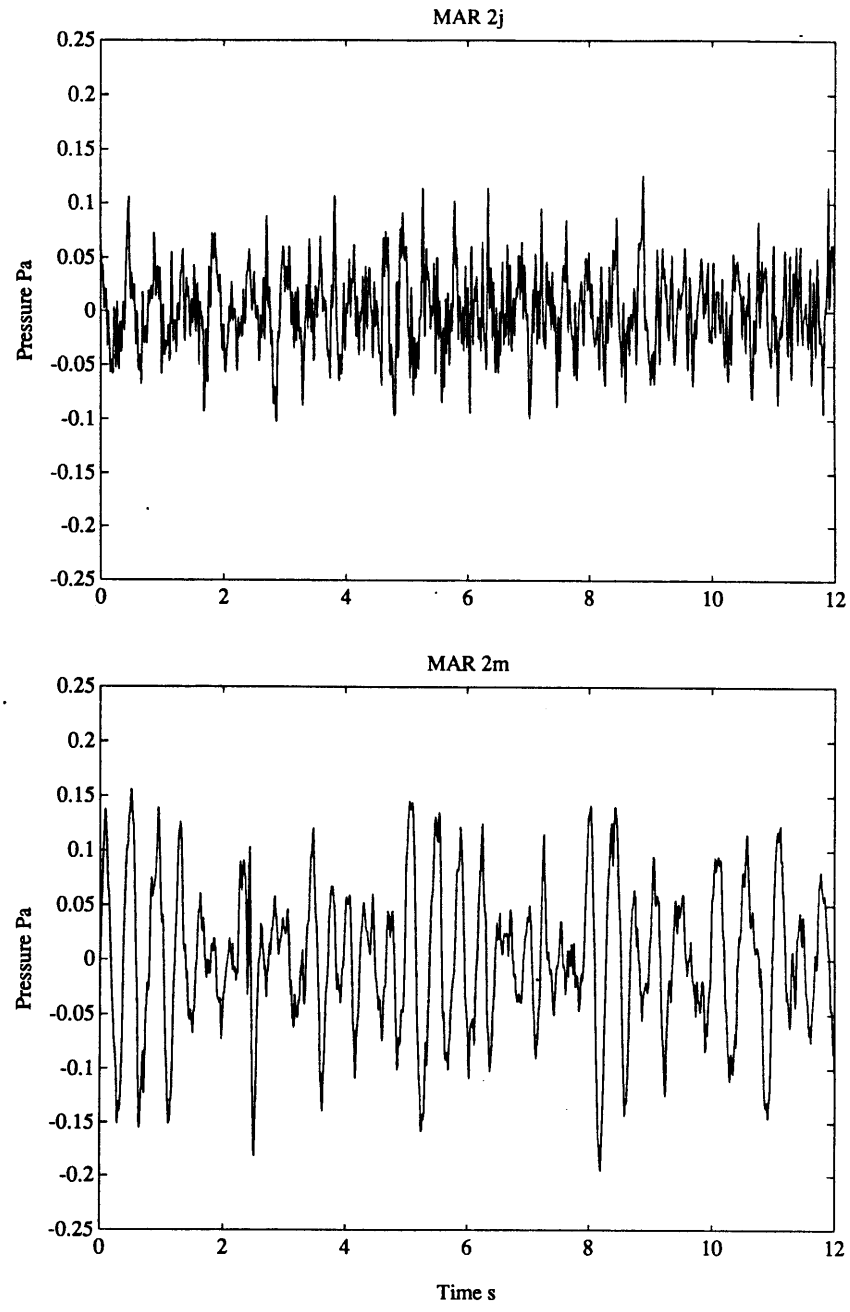

Figure D3
Time series record from instrument closest to hydrothermal vent, 750m, at two times eleven days apart showing variation in low frequency noise.

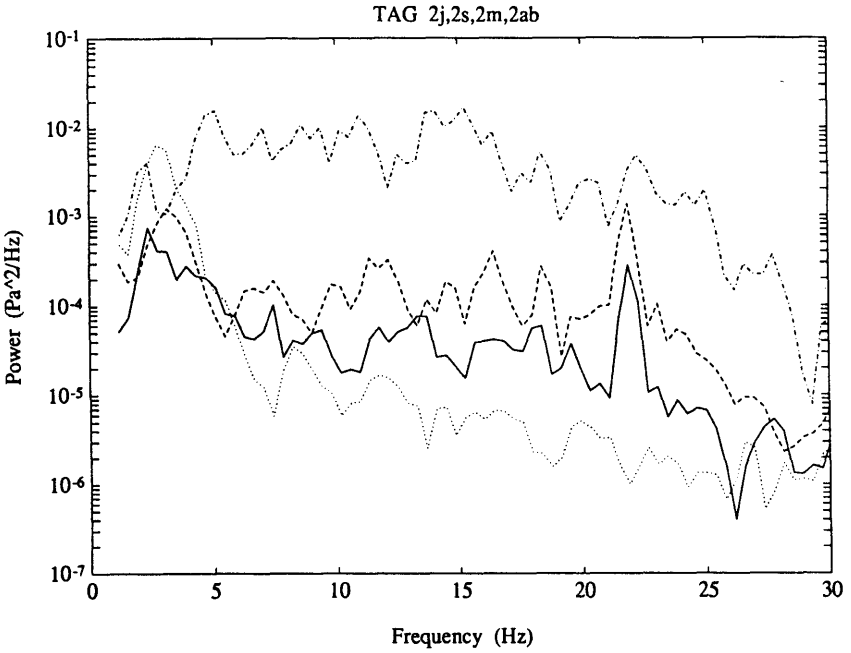

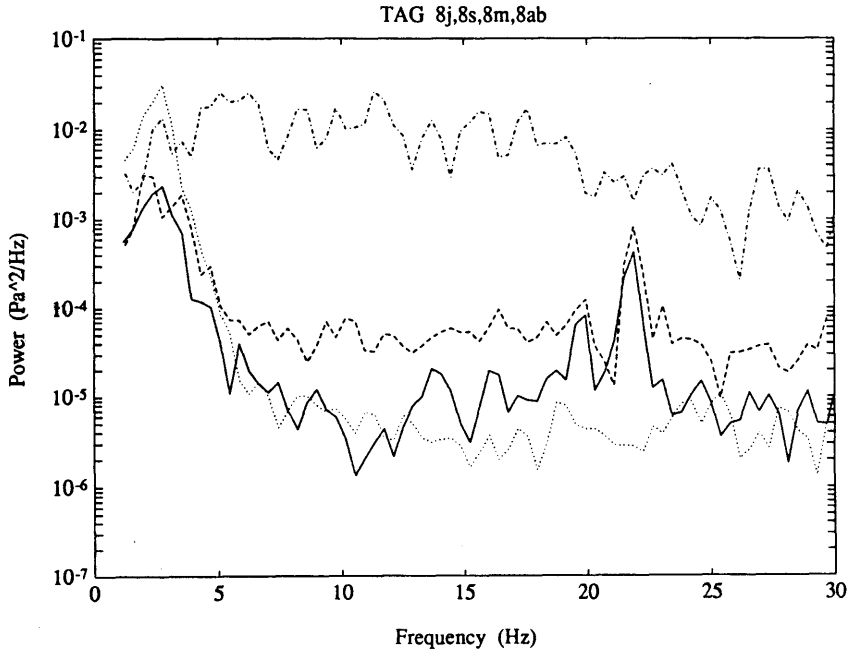

Figure D4

a) Power spectra for the first record (solid line), one hour later (dashed line), eleven days later (dotted line) and twelve days later (dot-dash line), from the instrument closest to the vent, 750m, showing temporal variation. The 22 Hz peak may be due to the R.V. Knorr. The anomalously high levels on day twelve are unexplained (dot-dash line).

b) Power spectra for the first record (solid line), one hour later (dashed line), eleven days later (dotted line) and twelve days later (dot-dash line), from the instrument 12 km from the vent showing the temporal variation. The 22 Hz peak may be due to the R.V. Knorr. The anomalously high levels on day twelve are unexplained (dot-dash line).

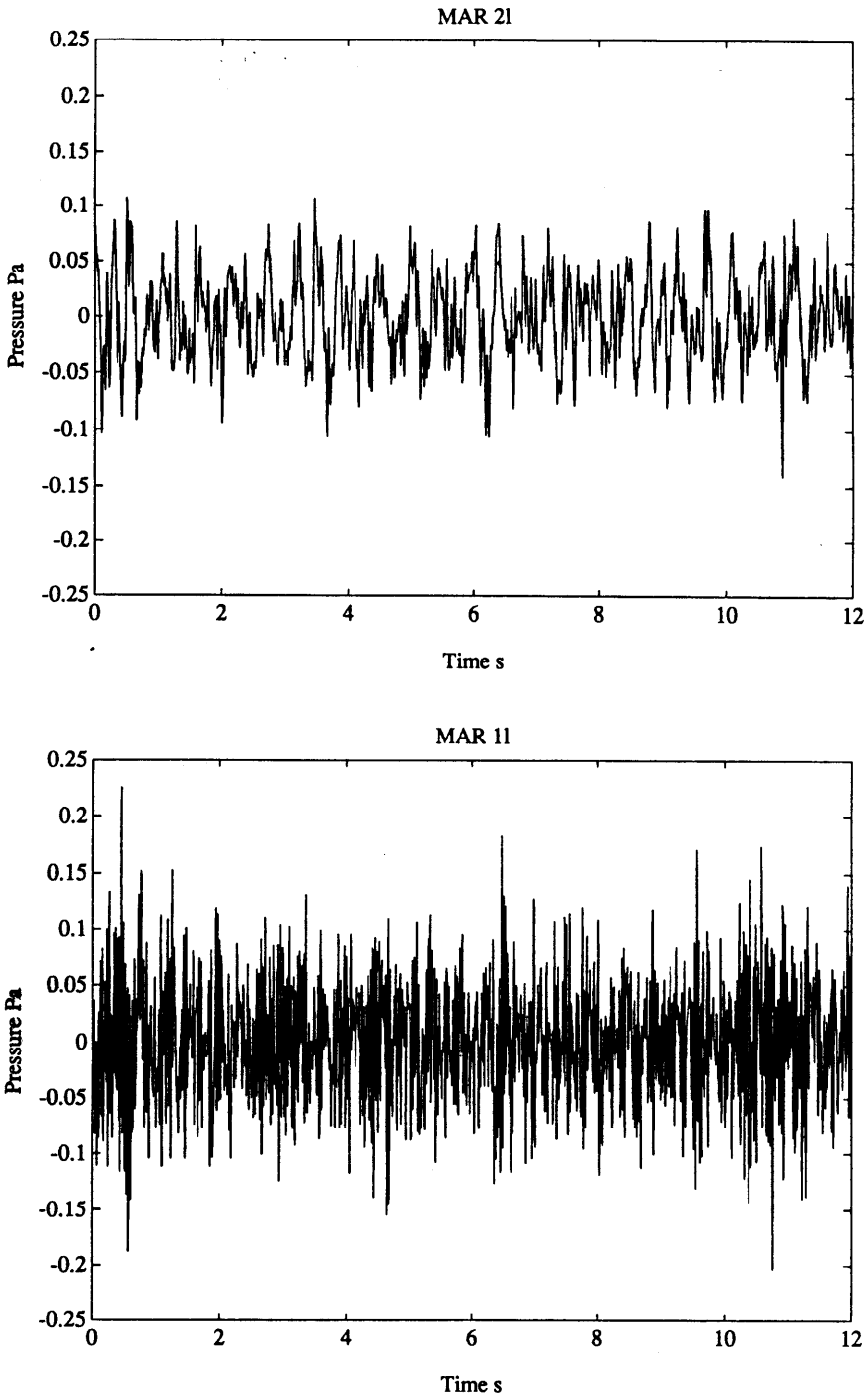

Figure D5
Time series, showing spatial variability, from instrument closest to vent (2), and instrument 6.5 km away (1).

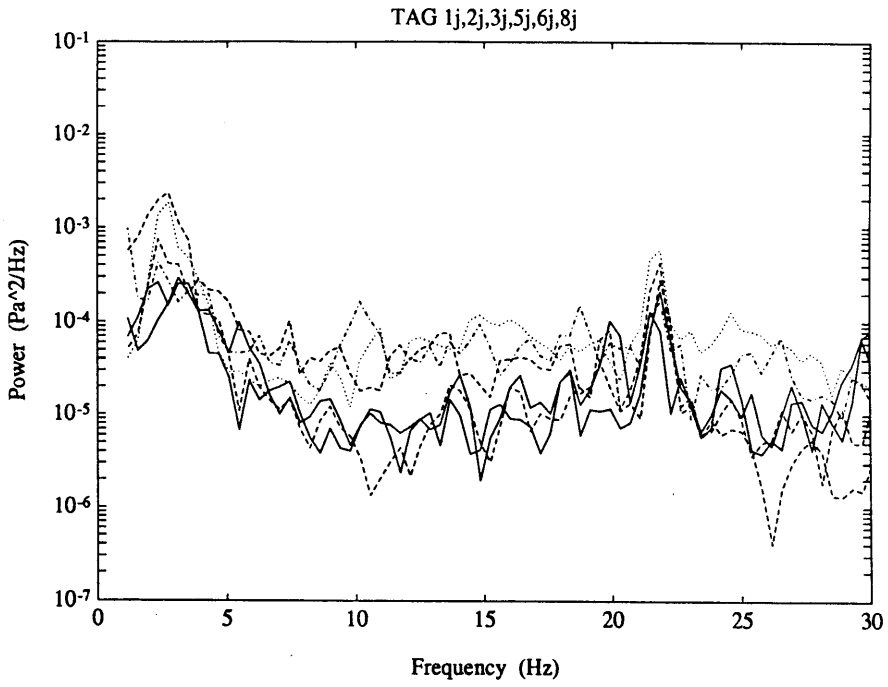

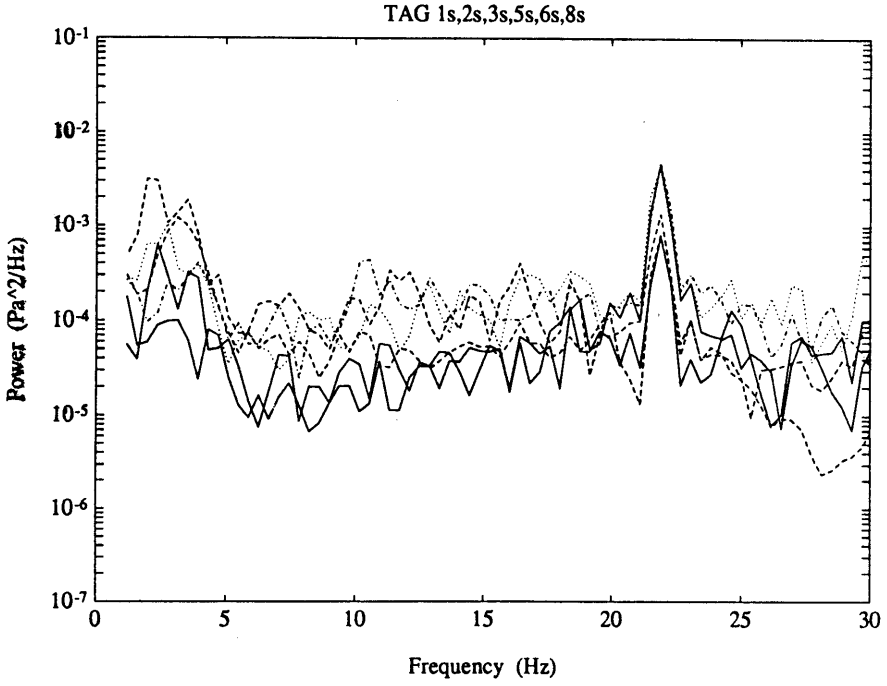

Figure D6

a) Power spectra recorded at each of six instruments for the first record show two orders of magnitude range. Note 22 Hz peak which may be caused by the ship or a whale.

b) Power spectra recorded at each of six instruments for record taken one hour after figure 6a. Note 22 Hz peak which may be caused by the ship or a whale.

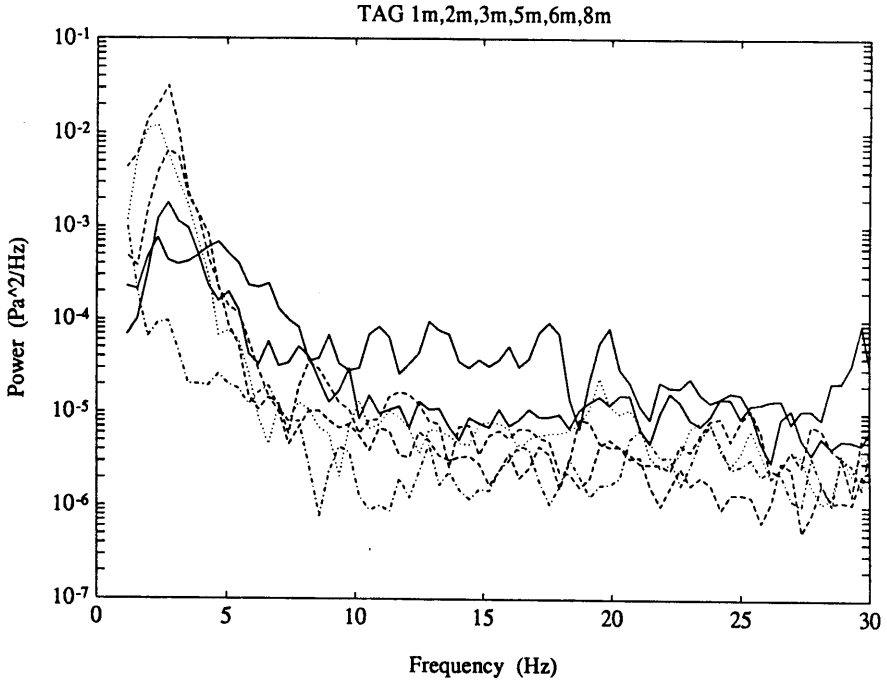

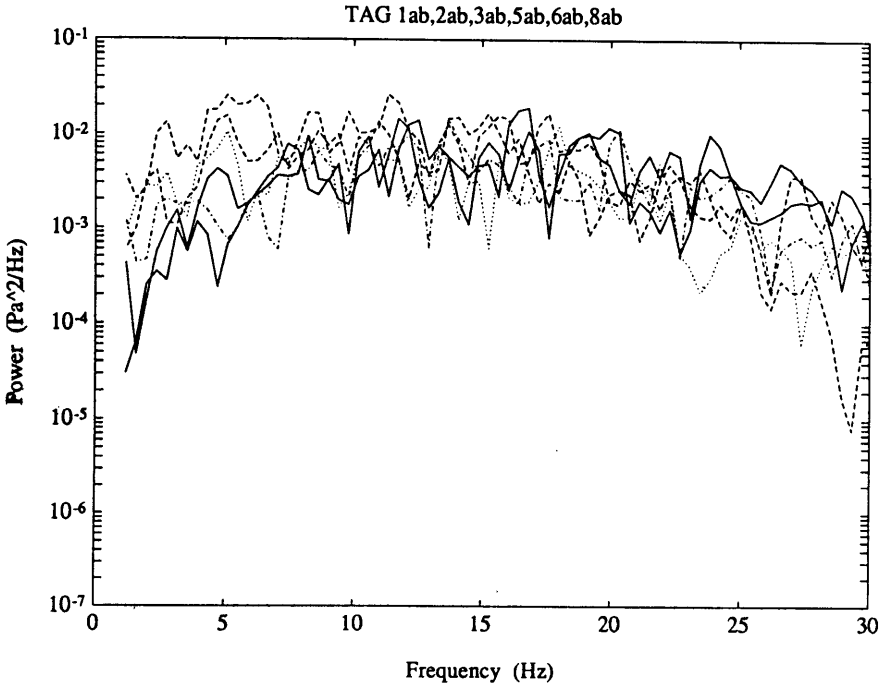

Figure D7

a) Power spectra recorded at each of six instruments for record taken eleven days after figure 6a. Ship is absent. Note high power at low frequencies.

b) Power spectra recorded at each of six instruments for record taken one day after figure 7a. Shows anomalously high broad band noise on all instruments.

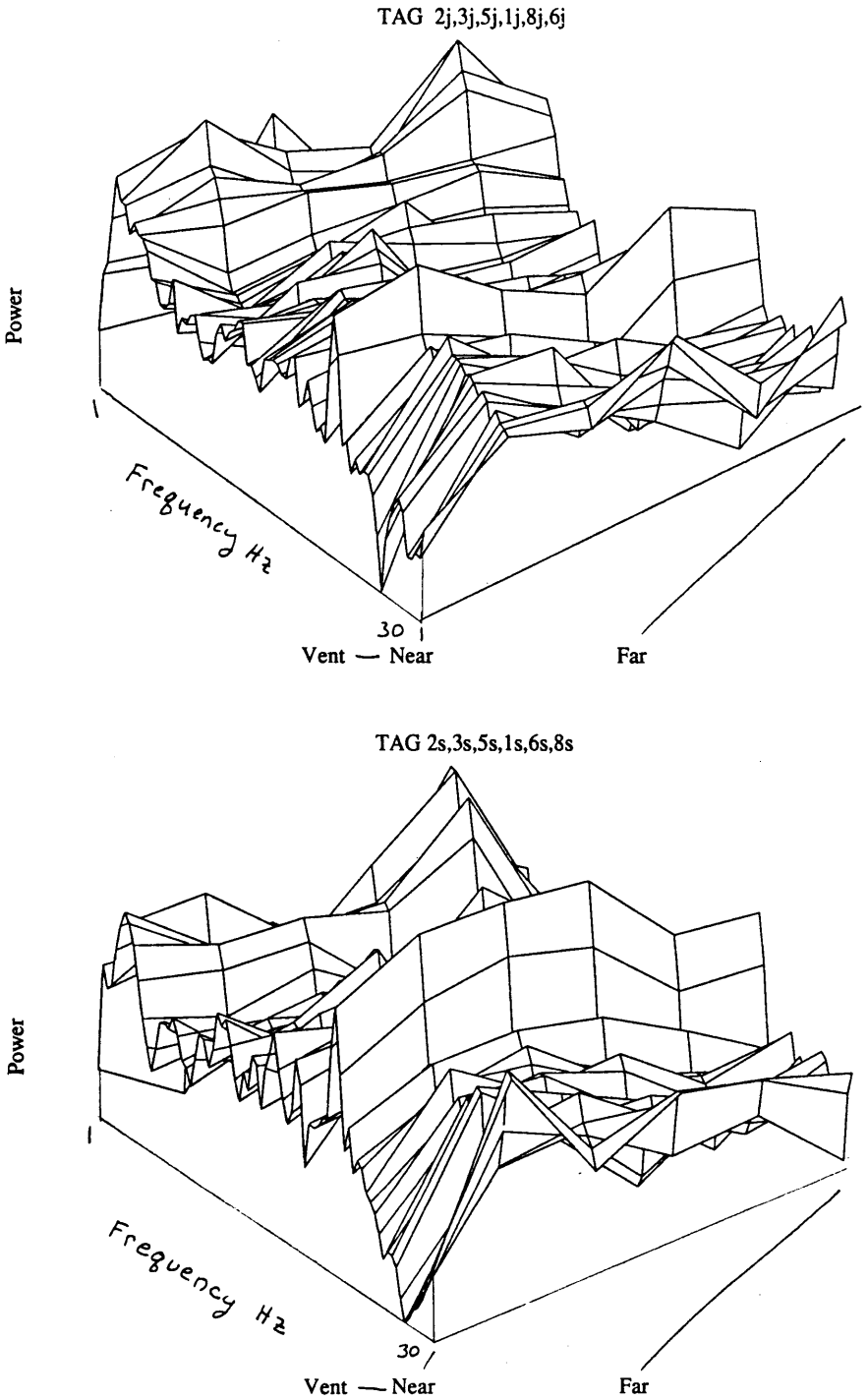

Figure D8

a) Power spectra vs. distance from vent site for first record (same as figure 6a). Note that at no frequency does power fall off monotonically with distance. The 22 Hz ship peak can be seen in all instruments.

b) Power spectra vs. distance from vent site for same record as figure 6b. Note that at no frequency does power fall off monotonically with distance. The 22 Hz ship peak can be seen in all instruments.

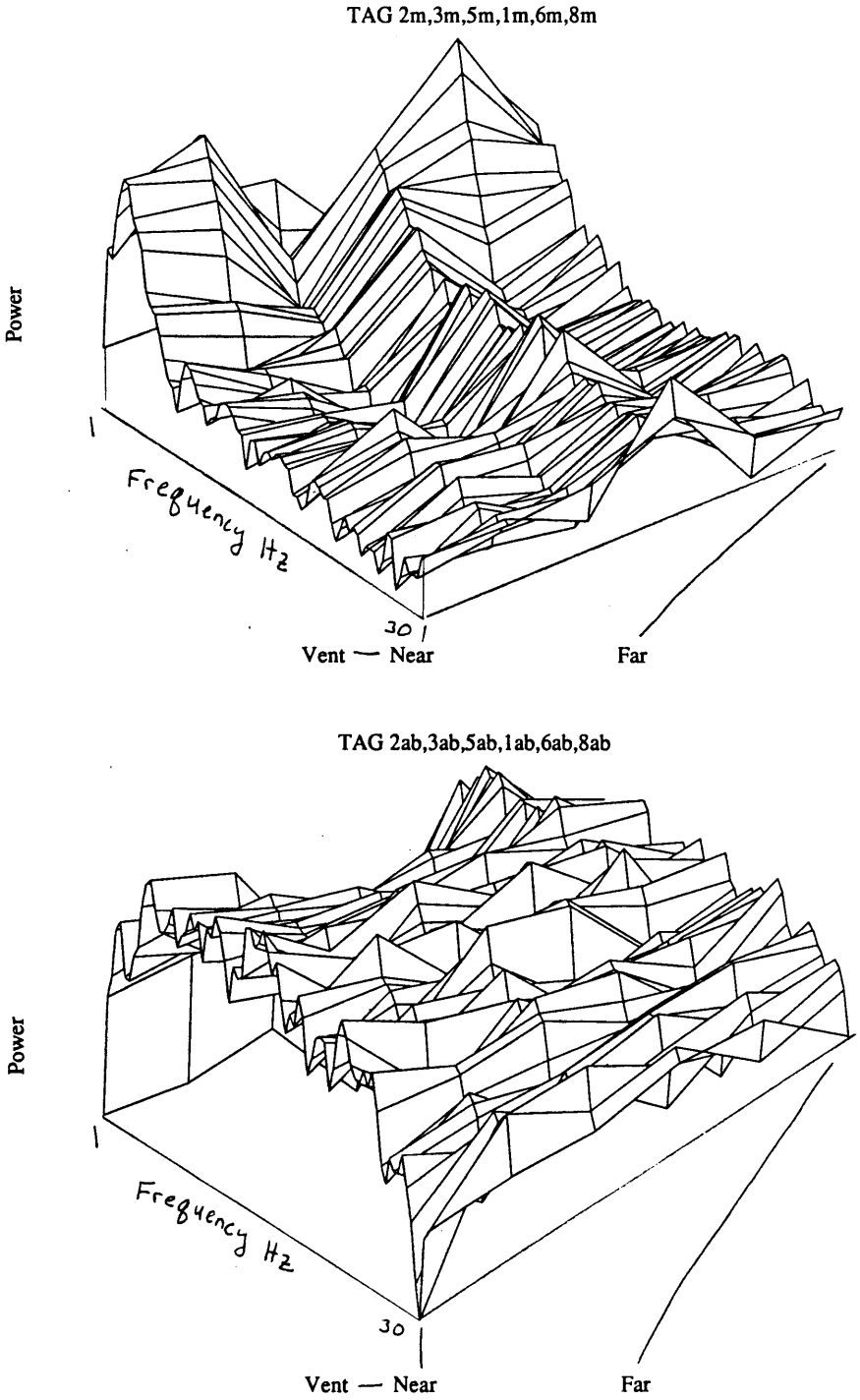

Figure D9

a) Power spectra vs. distance from vent site for same record as figure 7a. Ship is absent. There is high power at low frequencies but power does not fall off monotonically with distance.

b) Power spectra vs. distance from vent site for same record as figure 7b, showing anomalously high broad band noise on all instruments of relatively similar amplitude.

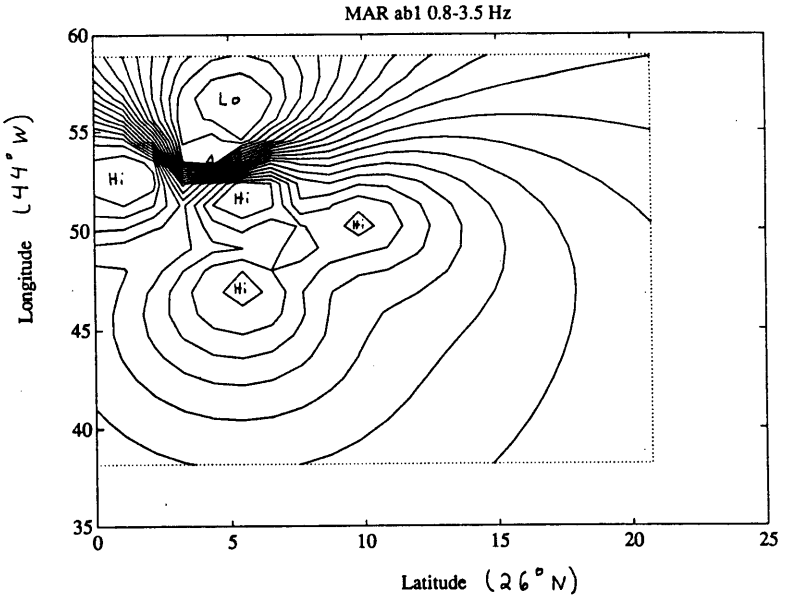

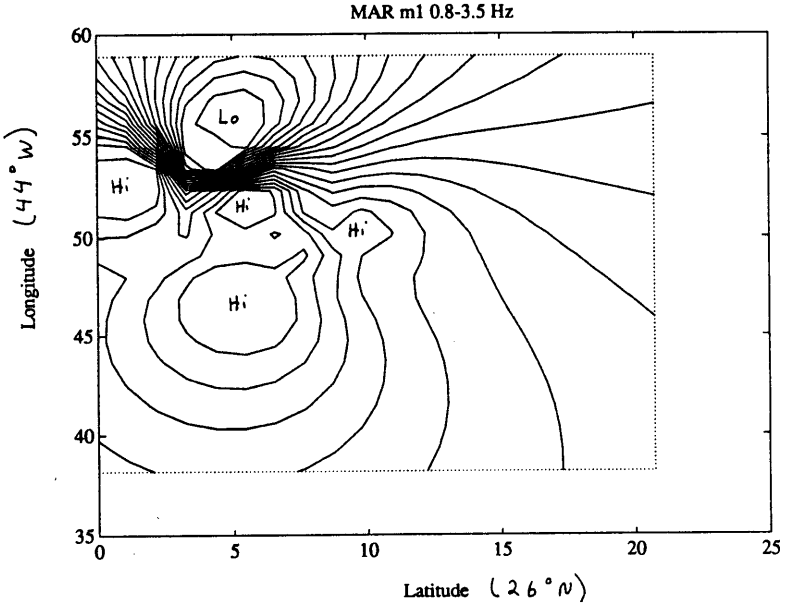

Figure D10

a) Contour of misfit between actual power vs calculated power for predictive sources within the study area. Contours are 1.95×10^{-4} Pa^2/Hz in a 3.1 Hz bandwidth of the rms misfit. Lowest point is the best fitting source location. The low in the north-west corner is the location of the source that produces the minimum misfit (0.0023 Pa^2/Hz) with recorded power levels for the bandwidth 0.8-3.5 Hz for the event shown in figures 7b and 9b. The rms power from the six instruments for this event was 0.0062 Pa^2/Hz.

b) Contour of misfit between actual power vs calculated power for predictive sources within the study area. Contours are 3.7×10^{-4} Pa^2/Hz in a 3.1 Hz bandwidth of the rms misfit. Lowest point is the best fitting source location. The low in the north-west corner is the location of the source that produces the minimum misfit with recorded power levels for the bandwidth 0.8-3.5 Hz for the records shown in figures 7a and 9a. Contour values are different from above because the total rms power is different for the two events. The rms power from the six instruments for this event was 0.0125 Pa^2/Hz.

REFERENCES

Adams, E. E., D. J. Cosler, K. R. Helfrich, S. Sengupta, and M. Chattree, Evaporation from heated water bodies: analysis of data from the East Mesa and Savannah River sites, Electric Power Research Institute report, April, 1986.

Akal, T., A. Barbagelata, G. Giudi, and M. Snoek, Time dependence of infrasonic ambient seafloor noise on a continental shelf. In Ocean Seismo-Acoustics: Low-Frequency Underwater Acoustics, Akal, T., and J.M. Berkson (ed.), Plenum Press, New York, p767-778, 1986.

Aki, K., and R.Y. Koyanagi, Deep volcanic tremor and magma ascent mechanism under Kilauea, Hawaii. J. Geophys. Res. 86, B8, 7095-7109, 1981.

Backer et al., Hydrothermal activity and sulfide formation in axial valleys of the East Pacific Rise crest between 18° and 22° S. Earth and Planet. Sci. Let, 72, 9-22, 1985.

Ballard, R. D., J .Francheteau, C. Rangan., W. Normark, East Pacific Rise at 21°N: the volcanic, tectonic and hydrothermal processes at the central axis. Earth Planet. Sci. Lett., 55, 1-10, 1981.

Ballard, R.D. et al., The Galapagos Rift at 86°W: 5. Variations in volcanism, structure, and hydrothermal activity along a 30km segment of the rift valley. J. Geophys. Res., 87, 1149-1161, 1982.

Ballard, R.D. et al., Geological setting of hydrothermal activity at 12°50'N on the East Pacific Rise: a submersible study. Earth Planet. Sci. Lett., 69, 176-186, 1984.

Bibee, L.D., and R.S. Jacobson, Acoustic noise measurements on Axial Seamount, Juan de Fuca Ridge, Geophys. Res. Lett., 13,9, 957-960, 1986.

Burdick, W.S., Underwater Acoustic System Analysis. Prentice-Hall, Englewood Cliffs, NJ, ch.10, 1984.

Canadian American Seamount Expedition (CASM), Hydrothermal vents and sulfide deposits, Axial Seamount, Juan de Fuca Ridge. Proc. Oceans '83, 801, 1983.

Canadian American Seamount Expedition (CASM), Hydrothermal vents on an axis seamount of the Juan de Fuca Ridge. Nature, 313, 212-214, 1985.

Cann, J.R., and M.R. Strens, Black smokers fuelled by freezing magma, Nature, 298, 147-149, 1982.

Cann, J.R., M,R. Strens, and A. Rice, A simple magma-driven thermal balance model for the formation of volcanogenic massive sulphides, Earth and Planet. Sci. Lett., 76, 123-134, 1986.

Chase, R.L., R.R. Delaney, H.P. Johnson, S.K. Juniper, J.L. Karsten, J.E. Lupton, S.D. Scott and V. Tunnicliffe. North caldera hydrothermal vent field, Axial Seamount, Juan de Fuca Ridge, EOS, 64, 723, 1983.

Cohen, J. and I. Wygnanski, The evolution of instabilities in the axisymmetric jet. Part 1. The linear growth of disturbances near the nozzle. J. Fluid Mech., 176, 191-219, 1987.

Converse, D. R., H. D. Holland, and J. Edmond, Flow rates in the axial hot springs of the East Pacific Rise (21^{o}N): Implications for the heat budget and the formation of massive sulfide deposits, Earth and Planet. Sci. Lett., 69, 159-175, 1984.

Corliss, J.B., J. Dymond, L.I. Gordon, J.M. Edmond, R.P. Von Herzen, R.D. Ballard, K. Green, D. Williams, A. Bainbridge, K. Crane and T.H. van Andel. Submarine thermal springs on the Galapagos Rift. Science, 203, 1073-1083, 1979.

Craig, H. et al., PAPATUA Expedition I: hydrothermal vent surveys in back-arc basins: the Lau, Fiji, Woodlark, and Manus Basins and Havre Trough. EOS, Trans. Am. Geophys. Union, 68 (7), 100, 1987.

Crane, K., F. Aikman, R. Embley, S. Hammond, A. Malahoff, and J. Lupton, The distribution of geothermal fields on the Juan de Fuca Ridge. J. Geophys, Res., 90, 727-744, 1985.

Curle, N., The mechanics of edgetones, Proc. Roy, Soc. Lon., A, 216, 412, 1953.

Delaney, J.R., and B. A. Cosens, Boiling and metal deposition in submarine hydrothermal systems, MTS Journal, 16, 3, 62-65, 1983.

Dowling, A.P., and J.E. Ffowcs Williams, Sound and Sources of Sound. Ellis Horwood, Publs., Chichester, p95, 1983.

Dowling, A.P., J.E. Ffowcs Williams, and M.E. Goldstein, Sound production in a moving stream. Philos. Trans. R. Soc. London, B 288, 321-349, 1978.

Embley, R.W., S.R. Hammond, and K. Murphy, The caldera of Axial Volcano - remote sensing and submersible studies of a hydrothermally active submarine volcano. NOAA Symposium Series for Undersea Research, 6, 2, 1988 (in press).

Ffowcs Williams, J.E., Hydrodynamic noise. Ann. Rev. Fluid Mech., 1, 197-222, 1969.

Ffowcs Williams, J.E., Aeroacoustics. Ann. Rev. Fluid Mech., 9, 447-468, 1977.

Fischer, H. B., J. E. List, R. C. Koh, J. Imberger, and N. H. Brooks, Mixing in Inland and Coastal Waters, p315-389, Academic, New York, 1979.

Francheteau, J. and R.D. Ballard, The East Pacific Rise Near 21°N, 13°N, and 20°S: Inferences for along-strike variability of axial processes of the Mid-Ocean Ridge, Earth and Planet. Sci. Lett., 64, 93-116.

Goldstein, M.E., Aeroacoustics of turbulent shear flows. Ann. Rev. Fluid Mech., 16, 263-285, 1984.

Hammond, S.R., et al., Pisces submersible exploration of a high-temperature vent field in the caldera of Axial Volcano, Juan de Fuca Ridge, (ASHES expedition). EOS, Trans. Am. Geophys. Union, 67, (44), 1027, 1986.

Hammond, S.R., et al. Discovery of high-temperature hydrothermal venting on the Endeavor Segment of the Juan de Fuca Ridge. EOS, Trans. Am. Geophys. Union, 65, (45), 1111, 1984

Hannington, M.D., and S.D. Scott, A caldera-hosted silica-sulfate-sulfide deposit, Axial Seamount, Central Juan de Fuca Ridge, N.E. Pacific Ocean. Geological Association of Canada/Mineralogical Association of Canada Abstracts, pA24, 1985.

Hawkins, J., Black smoker vent chimneys, EOS, Trans. Am. Geophys. Union, 67, 17, 430, 1986.

Hekinian, R., J. Francheteau, V. Renard, R.D. Ballard, P. Choukroune, J.L. Cheminee, F. Albarede, J.F. Minster, J.C. Marty, J. Boulegue, and J.L. Charlou, Intense hydrothermal activity at the axis of the East Pacific Rise near 13°N: submersible witness of the growth of sulphide chimney. Mar. Geophys. Res., 6, 1-14, 1983.

Hekinian, R., et al., Geology of massive hydrothermal deposits from fast spreading segments of the East Pacific Rise near 12°50'N and 11°30'N, Proc. Oceans '83, 816, 1983.

Hessler, R.R. and W.M. Smithey, The distribution and community structure of megafauna at the Galapagos hydrothermal vents. In: Rona, P.A., K. Bostrom, L. Laubier, K. Smith (ed.) Hydrothermal Processes at sea-floor Spreading Centers, Plenum Press, New York, p.735-770, 1983.

Hessler, R.R., W.M. Smithey, C.H. Keller, Spatial and temporal variation of giant clams, tube worms and mussels at deep-sea hydrothermal vents. In Jones, M.L., (ed.) Hydrothermal vents of the eastern Pacific: an overview, Bull. Biol. Soc. Wash., 6, 411-428, 1985.

Hoagland, P., and J. Broadus, Seabed material commodity and resource summaries, Tech. Rep. WHOI-87-43, p97-125, Woods Hole Ocean. Inst., Woods Hole, Mass., 1987.

Hodgkiss, W.S. and V.C. Anderson, Detection of sinusoids in ocean acoustic background noise. J. Acoust. Soc. Am., 67, (1), p214, 1980.

Johnson, P.H., and V. Tunnicliffe, Time-series measurements of hydrothermal activity on Northern Juan de Fuca Ridge. Geophys. Res. Lett., 12, (10), 685-688, 1985.

Jorgensen, D., "Near field" noise from turbulent jets, J.Acoust. Soc. Am., 33, 6, 817, 1961.

Karsten, J. et al., Regional setting and local character of a hydrothermal field/sulfide deposit on the Endeavor Segment of the Juan de Fuca Ridge. EOS, Trans. Am. Geophys. Union, 65, 45, 1111, 1984.

Klinkhammer, G., H. Elderfield, M. Greaves, P.A. Rona, and T. Nelsen, Manganese geochemistry near high temperature vents in the Mid-Atlantic Ridge rift valley. Earth and Planet. Sci. Lett., 80, 230-240, 1986.

Koelsch, D.E., and G.M. Purdy, An ocean bottom hydrophone instrument for seismic refraction experiments in the deep ocean. Mar. Geophys. Res., 4, 115-125, 1979.

Kong, L.S.L., S.C. Solomon, and G.M. Purdy, Microearthquakes near the TAG hydrothermal field , Mid-Atlantic Ridge, 26^{o}N. EOS Trans. Am. Geophys. Union, 67, 44, p1021, 1986.

Koyanagi, R. Y., B. Chouet, and K. Aki, Origin of volcanic tremor in Hawaii. U. S. Geological Survey Professional Paper 1350, in Volcanism in Hawaii, p 1221-1257, 1987.

Laufer, J., and T. Yen, Noise generation by a low-Mach number jet. J. Fluid Mech., 134, 1-31, 1983.

Lighthill, M.J., On sound generated aerodynamically, I. General theory. Proc. Roy. Soc. Lond. A 211, 564-587, 1952.

Lighthill, M.J., On sound generated aerodynamically II. Turbulence as a source of sound, Proc. Roy. Soc. Lon., 222, 1-32, 1954.

Lighthill, M.J., Jet noise. Am. Inst. Aero. Astro., 1, 7, 1507-1517, 1963.

Little, S.A., K.D. Stolzenbach, and R.P. Von Herzen, Measurements of plume flow from a hydrothermal vent field, J. Geophys. Res., 92, 2587-2596, 1987.

Little, S.A., and K.D. Stolzenbach, Sound production by hydrothermal vents, in prep.

Lonsdale, P.F., Hydrothermal plumes and baritic sulfide mounds at a Gulf of California spreading center, EOS, Trans. Am. Geophys. Union, 61, 995, 1980.

Lonsdale, P, and K. Becker, Hydrothermal plumes, hot springs and conductive heat flow in the Southern Trough of Guaymas Basin. Earth and Planet. Sci. Lett., 73, 211-225.

Lush, P.A., Measurements of subsonic jet noise and comparison with theory. J. Fluid Mech., 46, 3, 477-500, 1971.

Macdonald, K.C., K. Becker, R.N. Spiess, and R.D. Ballard, Hydrothermal heat flux of the "black smoker" vents on the East Pacific Rise, Earth Planet. Sci. Lett., 48, 1-7, 1980.

Macdonald, K.C., Mid-Ocean Ridges: Fine scale tectonic, volcanic and hydrothermal processes within the plate boundary zone, Ann. Rev. Earth Plan. Sci., 10, 155-190, 1982.

Macdonald, K.C., A geophysical comparison between fast and slow spreading centers: constraints on magma chamber formation and hydrothermal activity. In: Rona, P.A., K. Bostrom, L. Laubier, K. Smith (ed.) Hydrothermal Processes at Sea-floor Spreading Centers, Plenum Press, New York, p.27-51, 1983.

Mankbadi, R.R., On the interaction between fundamental and subharmonic instability waves in a turbulent round jet. J. Fluid Mech., 160, 385-419, 1985.

McConachy, T.F., R.D. Ballard, M.J. Mottl, R.P. Von Herzen, Geologic form and setting of a hydrothermal vent field at lat $10^{o}56'$N, East Pacific Rise: a detailed study using Angus and Alvin. Geology, 14, 295-298, 1986.

McGrath, J.R., Infrasonic sea noise at the Mid-Atlantic Ridge near 37^{o}N, J. Acoust. Soc. Am, 60, 6, 1290-1299, 1976.

Mellinger, E.C., K.E. Prada, R.L. Koehler, K.W. Doherty, Instrument Bus an electronic system architecture for oceanographic instrumentation. Woods Hole Oceanographic Institution technical report, WHOI-86-30, Woods Hole, Massachusetts, 1986.

Moores, E.M., and J.F. Vine, The Troodos Massif, Cyprus and other ophiolites as ocean crust: evaluation and implications, Philos. Trans. R. Soc. Lon., A, 268, 433-466, 1971.

Morfey, C.L., Amplification of aerodynamic noise by convected flow inhomogeneities. J. Sound and Vibration, 31, (4), 391-397, 1973.

Mottl, M.J., Metabasalts, axial hot springs, and the structure of hydrothermal systems at Mid-Ocean Ridges, Geo. Soc. Am. Bull., 94, 161-180, 1983.

Normark, W.R., et al., Active hydrothermal vents and sulfide deposits on the Southern Juan de Fuca Ridge. Geology, 11, 158-163, 1986.

Ocean Drilling Program (ODP) Leg 106 Scientific Party, Drilling the Snake Pit hydrothermal sulfide deposit on the Mid-Atlantic Ridge, lat. 23°N. Geology, 14, 1004-1007, 1986.

Ocean Science News, The soviet news agency TASS said Russian scientists observed hot-water springs on the floor of the Sea of Okhotsk near Paramushir, one of the northern islands of the Kurile chain. Washington: Nautilus Press, Inc. (February 3), p. 3, 1986.

Oppenheim,A.V., R.W. Schafer, Digital Signal Processing. Prentis-Hall Inc., Englewood Cliffs, New Jersey, 1975.

Owsley, N.L., and G.R. Swope, Time delay estimation in a sensor array. IEEE Trans. Acoustics, Speech, and Sig. Proc., ASSP-29, (3), 519-523, 1981.

Peter, J.M., and S.D. Scott, Mineralogy and geochemistry of hydrothermal vent deposits, Guaymas Basin, Gulf of California, In Geological Ass. of Canada and Mineralogical Ass. of Canada, Abstracts, A48, 1985.

Powell, A., Theory of vortex sound. J. Acoust. Soc. Am., 36, 1, 1964.

Riedesel, M., J.A. Orcutt, K.C. Macdonald and J.S. McClain, Microearthquakes in the black smoker hydrothermal field, East Pacific Rise at 21°N, J. Geophys. Res., 87, B13, 10,613-10,623, 1982.

RISE TEAM, Hot springs and geophysical experiments on the East Pacific Rise, Science, 207, 1421-1433, 1980.

Rona, P.A., Black smokers and massive sulfides at the TAG hydrothermal field, Mid-Atlantic Ridge 26°N, EOS, 66, 46, 936, 1985.

Rona, P.A., G. Klinkhammer, T.A. Nelsen, J.H. Trefry, and H. Elderfield, Black smokers, massive sulphides and vent biota at the Mid-Atlantic Ridge. Nature, 321, 6065, 33-37, 1986.

Rona, P.A., G. Thompson, M.J. Mottl, J.A. Karson, W.J. Jenkins, D. Graham, M. Mallette, K. Von Damm, and J.M. Edmond, Hydrothermal activity at the TAG hydrothermal field, Mid-Atlantic Ridge crest at 26°N, J. Geophys. Res., 89, B13, 11,365-11,377, 1984.

Ross, D., Mechanics of Underwater Noise. Pergamon Press, New York, 1976.

Ryan, P.J., D.R.F. Harleman, and K. D. Stolzenbach, Surface heat loss from cooling ponds, Water Resources Res., 10, (5), 930-938, 1974.

Schlichting, H., Boundary-layer theory, p278-289, McGraw Hill, New York, 1968.

Scott, S.D. et al., Tectonic framework and sulfide deposits of Southern Explorer Ridge, northeastern Pacific Ocean. EOS, Trans. Am. Geophys. Union, 65, 54, 1111, 1984.

Thompson, G., S.E. Humphris, B. Schroeder, M. Sulanowska and P.A. Rona, Active vents and massive sulfides at 26°N (TAG) and 23°N (Snakepit) on the Mid-Atlantic Ridge. submitted to Canadian Mineralogist, 1988.

Townsend, A. A., Structure of turbulent shear flow, Cambridge University Press, Cambridge, p 143, 1980.

Tivey, M.K., and J.R. Delaney, Sulfide deposits from the Endeavor Segment of the Juan de Fuca Ridge, Mar. Min. 5, 165-179, 1985.

Tivey, M.K., and J.R. Delaney, Growth of large sulfide structures on the Endeavour Segment of the Juan de Fuca Ridge. Earth Planet. Sci. Lett., 77, 303-317, 1986.

U.S. Geological Survey (USGS), Sulfide deposits on Gorda Ridge. EOS, Trans. Am. Geophys. Union, 68, 36, 1233, 1985.

Urick, R.J., Principles of Underwater Sound for Engineers, 2nd ed. New York, McGraw-Hill Book Company, 1975.

Urick, R.J., Ambient noise in the sea. Peninsula Publishing, Los Altos, 1986.

Van Dover, C.L., A comparison of stable isotope ratios ($^{18}O/^{16}O$ and $^{13}C/^{12}C$) between two species of hydrothermal vent decapods (Alvinocaris lusca and Munidopsis subsquamosa). Mar. Ecology, 31, 295-299, 1986.

Waltz, A., Boundary layers of flow and temperature, p62-72, MIT Press, Cambridge, 1969.

Watkins, W.A., Activities and underwater sounds of fin whales, Sci. Rep. Whales Res. Inst., 33, 83-117, 1981.

Webb, S.C., Observations of seafloor pressure and electric field fluctuations. PhD thesis, Scripps Inst. Oceanog., U.C. San Diego, California, 1984.

Wentz, G.M., Acoustic ambient noise in the ocean: spectra and sources. J. Acoust. Soc. Am., 34, p1936, 1962.

White, F. M., Fluid Mechanics, p410-419, McGraw Hill, New York, 1979.